Coverage dependence for structure of self-assembled monolayers of thiols on Au(111) and co-adsorption of water above them and on bare Au(111).

Per H. Borchardt

Thesis submitted in accordance with the requirements of the University of St. Andrews for the degree of **Doctor of Philosophy**.

Supervised by: **Prof. Neville V. Richardson**.

School of Chemistry, University of St. Andrews

September 2005

Abbreviations used in this thesis.

2ME = 2-Mercaptoethanol

BM = Benzylmercaptan

CA = Contact Angle

FTIR = Fourier Transform Infrared Spectroscopy

HREELS = High Resolution Electron Energy Loss Spectroscopy

LEED = Low Energy Electron Diffraction

LHe = Liquid Helium (temperature cooling)

RAIRS = Reflection Adsorption Infra Red Spectroscopy

RT = Room Temperature

STM = Scanning Tunnelling Microscopy

TPD = Temperature Programmed Desorption

UHV = Ultra High Vacuum

Abstract

Water is the most common liquid on Earth and a very important compound in biological life and science. It is therefore of great interest to study it in more detail.

Self assembled monolayers (SAMs) are another interesting feature in surface chemistry as they can act as a model in biological and industrial science. It is therefore important to know more about how to produce them, their structure and how they interact with other molecules, eg. water.

SAMs of two thiols have been studied in this project. The chosen ones were one aromatic and hydrophobic,benzyl mercaptan (BM), and one aliphatic and hydrophilic, 2-mercaptoethanol (2ME). Both were investigated by gaseous dosing the thiols onto Au(111) in vacuum (UHV) at different exposures.

The structure of BM were determined by LEED, HREELS, RAIRS and STM and the molecules were found to have different orientation depending on the coverage. At low (sub monolayer) covererage the BM molecules are orientated with the aromatic ring parallel to the surface without any long range order. On the other hand, at high coverage (saturated monolayer) they were standing up with the ring perpendicular to the surface and a long range $(\sqrt{7}x\sqrt{7})R19.1^{o}$ structure relative to the Au(111) surface.

A similar coverage dependence was found for 2ME by HREELS and RAIRS. At low coverage the molecules were found to be orientated with the C-C-O plane parallel to the surface while at higher coverage they are orientated more vertically. Even an intermediate orientation was found for a short range of exposure between the low and high coverage with the molecules partly standing up. There are also intermolecular hydrogen bonding between the O-H end groups of the molecules.

For both thiols, the molecules becomes deprotonated upon adsorption and the thiolate binds to the surface during the build up of a monolayer at both room temperature and reduced temperatures (below 100K). There was no sign of multilayer for BM and a little for 2ME above the saturated monolayer with additional exposure at room temperatures, but both grow multilayer at low temperatures (below 100K) where the molecules are not ordered nor deprotonated. By gaseous deposition of pure BM or 2ME in UHV, 2ME sticks better of the Au(111) surface than BM while the opposite is true when growing the SAMS from a mixture of them in ethanol solution.

The adsorption of water onto bare Au(111) and different coverages of 2ME and BM has been carried out below 100K in UHV.

On bare Au(111) STM shows that water molecules form clusters containing rings of six water hexamers. The dominating frequency of the O-D hydrogen bond stretch in RAIRS show that the first layer of D_2O seems to be less amorphous then the subsequent ones as the ice grows with further exposure. Similar ordering was also found for D_2O adsorbed on a saturated monolayer and multilayer of 2ME with more amorphous structure throughout the ice. On the other hand, for higher coverage of BM the D_2O molecules seem to have a higher degree of order. For all surfaces (bare Au and BM, 2ME) and all coverages of the SAM, the overall amount (thickness) of ice grown seems to be linear to the D_2O exposure according to the hydrogen bonded O-D band. The free O-D stretch band shows that these free O-D only exists only on the surface facing the vacuum for ice on bare Au(111) and 2ME while on BM there is no maximum in the intensity of that band suggesting that there are also free O-D in the interior of the ice from clusters.

Acknowledgements

My greatest thanks goes to my supervisor Prof. Neville V. Richardson for organising and bringing me in to the project, his patience and help when there are problems and I need help and also for teaching me some surface science theory.

Many thanks also to Dr. Euan Sturrock for instructing me to use the techniques as HREELS, STM, LEED, sample preparation and working with the UHV systems. And thanks to Dr. Steve Francis for guiding me how to use the RAIRS and also helping me when any troubles with the machines appear, which I also thank Dr Qiao Chen for his assistance very much.

Also the Surface Science group, including Sandy, Emma, Tim, Wendy, Manfred, Ian, Tomas, Christel, Piotre, Aoife, Chris, and other present and former people over there for some help and nice social atmosphere deserve my acknowledgement.

Students and other people I know in St Andrews and elsewhere in Scotland deserve my thanks for a social and funny non-academic life. In particular two university clubs for keeping me fit: Celtic Society for teaching me Scottish Dances and Breakaway for bringing me out on the hills and into the sport "Munro Bagging" (you can guess how many of those 3000ft+ summits I climbed – it is more than the number of pages in this thesis).

Finally I would like to thank my family and friends home in Sweden, including my father Peter, mother Ulla and brother Lars and his family (wife and two lovely girls) for all support. Tack så hemskt mycket för all hjälp och stöd när det som bäst behövdes, samt att ni alltid fanns till hands för att prata och att hålla kontakt med släkt och vänner hemma. Likaså att det var trevligt att ses varje gång jag åkte hem.

List of papers

This thesis is based on the following papers:

- E.J. Sturrock, Q. Chen, P.H. Borchardt, N.V. Richardson, "*Coverage dependent change in orientation for the adsorption of benzyl mercaptan on Au(111)*", ***Journal of Electron Spectroscopy and Related Phenomena*** 135 (2004) 127-134.
- E.J. Sturrock, P.H. Borchardt, N.V. Richardson, "*STM study of water and benzyl mercaptan on Au(111)"* – unpublished work 2004.

Table Of Contents

Declarations

I, Per H. Borchardt, hereby certify that this thesis, which is approximate 23,000 words in length, has been written by me, that it is the record of work carried out by me and that it has not been submitted in any previous application for a higher degree.

Date: 26/08/2005 Signature of candidate:

I was admitted as a research student in September 2001 and as a candidate for the degree of PhD in July 2002; the higher study for which this is a record was carried out in the University of St Andrews between 2001 and 2005.

Date: 26/08/2005 Signature of candidate:

I hereby certify that the candidate has fulfilled the conditions of the Resolution and Regulation appropriate for the degree of PhD in the University of St Andrews and that the candidate is qualified to submit this thesis in application for that degree.

Date: 27/8/05 Signature of supervisor

Declarations, continued

In submitting this thesis to the University of St. Andrews I am understood that I am giving permission for it to be made available for use in accordance with the regulations of the University Library. I also understand that the title and abstract will be published and that copy of the work may be made and supplied to any *bona fide* library or research worker.

Date: 30/09/2005 Signature of candidate: Per Backandt

Chapter 1: Introduction

1.1 About the project.

Water is known to be the most common liquid on Earth. But despite the small size and simple structure of its molecule, the nature of this liquid is very complex [1-2]. Although many of its properties are known, there are others which are not. The roles this molecule plays on surfaces are in particular interesting. Some examples are in medicine, biochemical processes and corrosion [3]. Therefore it is important to learn more, both how the structures of the surfaces (e.g. SAMs) are formed and ordered and how the water molecules interact with different type of surfaces.

In this project there are two main things we need to do.
First, we want to produce well defined surfaces and examine the structures of them using a range of electronic, spectroscopic and microscopic methods. Using two different thiols, one hydrophilic and one hydrophobic, SAMs on single crystal metals are formed and their structures at different coverage of each are investigated.

Once a particular surface structure is known, water is then adsorbed above it (also at different coverages) and then examined using the same methods.

1.2 The hydrogen bond [1, 2].

A non-covalent bond between two electronegative atoms via a hydrogen atom is called a hydrogen bond. Commonly the hydrogen atom is covalently bound to one of the electronegative atoms (X) in a polar compound or functional group, X - H. Because the electrons are attracted towards X, the hydrogen atom is slightly positive charged. The polar group is then attracted to another electronegative atom (Y) whose lone pair electrons act as an acceptor of the hydrogen atom. So an electrostatic bond is formed, X – H ····· Y. This is the hydrogen bond. X and Y may be the same type of atom (e.g. O for bonding between water molecules) or two different ones. Depending on the electronegative atoms, the strength of the hydrogen bond varies. However, it is the most electronegative elements (oxygen, nitrogen and fluorine) that are most characteristic for hydrogen bonding and form the strongest bonds. The bonding energy for those is around 15-40 kJ/mole. It is much weaker than a covalent bond but stronger than other dipole attractions and van der Waals' forces. This makes the properties of ammonia, water and hydrogen fluoride much different from their analogues with the (less electronegative) elements further down in their respective groups in the periodic chart.

Hydrogen bonding can occur both between two separate molecules and within the same molecule. This is called intermolecular and intramolecular hydrogen bonding respectively.

The hydrogen bond plays many important roles in biological processes. Since it lies energetically between covalent bond and Van der Waal's interactions, it allows molecules to both associate and dissociate rapidly at room temperature because the hydrogen bonding energy is similar to the thermal

fluctuation energy (~25kJ/mol at room temperature). It also enables specific conformations to be formed. So the 3D conformation of an active protein, the specific base-pairing in DNA, the formation of monolayers and vesicles and enzymatic catalyses etc are possible due to this bond.

1.3 The water molecule [1, 3].

Water is an important compound and the most abundant liquid on Earth [1]. One may think it is the liquid we use for cooking, drinking, swimming, washing etc. But it is more than that, it is essential for life. In all biochemical reactions water is required as solvent, reactant and/or catalyst. In a human body about 2/3 of the weight is water.

The molecule itself is very simple, containing only two hydrogen and one oxygen atoms. The molecule is described as V-shaped, rather than linear, due to the two non-bonding pairs of electrons in the oxygen atom. It has C_2v symmetry with one 2-fold rotation axis and two mirror planes. The atoms are covalently bonded with a bond length (H-O) of 0.96Å and a bond angle (H-O-H) of 104.5º. The oxygen is sp^3-hybridized with two of the orbitals hosting the bonding electron pairs to the hydrogen atoms and the other two the lone pairs. However there is no complete evidence for this. If we include the hydrogen bonding, the oxygen atom in water can be considered being tetrahedral. Proton transfer constantly exchanges the hydrogen atoms in liquid water. One molecule acts as an acid and another as a base.

$H_2O + H_2O \leftrightarrow H_3O^+ + OH^-$

This process is catalysed by both acids and bases, but even at pH 7 and room temperature, it is occurs in milliseconds.

Despite the small size of the molecule, many properties of water are special and complex compared to other liquids. Some examples are the boiling point, melting point, critical point, surface tension, viscosity and heat of vaporisation, which all are unusually high for water. The main reason for these is the hydrogen bond. The length of the hydrogen bond and O-H···O angle in water varies with temperature, pressure and structure. A typical value of tetrahedral structure of ice is 2.82 Å for the O-H···O length and the H-O···H angle is 109.47º. In contrast, the H-O···H angle for a dimer is much different, at 162º while the distance between the two O is about the same [3].

1.4 Clustering:

The hydrogen bonds will keep the network based on 14-water molecule units (proposed computer modelling [3]) in shape [4], as long the environmental conditions do not change, because the lifetime of the hydrogen bond is about 10-200 times longer than the broken bonds [1]. If one hydrogen bond breaks, but not the others around it, it will probably reform again.

The hydrogen bonds help to form an infinite network of water molecules. This is made of large clusters of water molecules that are formed by smaller ones. According to one proposed model [1], two clusters of four H_2O molecules each form a stable octamer, which further form dodecahedrons and icosahedrons as illustrated in Figure 1-1. Depending on the temperature, these

clusters can be of either low-density or high-density forms. Bending rather than breaking some hydrogen bonds causes the interconversion between these two forms.

Which density structure that is favoured depends on the presence of ions and macromolecular surfaces. If the surface is hydrophobic, hydrogen bonds, which should point towards it, are lost and the water molecules compensate for this by expanding the network to form a lower density structure with lower entropy.

As one molecule reorientates, corresponding motions will be induced in the neighbours and so on further away. So information about surfaces and ions etc will be spread over a long distance in liquid water.

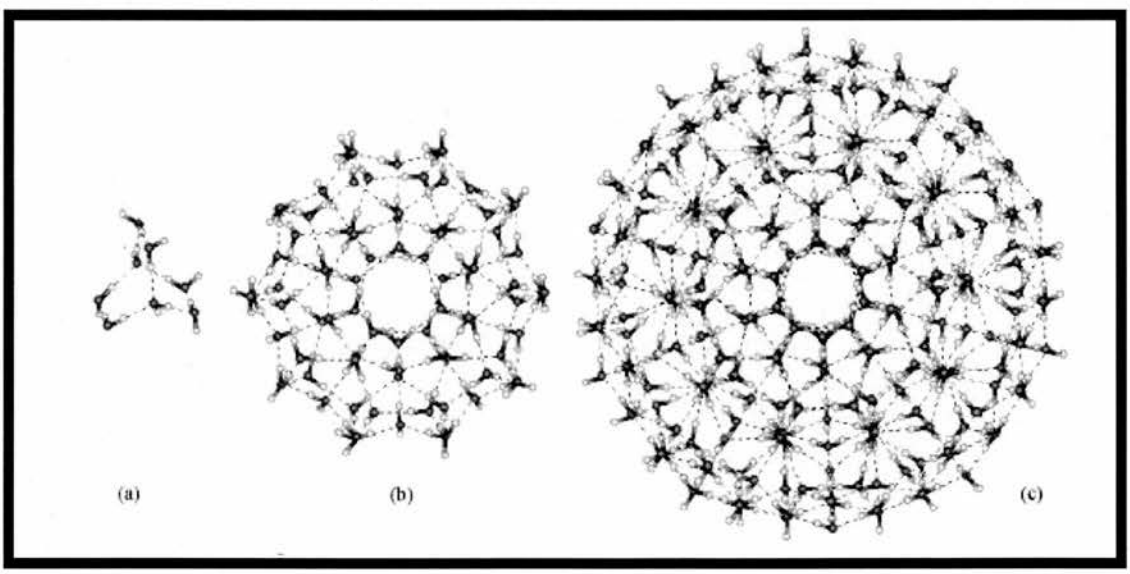

Figure 1-1. Water clusters that build up the hydrogen bonding network in water. (a) A stable octamer $(H_2O)_8$, (b) water dodecahedron made up from twenty octamers, (c) Icosahedral cluster of 280 water molecules. M. Chaplin [1]

1.5 Self-assembled monolayers (SAM)

The presence of thin organic films at interfaces between two phases (eg. solid/liquid, solid/gas and liquid/gas) has been well studied [5]. These studies have been useful in many areas of research, in particular medicine and biotechnology. Such a film can show many interesting physical and chemical properties and can today easily be prepared and analysed in a laboratory with a wide range of methods. Some examples are cell membranes, Langmuir films (amphiphilic molecules at liquid/air inferface) [6] and the latter transferred to a solid surface (Blodgett-Langmuir films) [7].

In this project we will use a special type of organic film called Self Assembled Monolayer (SAM) [8, 9]. Such layers are formed when organic molecules of one (or mixture of two or more) compound adsorb onto a solid surface, usually forming an ordered layer from a solution of the compound(s). It is arguable whether this term should be used also for gas-phase adsorption in UHV although this is quite common too. The monolayer forms spontaneously, hence the word "self assembled" [5], and is then usually energetically stable and no external force is needed to keep it in shape.

Figure 1-2 show a simple model of a SAM and the typical structure of the molecules it is built from.

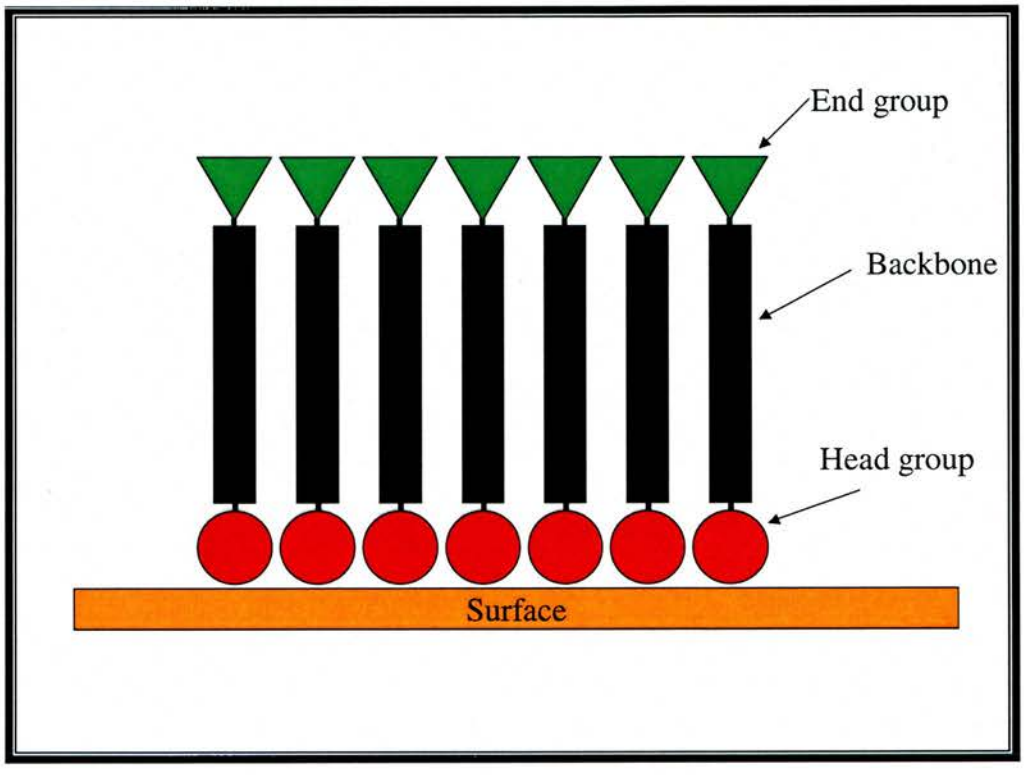

Figure 1-2: A schematic description of a self assembled monolayer.

The structure of a typical molecule involved in a SAM formation consists of three parts. The head group is responsible for binding to the surface. It forms a chemical bond with the atoms in the surface, and this is the main driving force for the adsorption. The type of surface (substrate) and functional groups in the molecule (adsorbate) both play important roles in the formation of the SAM. The backbone is usually an alkane chain, $-(CH_2)_n-$, but can also contain other groups, for example aromatic rings and ether bonds. The tail group can be of any functional group and can be chosen accordingly for the required surface properties. Interactions (van der Waals, hydrogen bonding etc) between the backbones and tail groups of adjacent molecules help the SAM to be highly ordered and retain its structure [9].

One major advantage of many SAMs is that they can be easily prepared in a laboratory, and there are several different methods of doing it. One method is simply to dip the substrate in a solution containing the adsorbate in low concentration (typically around 1mM) for a specified time, perhaps many hours [5]. Then the substrate is washed with the same solvent and blow dried using an inert gas such as nitrogen. An alternative method of forming an ordered molecular monolayer is to place the substrate in an ultra high vacuum system (UHV) chamber and evaporate the adsorbate in the gas phase [5]. Conventionally this is not usually termed self-assembly although the outcome of the liquid phase and gas-phase depositions may be similar.

The cleanliness of the substrate as well as the concentration of the adsorbate affects the SAM formation. The more clean the surface the fewer defects the monolayer will contain. If the adsorbate concentration is too high and/or the adsorption process is running for a long time, and the tail group is reactive (e.g. an aliphatic thiol with –OH, $-NH_2$ or –COOH in the other end of the chain), a multilayer rather than a monolayer may be formed. Also, the length of the chain is important. In the case of SAMs formed from long chain alkane thiols, longer chains (usually over 10 methylene units) enable better ordered 2D monolayers to be obtained. It has also been found that final ordered surface develops over time (many hours) with an initially rapid uptake followed by lateral ordering, untangling of chains and larger, well-ordered domains [5].

There are several methods for characterising the SAMs. Some examples are X-ray photoelectron spectroscopy (XPS) [7], infrared spectroscopy (RAIRS) [10, 11], scanning tunneling microscopy (STM) [12], contact angle and wettability measurement [7, 13], and quartz crystal microbalance (QCM) [14].

1.6 Thiols:

One of the most common and widely used class of molecules for SAM formation is thiols [5, 15]. A typical thiol used to form a SAM has the SH-group as head, one or more methylene groups (alkane chain) and/or aromatic rings in its backbone. The tail is any functional group (CH_3, OH, COOH, NH_2 etc) as appropriate. A thin film of gold, usually evaporated onto glass, mica or a silicon wafer or, alternatively, a gold single crystal surface, are useful substrates as the sulfur atom strongly interacts with gold atoms. The adsorption process involves the following reaction, [9]:

$R\text{-}S\text{-}H + Au_n^0 \rightarrow R\text{-}S^-Au^+ \bullet Au_n^0 + \frac{1}{2}H_2$

where the alkane chain with functional group is directed away from the surface, and hydrogen is lost from the surface.

Such alkane thiol/gold SAMs are easy to prepare by dissolving the desired thiol in any solvent of high purity, eg ethanol, and then placing the substrate in this solution (thiol concentration between 1 and 10 mM). For optimum coverage and 2D order, the substrate should remain in the solution for many (>15) hours [15]. Then it should be taken out, rinsed with the same solvent and dried, preferably in a vacuum dessicator.

By dissolving two different thiols in a certain proportion, a mixed monolayer will be the result [15]. The hydrophilicity of the surface can then be fine-tuned, from completely hydrophobic (pure non-polar thiol) through many intermediates (specific molar ratio between a polar and non-polar thiol) to completely hydrophilic (pure polar thiol). For example mixtures of HS-R-CH_3 and HS-R-OH molar ratios can achieve this [*15*, *16*].

1.7 Adsorption of water on well defined surfaces.

Because of the important role of the water molecule in nature described above, the adsorption of water molecules onto different surfaces has been widely examined. Water adsorption on a wide range of metal crystal surfaces, mainly close-packed hexagonal (111), has been studied in UHV conditions at low temperature (from 40K up to about 140K), for example Pd(111) [17], Cu(111) [18], Ag(111) [19], Pt(111) [20 - 23] and Au(111) [24 - 34].

On Pd(111) at 40K, water adsorbs as single molecules [17]. They then diffuse by moving from one adsorption site to the next, and by collision with another water molecule form dimers, trimers and so on up to cyclic hexamers with the (√3x√3)R30° structure relative to Pd(111), which was found to be the most stable [17]. Figure 1-3 shows two bilayers of the (√3x√3)R30° structure (one with H pointing up and the other down).

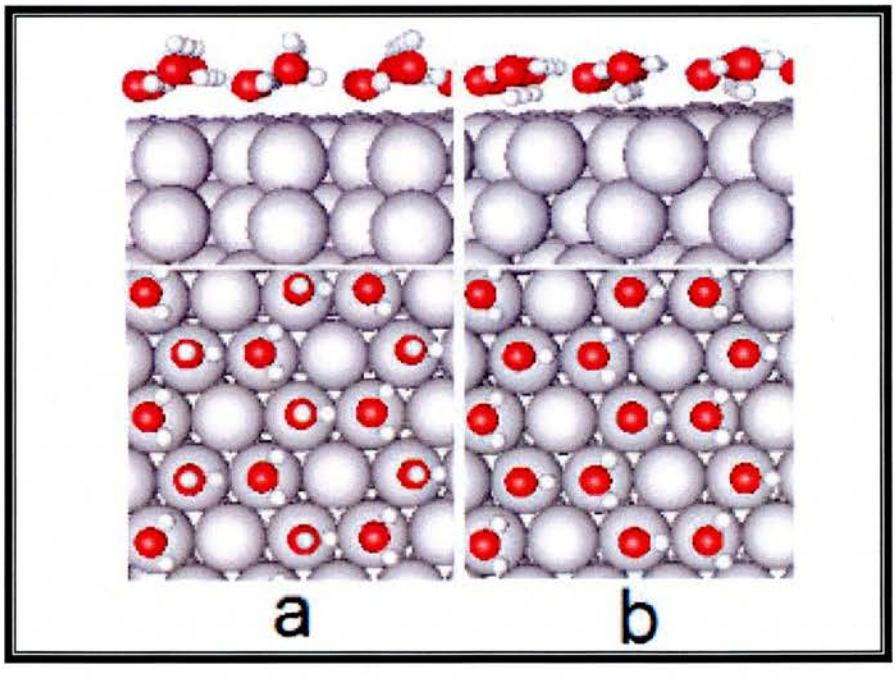

Figure 1-3. Bilayers of water hexamers on Pt(111) and other (111) metal surfaces with the $(\sqrt{3}x\sqrt{3})R30^{o}$ structure where a) H is up and b) H is down. S. Meng et. al. [35].

It was also noted in this study that the rate of diffusion increases with cluster size up to tetramer and then decreases.

On Pt(111), water adsorbs as monomers under 40K while the molecules are more stable in di- and trimers above that temperature [20]. At higher temperatures around 135K, when the water molecules are more mobile and almost at their desorption temperature, a bilayer of crystalline ice consisting of hexamers of water molecules is formed. At low coverage, this has a (√37x√37)R25.3° structure while it at higher coverage has a (√39x√39)R16.1° [21, 23]. These structures were also the result of DFT studies [35], which are shown in figure 1-4. These structures have a few % expansion and compression respectively compared to bulk ice.

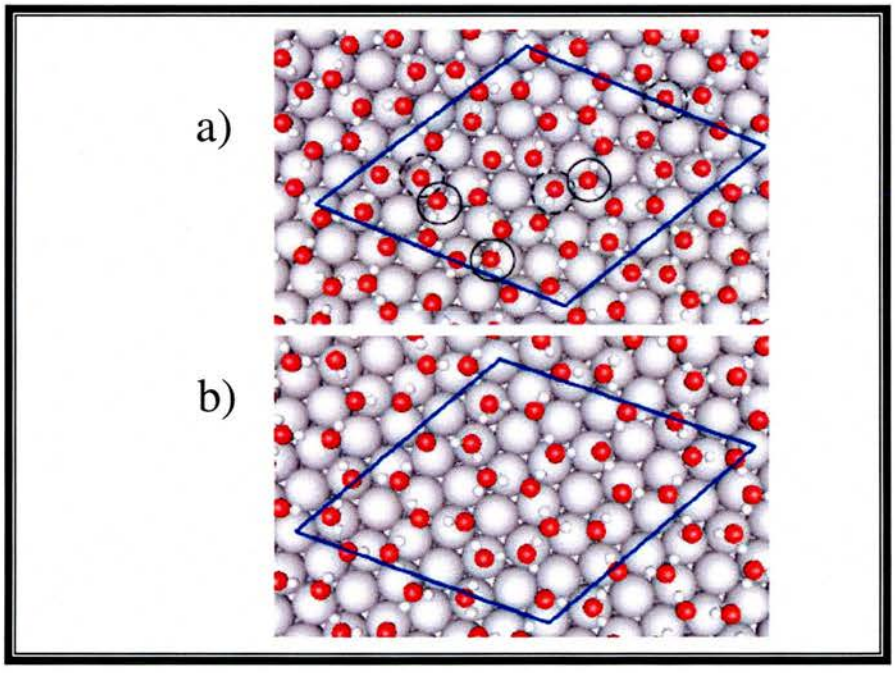

Figure 1-4: The a) $(\sqrt{37}x\sqrt{37})R16.1^{o}$ **and b)** $(\sqrt{39}x\sqrt{39})R25.3^{o}$ **structure of water on Pt(111). S. Meng et. al. [35].**

For Au(111), which has been used in this work for most experiments, many investigations have been done. Ikemiya et.al. have found that the adsorbed water molecules do not change the reconstructed surface of Au(111) [24] and the interaction between the water molecules and the gold surface is weak [25]. They also found that the hydrogen bonding between the water molecules is stronger than to the gold surface at 85K and that water desorbs completely at 170K. The desorption spectrum is shown in figure 1-5.

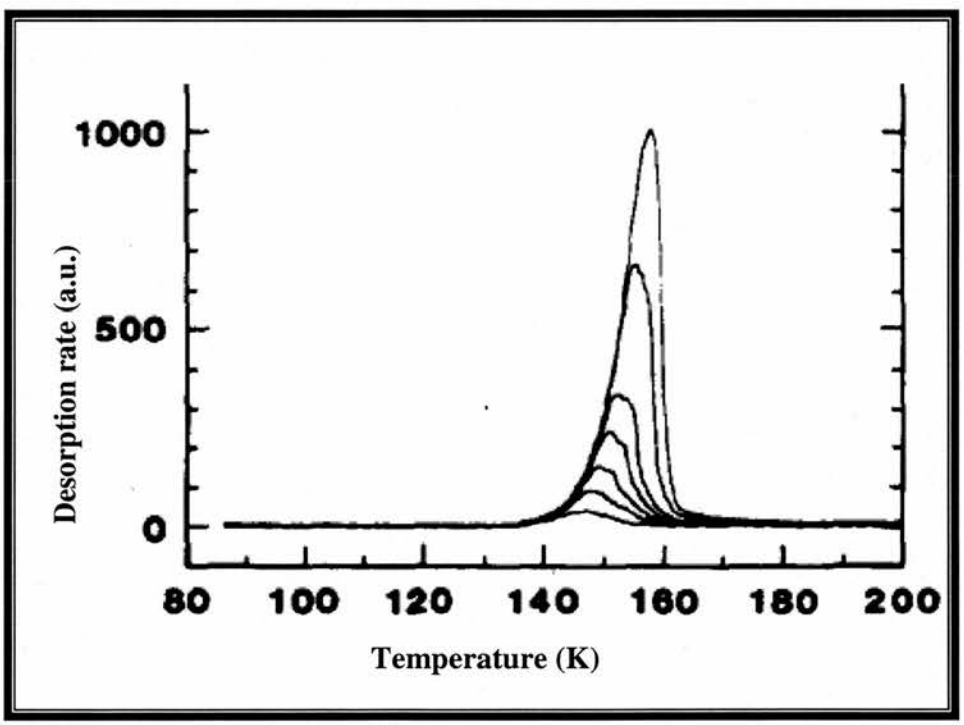

Figure 1-5: Thermal desorption spectra for H_2O on Au(111) as a function of increasing H_2O exposure. The molecules were adsorbed at 85K and the desorption rate was 2K/s. Kay et al. [25].

Any peak for the sub monolayer in this spectrum is not resolved so this is a sign that the water molecules bind more to themselves than the Au atoms on the surface. Each water molecule can form hydrogen bonds to four neighbours and clustering occurs before adsorption. Pirug et al. also observed the

unaltered reconstructed Au(111) using LEED when studying water adsorption on to the surface [28]. The water formed an (√3x√3)R30° structure up to saturation coverage of an bilayer and an 9% compression of this structure at higher coverage. The LEED patterns are shown in figure 1-6.

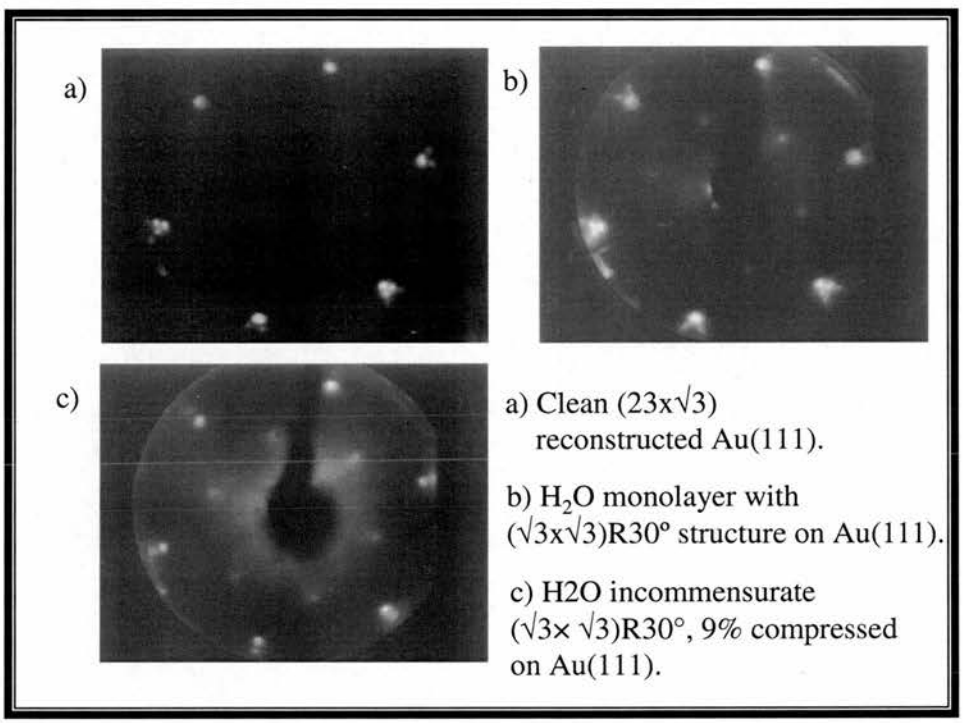

Figure 1-6: LEED pattern for a clean Au(111) surface and coverages of water on Au(111). Pirug et.al. [28].

The adsorption of water has also been studied on thin organic films with ordered structure adsorbed on metal crystal surfaces, in particularly thiols on Au(111). Liedberg et al. examined the full range of mixed SAMS of two thiols of the type HS-$(CH_2)_{16}$-X, where X = H and X = OH respectively [15]. The wettability was confirmed with contact angle measurements. Water was then adsorbed at reduced temperatures (80-120K) in UHV and studied with RAIRS when running TPD (temperature programmed desorption). It was found that the structure of the ice is amorphous below 100K for all wettabilities, but when

heated to higher temperature, the ice structure becomes polycrystalline. The transition temperature is dependent of the hydrophilicity of the SAM, and ranges from 110K for the most hydrophobic to 150K for the most hydrophilic SAM [36]. Figure 1-7 show a phase diagram for these ice structures.

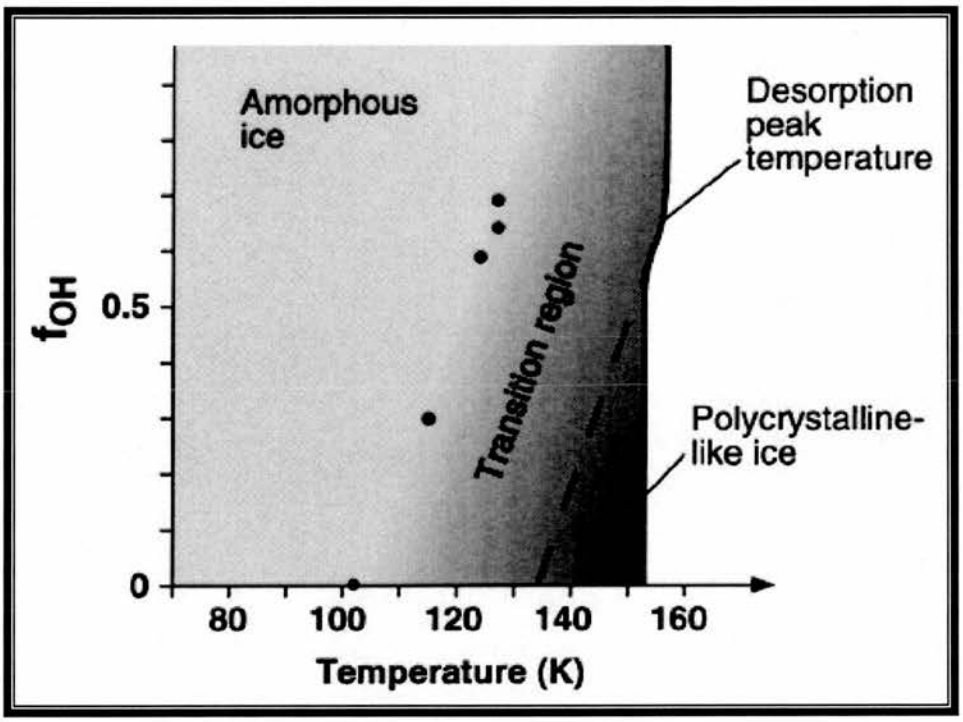

Figure 1-7: Phase diagram for the whole wettability range of the mixtures between HS-$(CH_2)_{16}$-H and HS-$(CH_2)_{16}$-OH. Liedberg et. al. [36].

It can also be noted that for the more hydrophilic mixed SAM, the phase transition to polycrystalline structure is not complete before the water molecules desorb.

1.8 Adsorption of benzyl mercaptan and other aromatic thiols on Au(111) and related surfaces.

Self assembled monolayers containing one or more aromatic rings are of great importance, in particularly because they can be used in applications involving electron transport and optoelectronic properties [37]. It has been shown that these thiols bind to the surface with the sulfur atom rather than the aromatic ring [38]. There are several reported studies of BM and other aromatic thiols adsorbed on Au(111).

Whelan et al. studied the simplest aromatic thiol, benzene thiol, adsorbed on Au(111) by gaseous deposition in UHV. Using HREELS, they found that the molecules are aligned with the aromatic ring parallel to the gold surface independent of the coverage [39]. In another study, Dhirani et al. grew SAMs of conjugated phenylethynyl benzene thiols from solution on Au(111) and imaged them with STM. Three different ones were used: H-(Ar-C≡C)$_n$-Ar-SH, (Ar = aromatic ring, para-substituted) where n = 0 (i.e. benzene thiol), 1 and 2. They concluded that the longer the chain the more ordered the molecules are in the SAM, with a highly ordered $(2\sqrt{3}x\sqrt{3})R30^o$ pattern for the longest [40]. Zharnikov and Grunze compared aliphatic and aromatic thiols grown in ethanol solution on Au(111) and Ag(111), and from their analyses with XPS and RAIRS they found that the intermolecular interactions were dominant in determining the structure and the packaging of the aromatic SAMs, in contrast to the headgroup-substrate interaction which dominates the aliphatic SAMs [41]. There are other studies that agree that for any thiol with the sulfur atom bond directly to the aromatic ring it is necessary to add more aromatic rings for stronger intermolecular

interactions to obtain a well ordered SAM [38,42]. However, by inserting a methylene group between the sulfur atom and the aromatic ring, the resulting benzyl mercaptan adsorbs in well ordered SAMs, and by varying the end groups these structural properties can be controlled [37].

Self assembled monolayers of benzyl mercaptan have previously been studied. Using RAIRS and STM, Tao et al. compared BM and benzene thiol and some para-substituted analogues containing an additional aromatic sing and/or alkoxy group [37]. These thiols were grown from ethanol solution on Au(111). The benzene thiol formed a very poorly ordered monolayer while in the case of benzyl mercaptan an ordered SAM of the $(\sqrt{3}x\sqrt{3})R30^o$ structure was formed. This confirmed that the inserted methylene group makes the molecule more flexible and allows stronger intermolecular interactions. Gui et al. studied BM adsorbed in aqueous solution on Ag(111) and Pt(111) using LEED and RAIRS. They found that the BM molecules adsorb in a commensurate $(2\sqrt{3}x2\sqrt{3})R30^o$ structure on Ag(111) while no long range order of the molecules was found on Pt(111) [43]. Baunach and Kolb deposited BM on Au(111) from ethanol solution. They showed that a disordered structure of the BM molecules can be obtained by modification of the Au(111) surface in acidic solution. But by partial reductive desorption, striped $(2x\sqrt{3})$ and $c(15x\sqrt{3})$ structures at a potential of +0.65 and -0.22V respectively were obtained [44]. There were no references for the orientation of these species. Molecular dynamics simulations were performed by Jung et al. Their work showed that BM adsorbed in a well ordered SAM while benzene thiol molecules were disordered on Au(111). This shows the importance of the flexible methylene group, bridging the aromatic ring and sulfur

head group, and allows close-packed structures of aromatic thiols to be formed on Au(111) [45].

1.9 Adsorption of 2-mercaptoethanol and other aliphatic thiols on Au(111) and related surfaces.

Long alkane chain thiols have been well used in studying properties of SAMs. Baltzer et al. prepared SAMs of unbranched aliphatic thiols (referred as C_n-SH, n=4-12) by gaseous deposition on Au(111) in UHV which was characterized by LEED [46]. They found that at low coverage the molecules are orientated with the carbon axes parallel to the surface and in a structure with a linearly increase of the unit cell length with increasing carbon chain length. At higher coverage the molecules are orientated with the carbon chain perpendicular to the surface, with an ordered $c(4\sqrt{3}x2\sqrt{3})R30^o$ structure independent of chain length for the longer chains (n>9). The same structure was found by Camillone et al. for octanethiol (C_8-SH) grown from solution in ethanol [47] on Au(111) and analysed by helium diffraction. Poirier et al. studied monolayers of C_n-SH (n=4, 6, 8, 10) adsorbed on Au(111) in ethanol solution which were analysed with STM in UHV [48]. At saturation coverage they found that the SAMs from all those thiols pack in a $(\sqrt{3}x\sqrt{3})R30^o$ structure with a c(4x2) super lattice.

For SAMs of thiols with a hydroxy-group (-OH) as tail group the structure is much different than the ones of the corresponding unsubstituted alkane thiol.

Poirier et al. found that SAMs of mercaptohexanol, gaseously adsorbed on Au(111) in UHV and imaged by STM, pack in an oblique commensurate lattice with unit-cell-dimensions, a=3c, b=$\sqrt{13}$ c and tanα= $2\sqrt{3}$ relative to the Au(111) unit cell (length = c) [49]. Another example is a study by Sprik et al. who compared SAMs of dodecanethiol and mercaptoundecanol grown on Au(111) in ethanol solution and imaged by STM. A $(\sqrt{3}x\sqrt{3})R30^{o}$ structure was observed for the SAMs of dodecanethiol while a striped pattern was imaged on the SAMs of mercaptoundecanol [50]. A possible explanation for the latter is that the OH-groups in the molecules hydrogen bond to each other in a linear direction.

Previous works on 2-mercaptoethanol adsorbed on Au(111) and similar surfaces are very limited. Hyun & Rhee performed an extensive STM study of 2ME adsorbed on Au(111) in ethanol solution followed by annealing to 353K. They found four different striped ordered structures of 2ME on Au(111): $(6x\sqrt{3})$, $(5x\sqrt{3})$, $(4x\sqrt{3})$ and compact-$(5x\sqrt{3})$ relative to the gold surface [51]. These four structures are produced from a combination of one or more of the three crystallographic non-equivalent $(\sqrt{3}x\sqrt{3})R30^{o}$ assemblies which are the basic fundamental units. The $(6x\sqrt{3})$ structure consists of rows of one $(\sqrt{3}x\sqrt{3})R30^{o}$ assembly with a separation of 6 gold atoms between the rows. Two rows of different $(\sqrt{3}x\sqrt{3})R30^{o}$ assemblies build up the $(5x\sqrt{3})$ and $(4x\sqrt{3})$ structures where the rows are separated by 5 and 4 gold atoms respectively. Finally, the compact-$(5x\sqrt{3})$ structure was obtained by overlapping all three different $(\sqrt{3}x\sqrt{3})R30^{o}$ assemblies. Compared with the corresponding hydrophobic analogue, ethanethiol, this result probably depends on the strong

hydrogen bonding between the hydroxyl groups. In addition, because of the short hydrocarbon chain, the van der Waals interactions between the molecules are very small.

Kudelski studied 2ME grown in aqueous solution on gold, silver and copper (crystallographic surface not mentioned) by surface-enhanced Raman scattering. He found that the orientation of the 2ME molecules is strongly pH sensitive but independent of neutral salts in the solution. In acidic solution the C-C "chain" are orientated parallel along the surface, otherwise it is tilted away from the surface [52].

1.10 References

1. M.F. Chaplin, ***Biochemistry and Molecular Biology Education*** 29 (2001) 54.
2. G.R. Desiraju, T. Steiner ***"The Weak Hydrogen Bond : in structural chemistry and biology"***, Oxford University Press, 1999
3. M. Chaplin, web pages about Water, London South Bank University, http://www.sbu.ac.uk/water/
4. M.F. Chaplin, ***Biophysical Chemistry*** 83 (1999) 211.
5. F. Schreiber, ***Progress in Surface Science*** 65 (2000) 151.
6. G.L. Gaines Jr., ***Insoluble Monolayers at Liquid-Gas Interfaces***, Interscience, New York, 1966.
7. A. Ulman, ***An Introduction to Ultrathin Organic Films: From Langmuir-Blodgett to Self-Assembly***, Academic Press, Boston, 1991

8. K. Nirmalya, K. Chaki, K. Vijayamohanan, ***Bioelectronics & Biosensors*** 17 (2002) 1.

9. A. Ulman, ***Chemical Reviews*** 96 (1996) 1533.

10. R.G. Nuzzo, L.H. Dubois, D.L. Allara, ***Journal of Americal Chemical Society*** 112 (1990) 558.

11. A.N. Parikh, D.L. Allara, ***Journal of Chemical Physics*** 96 (1992) 927.

12. G.E. Poirier, ***Chemical Review*** 97 (1997) 1117.

13. C.D. Bain, G.M. Whitesides, ***Angewandte Chemie International Edition English*** 28 (1989) 506.

14. A. Ulman (Ed.), Self-assembled monolayers of thiols, Thin Films, vol. 24, Academic Press, San Diego, 1998.

15. I. Engquist, I. Lundström, B. Liedberg ***Journal of Physical Chemistry*** 99 (1995) 12257.

16. I. Engquist, B. Liedberg, ***Journal of Physical Chemistry*** 100 (1996) 20089.

17. T. Mitsui, M.K. Rose, E. Fomin, D.F. Ogletree, M. Salmerson, ***Science*** 297 (2002) 1850.

18. K. Morgenstern, K.H. Rieder, ***Journal of Chemical Physics*** 116 (2002) 5746.

19. K. Morgenstern, ***Surface Science*** 504 (2002) 293.

20. A.L. Glebov, A.P. Graham, A. Menzel, ***Surface Science*** 427-8 (1999) 22.

21. J. Harnett, S. Haq, A. Hodgson, ***Surface Science*** 528 (2003) 15.

22. N. Materer, U. Starke, A. Barbieri, M.A. Van Hove, G.A. Somorjai, G.J. Kroes, C. Minot, ***Surface Science*** 381 (1997) 190.

23. S. Haq, J. Harnett, A. Hodgson, ***Surface Science*** 505 (2002) 171.

24. N. Ikemiya, A.A. Gerwin, ***Journal of Americal Chemical Society*** 119 (1997) 9919.

25. B.D. Kay, K.R. Lykke, J.R. Creighton, S.J. Ward, ***Journal of Chemical Physics*** 91 (1989) 5120.

26. R.S. Smith, C. Huang, E.K.L. Wong, B.D. Kay, ***Surface Science*** 367 (1996) L13.

27. P. Löfgren, P. Ahlström, D.V. Chakarov, J. Lausmaa, B. Kasemo, ***Surface Science*** 367 (1996) L19.

28. G. Pirug, H.P. Bonzel, ***Surface Science*** 405 (1998) 87.

29. P.A. Thiel, T.E. Madey, ***Surface Science Reports*** 7 (1987) 211.

30. L.H. Dubois, B.R. Zegarski, R.G. Nuzzo, ***Journal of Americal Chemical Society*** 112 (1990) 570.

31. M. Hara, H. Sasabe, W. Knoll, ***Thin Solid Films*** 273 (1996) 66.

32. D.D. Chambliss, R.J. Wilson, S. Chiang, ***Physical Review Letters*** 66 (1991) 1721.

33. T. Boland, B.D. Ratner, ***Langmuir*** 10 (1994) 3845.

34. J.V. Barth, H. Brune, G. Ertl, R.J. Behm, ***Physical Review B*** 42 (1990) 9307.

35. S. Meng, E.G. Wang, S. Gao, ***Physical review B*** 69 (2004) 195404.

36. I. Engquist, I. Lundström, B. Liedberg, ***Journal of Chemical Physics*** 106 (1997) 3038.

37. Y.-T. Tao, C.-C. Wu, J.-Y. Eu, W.L. Lin, ***Langmuir*** 13 (1997) 4018.

38. J.M. Tour, L. Jones, D.L. Pearson: J.J.S. Lamba, T.P. Burgin, G.M. Whitesides, D.L. Allara, A.N. Parikh, S.V. Atre, ***Journal of the American Chemical Society*** 117 (1995) 9529.

39. C.M. Whelan, C.J. Barnes, C.G.H. Walker, N.M.D. Brown, ***Surface Science*** 425 (1999) 195.

40. A-A. Dhirani, R.W. Zehner, R.P. Hsung, P. Guyot-Sionnest, L.R. Sita, ***Journal of the American Chemical Society*** 118 (1996) 3319.

41. M Zharnikov, M Grunze, ***Journal of Physics: Condensed Matter*** 13 (2001) 11333.

42. E. Sabatani, J. Cohen-Boulakia, M. Bruening, I. Rubinstein, ***Langmuir*** 9 (1993) 2974.

43. J.Y. Gui, D.A. Stern, D.G. Frank, F. Lu, D.C. Zapien, A.T. Hubbard, ***Langmuir*** 7 (1991) 955.

44. T. Baunach, D.M. Kolb, ***Analytical and Bioanalytical Chemistry*** 373 (2002) 743.

45. H.H. Jung, Y.D. Won, S. Shin, K. Kim, ***Langmuir*** 15 (1999) 1147.

46. F. Balzer, R. Gerlach, G. Polanski, H.-G. Rubahn, ***Chemical Physics Letters*** 274 (1997) 145.

47. N. Camillone, C.E.D. Chidsey, G. Liu, G. Scoles, ***Journal of Chemical Physics*** 98 (1993) 3503.

48. G.E. Poirier, M.J. Tarlov, ***Langmuir***, 10 (1994) 2853.

49. G. E. Poirier, E.D. Pylant, J.M. White, ***Journal of Chemical Physics*** 105 (1996) 2089.

50. M. Sprik, E. Delamarche, B. Michel, U. Röthlisberger, M.L. Klein, H. Wolf H. Ringsdorf, ***Langmuir*** 10 (1994) 4116.

51. M. Hyun and C.K. Rhee, ***Bulletin of Korean Chemical Society*** 22 (2001) 213.

52. A. Kudelski, ***Langmuir*** 19 (2003) 3805.

Chapter 2: Surface Chemistry Techniques used.

2.1 Ultra High Vacuum (UHV)

One of the most important requirements in surface science is to obtain a very clean substrate for good results. One may think of cleaning it for example with acetone or ethanol in an ultrasonic bath, or by treatment in an ozone-UV chamber. But once out in the atmosphere again, there is a large risk of contamination by molecules such as O_2, CO_2, H_2O etc. So another environment has to be chosen to prevent this.

Working in UHV conditions is necessary for many experiments in surface chemistry. This means a pressure at around 10^{-9} mbar or less. It allows surfaces to be atomically cleaned before an analysis, and a much better control of what will be adsorbed on it later. For some techniques, particularly those using low energy electron beams and ions, this is required to prevent scattering by gas molecules. Also, the oxidising effect of oxygen on the sample as well as the risk of burning filaments (e.g. for annealing) is avoided in UHV.

The following equations will explain the effect of the vacuum [1].

First the ideal gas law: $pV = n_m RT$

p = pressure (Pa)

V = volume (m^3)

n_m = moles of gas

R = ideal gas constant = 8.31447 J K^{-1} $mole^{-1}$ [2]

T = temperature (K)

And

$$k_B = \frac{R}{N_A} \quad \text{and} \quad N = n_m N_A$$

N = number of gas molecules.

N_A = Avogadro's number = 6.02×10^{23} mole^{-1}

k_B = Boltzmann's constant = 1.38×10^{-23} J K^{-1}

With all these together we get $pV = Nk_BT$

To estimate the gas density the number of gas molecules per unit of volume (n) the equation above can be rewritten as: $n = \frac{N}{V} = \frac{p}{k_BT}$

When a surfaced has been cleaned, the next question is for how long it will remain clean in the UHV chamber. The gas molecules around it will of course have an adsorbing ability on the surface. To estimate this, the incident flux (F) is a measure of it.

First, the following equation relates the flux to the gas density (n) and the average speed of the molecules ($\bar{v}$).

$$F = \frac{n\bar{v}}{4}$$

Second, the molecular gas density is given from above.

$$n = \frac{N}{V} = \frac{P}{k_BT}$$

Third, the Maxwell-Boltzmann distribution of gas velocities will by integration give the mean molecular speed, $\bar{v} = \sqrt{\frac{8k_BT}{m\pi}}$

By combining these three equations, we get this:

$$F = \frac{\frac{p}{kT}\sqrt{\frac{8k_BT}{m\pi}}}{4} = \frac{p}{\sqrt{2\pi mk_BT}}$$

Where m is the mass of the molecule. It is necessary to use SI units, then F will be expressed in molecules per square metre and per second.

Here we can see that the molecular flux is proportional to the pressure in the chamber.

The mean free path of a particle, λ, is given by [1]:

$$\lambda = \frac{RT}{\sqrt{2}\pi d^2 N_A P} = \frac{kT}{\sqrt{2}\pi d^2 P}$$

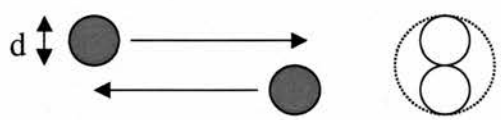

The effective collision area = πd^2

This is calculated from a simple hard-sphere model [2] and applies for neutral molecules.

2.2 Low Electron Energy Diffraction (LEED)

To check the structure and cleanliness of the surface, LEED is a very useful method. It can be used both for quantitative and qualitative analyses, of which the latter is most common. [1]

A beam of electrons at low energy (usually between 20 and 200eV) is directed perpendicular towards the surface, which has a well ordered crystalline surface.

λ_e = wavelength (m)

h = Planck's constant = 6.62×10^{-34} J s

p_e = electron momentum

m_e = mass of the electron = 9.11×10^{-31} kg

v_e = velocity of the electron (m/s)

E_e = kinetic energy of the electron (J)

q_e = charge of the electron = 1.602×10^{-19} C

V = acceleration energy (eV)

In classical mechanics the momentum of a particle is the product of its mass and velocity. So for an electron it is simply:

$$p_e = m_e v_e$$

The kinetic energy of the electron is

$$E_e = \frac{m_e v_e^2}{2}$$

By combining the two equations above:

$$E_e = \frac{m_e \frac{p_e^2}{m_e^2}}{2} = \frac{p_e^2}{2m_e}$$

which can be written as

$$p_e = \sqrt{2m_e E_e}$$

The kinetic energy of a charged particle (for example an electron with the charge q_e) accelerated in the voltage V is given by:

$$E_e = q_e V$$

If we now use the De Broglie relation

$$\lambda_e = \frac{h}{p_e}$$ (here using the subscript "e" to denote the electron)

and combine it with equation above, we get

$$\boxed{\lambda_e = \frac{h}{p_e} = \frac{h}{m_e v_e} = \frac{h}{\sqrt{2m_e q_e V}}}$$

For example, an acceleration voltage of 20eV will give λ_e = 2.74Å and a 200eV beam will have λ_e = 0.87Å. For diffraction to be useful in the atomic scale, the wavelength of the electron beam has to be around the same as the distance between the atoms in the crystal.

How the diffraction works:

First, a simple one dimensional model of a row of atoms in the crystal, which could represent a cross section of the surface. Figure 2-1 shows how the electrons are diffracted.

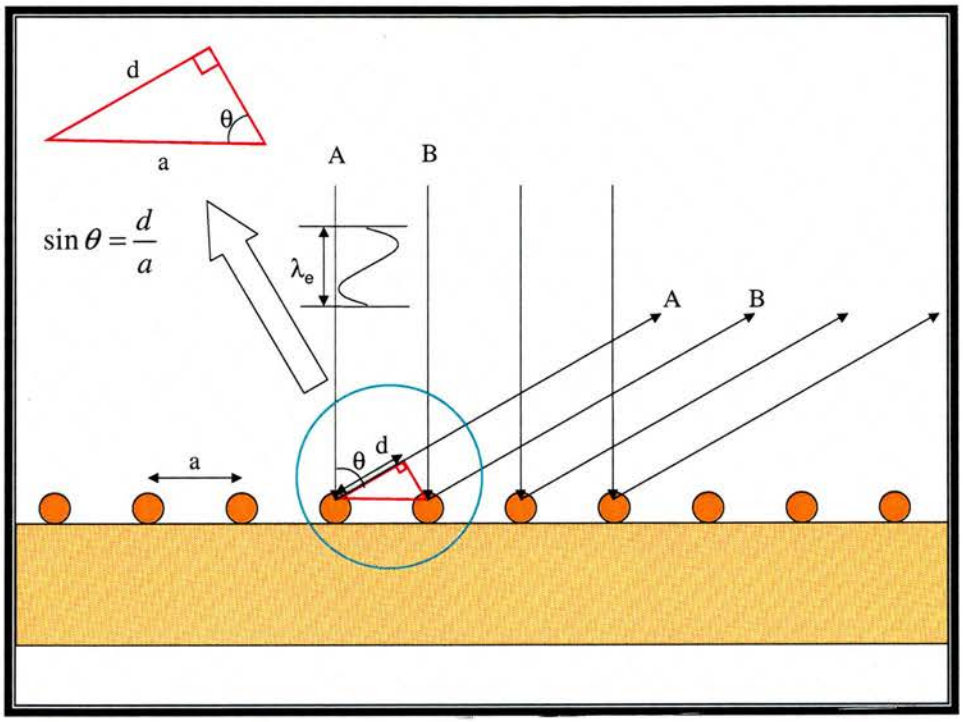

Figure 2-1: Diffraction of electrons from a well defined surface.

If one looks at the two adjacent electrons A and B, the radiation scattered from A has to travel a longer distance to the detector than the one for B. The difference is d, and if the angle between the incoming and the scattered beam is θ, using simple trigonometry gives

$$\sin\theta = \frac{d}{a} \quad \text{or} \quad d = a\sin\theta$$

where a is the distance between the nucleus of the atoms. These two scattered beams will interfere with each other, and for maximum constructive interference, d has to be equal of a multiple of whole wave lengths, that is

$$d = a\sin\theta = n\lambda \qquad \text{(Bragg's law)}$$

where λ is the wave length and n is an integer (0, 1, 2, ... and equivalent negative values). On the other hand, mid way between these two adjacent

maxima, at d=(n+½)λ, total cancellation occurs. An example of a typical plot of the intensities vs sinθ is shown in figure 2-2 [1]

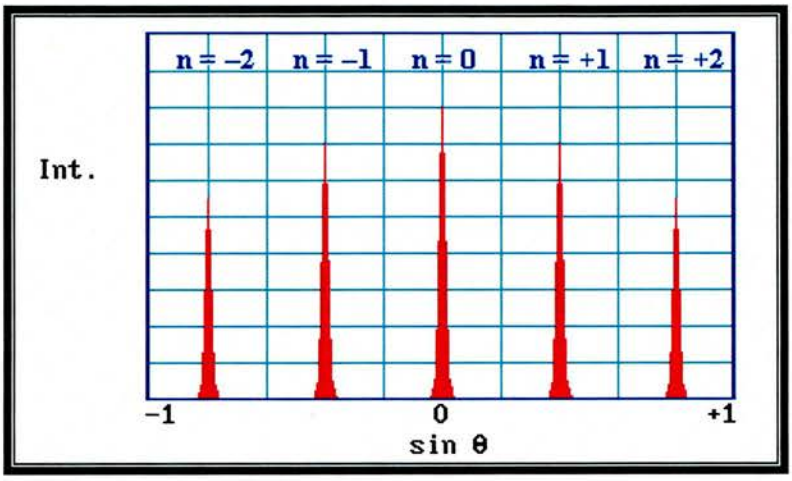

Figure 2-2: A typical intensity profile for the diffraction. Dr R.M. Nix [1].

Here we can see that it is symmetric around θ=0 (and n=0) and the intensity for the next n on each side decreases slightly. Also sinθ is inversely proportional to both the lattice parameter (a) and the square root of the acceleration voltage (V).

Using two diffraction indices m and n, the one dimensional patterns above can then be extended to two dimensions. A simple description of the experimental setup is shown in figure 2-3.

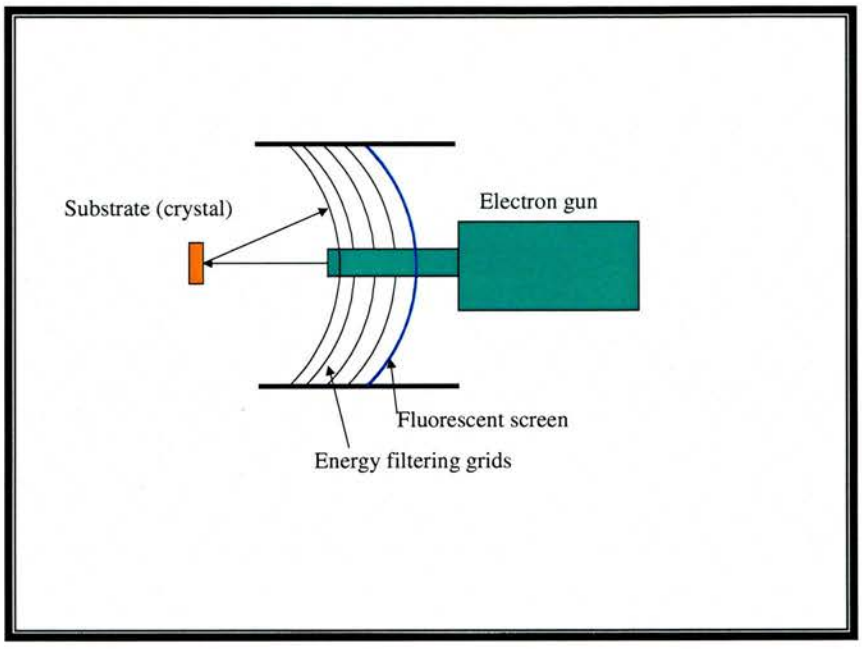

Figure 2-3: A simple and typical experimental setup for LEED.

The grids are used to filter out the inelastically scattered (lower energy) electrons so that only the elastic scattered ones (which give the diffraction pattern) hit the fluorescent screen. By using a camera the pattern can be recorded for each sample (clean and with one or more overlayer) and as the beam energy is known, the structure of any overlayer can be determined by comparisons and recalculations.

2.3 Scanning Tunnelling Microscopy (STM):

The basic principle of this technique, developed by Binnig & Rohrer [3], is a metallic tip moving over a conducting substrate. The tip is made in such way that the very end of it is just one atom wide. It is approached (along the z-axis) to the surface as close as nanometres but not physically touching it. At such a

small distance, a current will flow through the gap during certain conditions. This is called tunnelling. The following will describe how it works.

Consider a solid which is built up from one atom, then adding another one, and so on until we have "a huge amount of atoms", as indicated in figure 2-4. The electronic properties will change from atomic orbitals via "molecular" orbitals, which will increase in number and be energetically closer together as the number of atoms increases, eventually forming bands. The lower energy bands will be filled and the upper ones empty, and the energy level separating them is called the Fermi level (E_F). For conducting solids such as metals the empty and filled bands will be close together, see figure 2-4 a.

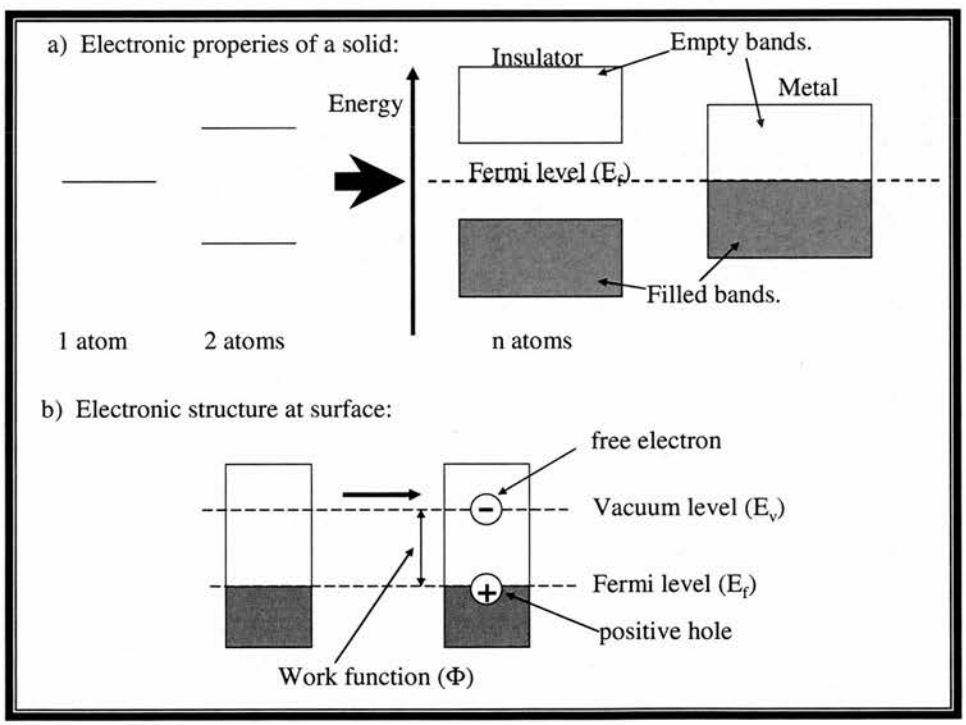

Figure 2-4. The electronic properties of a solid.

The highest band, which is partly or completely filled, is called the valence band and the lowest empty band is called the conduction band. The removal of an electron at the surface out to the vacuum (to a certain vacuum level, E_V,

where it is a free electron) require energy which is called the work function, $\phi = E_V - E_F$ (figure 2-4 b). The size of the work function depends not only on the solid itself (typically 2 to 5 eV for most metals) but also on the presence of adsorbates, external electric fields and reconstruction.

Near the surface, there is a barrier, represented by the work function, which prevents the electrons from leaving the surface and entering the vacuum [4]. So the electron can be considered as a particle in a box [2]. The graph for the solution of the wave function is shown in figure 2-5. Within the solid it is sinusoidal but it decays exponentially in vacuum with the distance from the surface. This is called "leak out electron wave function" [5].

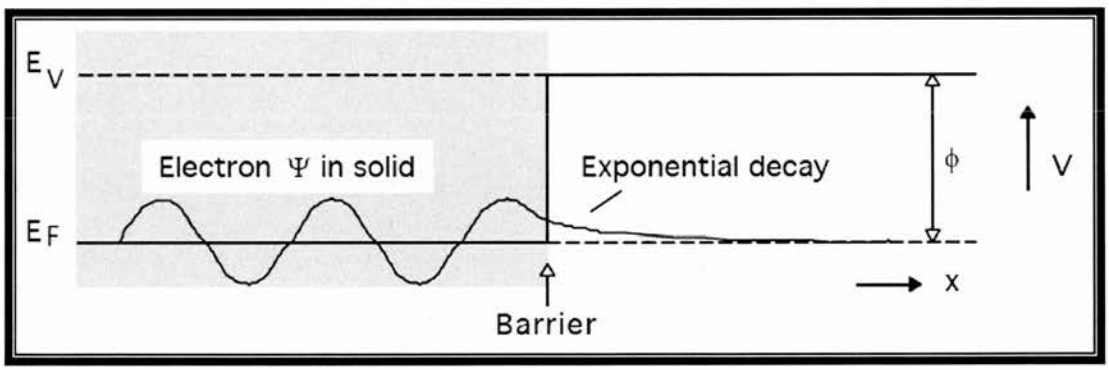

Figure 2-5. The wave function within and outside the solid. The wave function decays exponentially with the distance from the surface (x). Michigan State Univiversity web site [4].

When two metals (or other conducting solids) are close together their decay overlap as shown in figure 2-6 a. The current flow is equal in the two directions. However, if an external voltage is applied between the conductors, a current will flow between them (figure 2-6 b), referred to as a tunnelling current.

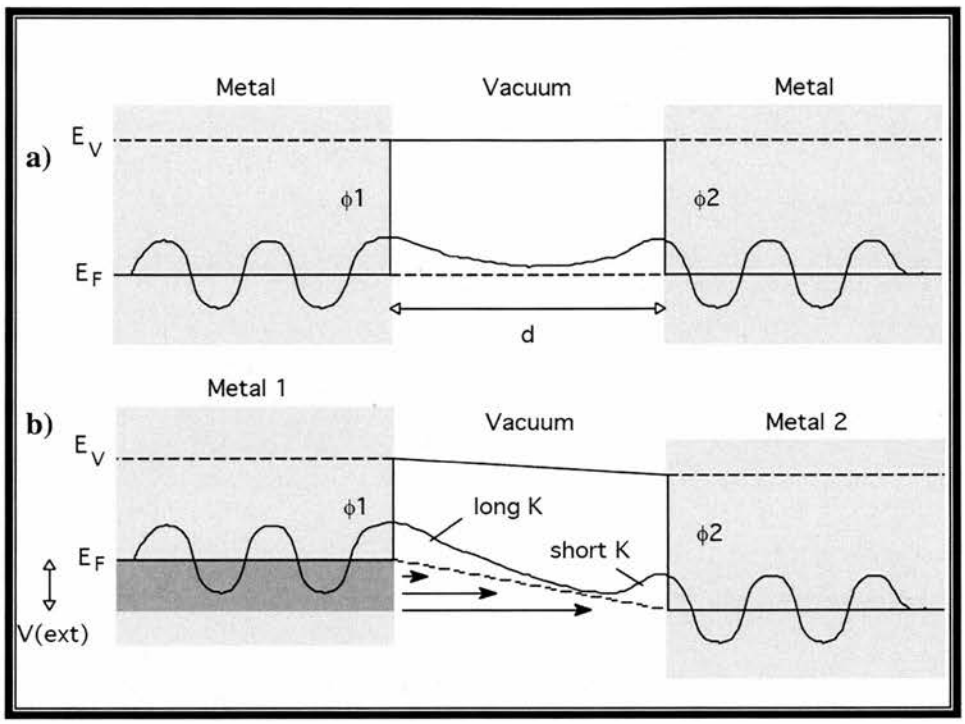

Figure 2-6. a) The overlap of the decays from two metals which are close together and b) when a voltage is applied is applied between the conductors. Michigan State Univiversity web site [4].

This current (I) is exponentially related to the gap between the tip and the surface (z) in the following way, $I \sim e^{-kz}$. By moving the tip across the surface in the other two dimensions (x- and y-axis) and recording the tunnelling current, one can get a topographical map of the surface in the atomic scale. The STM imaging can be performed in two different ways. One way is to keep the tunnelling current constant and let the tip move up and down recording the height. The other is to keep the height constant and record the tunnelling current whose value can be transformed to a colour (dark to bright) scale and give an topographical image. It is the magnitude of k which gives STM its extreme surface sensitivity [4].

2.4 Reflection Absorption Infra Red Spectroscopy (RAIRS)

Vibrational spectroscopic methods are very useful in surface science. First, they are helpful for providing information about what kind of molecule(s) is adsorbed on the substrate by identifying functional groups. One can then check that a desired adsorbant is attached to the surface, or that the surface is free from unwanted impurities. Second, the orientation of certain bonds can be determined from various selection rules.

For a molecular vibration to absorb any radiation it needs to be *infrared active*. This happens if the electric dipole of the molecule changes when the atoms in the molecule move relative to each other. It does not mean that the molecule has to have a permanent dipole, simply a change in the dipole moment. The intensity of the vibrational mode depends on $|\delta\mu/\delta q|^2$, where μ is the dipole moment and q is the relevant vibrational co-ordinate. In a diatomic molecule there is only one type of vibration, a stretch along the only bond, while in polyatomic molecules there are additional vibrations like asymmetric and symmetric stretches as well as bends, see figure 2-7.

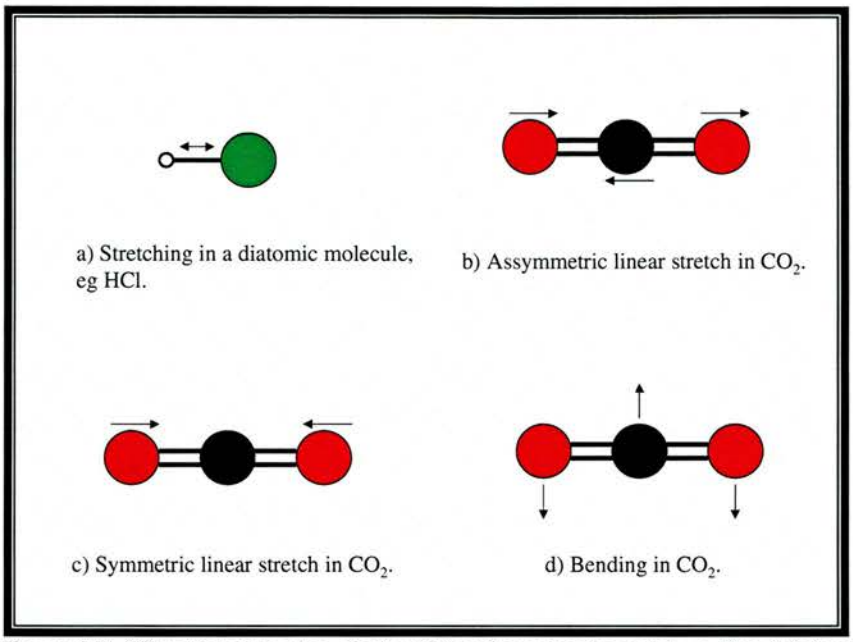

Figure 2-7. Vibrational modes of a) a diatomic molecule and b, c, d) a triatomic molecule.

From the Schrödinger equation [2] and the harmonic oscillator approximation, the permitted energy for a molecular vibration expressed in wave numbers can be written as

$$G_n = (n+\frac{1}{2})\frac{1}{2\pi c}\sqrt{\frac{k}{m_{eff}}}$$

Where n is an integer (0, 1, 2, ...), c = speed of light, k = the force constant of the bond, and m_{eff} = the effective mass of the molecule. For a diatomic molecule, it is defined as $m_{eff} = \frac{m_1 m_2}{m_1 + m_2}$ where m_1 and m_2 are the masses of the atoms. The transition between two adjacent energy levels (n and n+1) are in the infrared region, so molecular vibrations absorbs and emit infrared radiation with the size of $\bar{\upsilon} = \frac{1}{2\pi c}\sqrt{\frac{k}{m_{eff}}}$ (in wave numbers). Almost all molecules are in the vibrational ground state (Boltzmann distribution) so the transition to n=1 from n=0 will be the dominant part of the absorption. However, for higher vibrational excitations the harmonic oscillation model is not sufficient as the steps between

the energy level decreases with higher n. So an anharmonic solution of the Schrödinger equation is necessary [2] which is not described further here.

For polyatomic molecules, each normal mode ("an independent and synchronous motion of an atom or groups of atoms" [2]) can be considered as independent from other normal modes and each of them can be treated as an harmonic oscillator. So the equation above can be applied and each of them has its own force constant and effective mass (which is a complex function of the masses of the atoms involved).

IR spectroscopy can be used in either transmission mode or reflection mode. In surface science the latter is widely used (as most substrates are insufficiently transparent to IR) and will be described further.

Figure 2-8 show how the IR radiation is reflected (and transmitted if applicable).

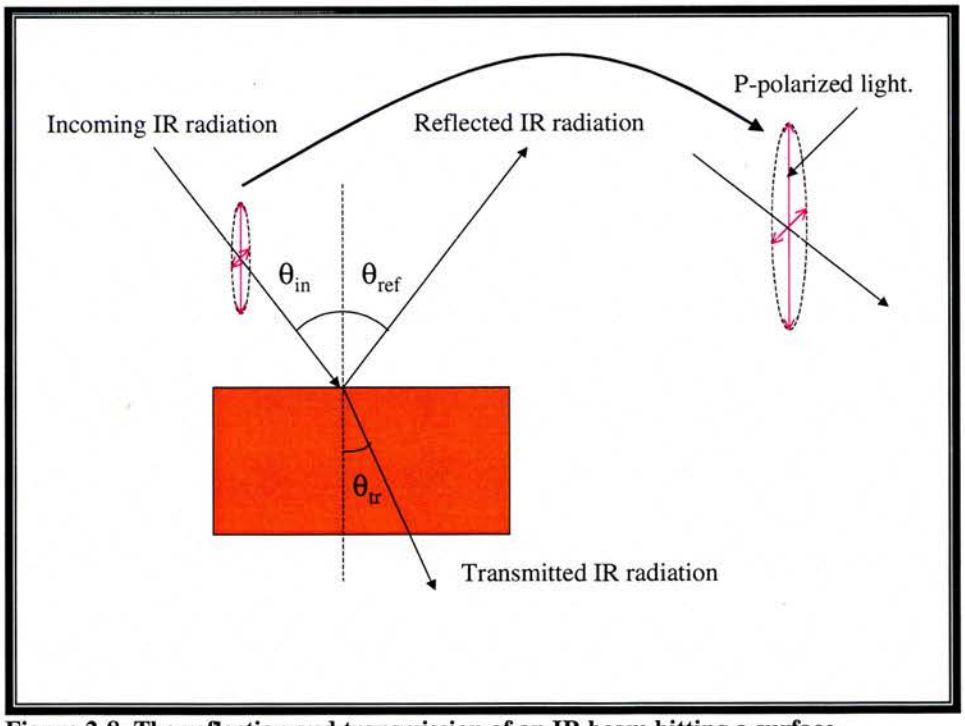

Figure 2-8. The reflection and transmission of an IR beam hitting a surface.

Snell's law: $\frac{n_1}{n_2} = \frac{\sin\theta_I}{\sin\theta_T}$ where n_1 and n_2 are the refractive indices for air/vacuum (=1.00) and the substrate respectively and θ the angles shown in figure 2-8. For the reflective part, $\theta_I = \theta_R$.

It has been shown [6] that the best sensitivity for RAIRS measurement is obtained when the incident radiation angle approaches 90° (usually around 85°). At this angle, only the p-polarized component of the light contributes any significant field strength at the surface. This means only vibrations components perpendicular to the surface will be IR active, the so called surface selection rule [7]. This is also called the image charge effect, as the dipole causes a response of the substrate electrons which behaves as "a twin" with opposite sign at the same distance on the other side of the surface plane, normal to the surface. This enhances the perpendicular component while the parallel component is cancelled, see figure 2-9.

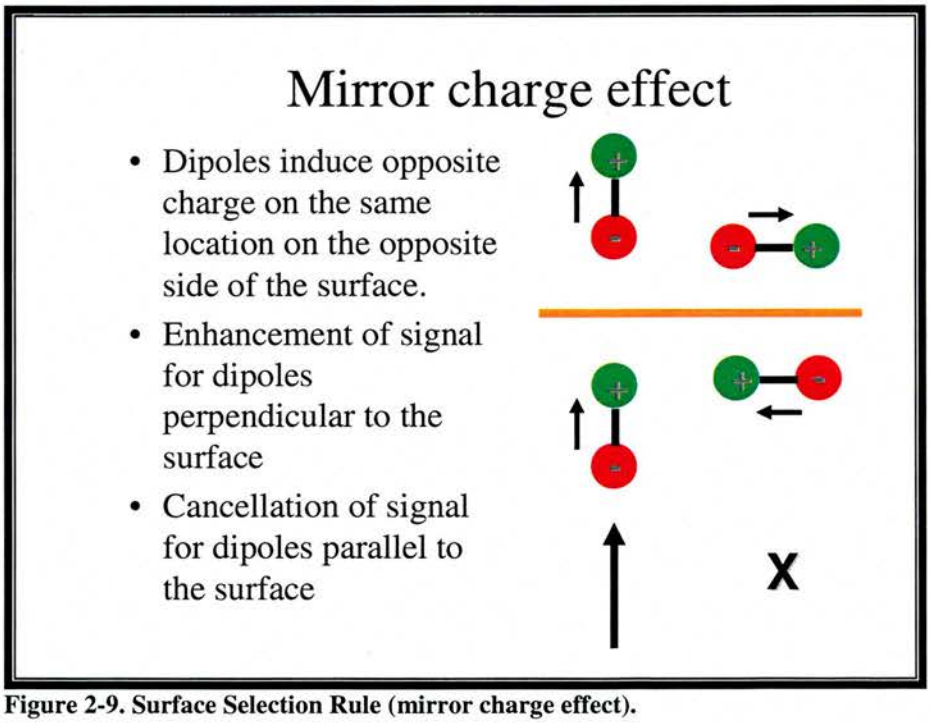

Figure 2-9. Surface Selection Rule (mirror charge effect).

2.5 Electron Energy Loss Spectroscopy (HREELS)

Similar to infrared spectroscopy, this technique measures vibrational spectra of a compound adsorbed on a well-defined surface. But instead of infrared radiation, a beam of low energy electrons is used as source. This has to be used in UHV conditions.

The incoming beam of electrons at a fixed energy (up to 10eV) hits the sample and electrons are scattered after losing some energy to the vibrational excitations of the adsorbed molecules as shown in figure 2-10. The energy conserved is given by the equation.

$$E_{sc} = E_{in} - h\nu = E_{in} - \frac{hc}{\lambda} = E_{in} - hc\,\bar{\nu} \quad \Leftrightarrow \quad \bar{\nu} = \frac{E_{in} - E_{sc}}{hc}$$

where the E_{in} and E_{sc} are the energy of the incoming and scattered electrons respectively, and λ and $\bar{\nu}$ are the wavelength and wavenumber respectively of the excited vibrational mode.

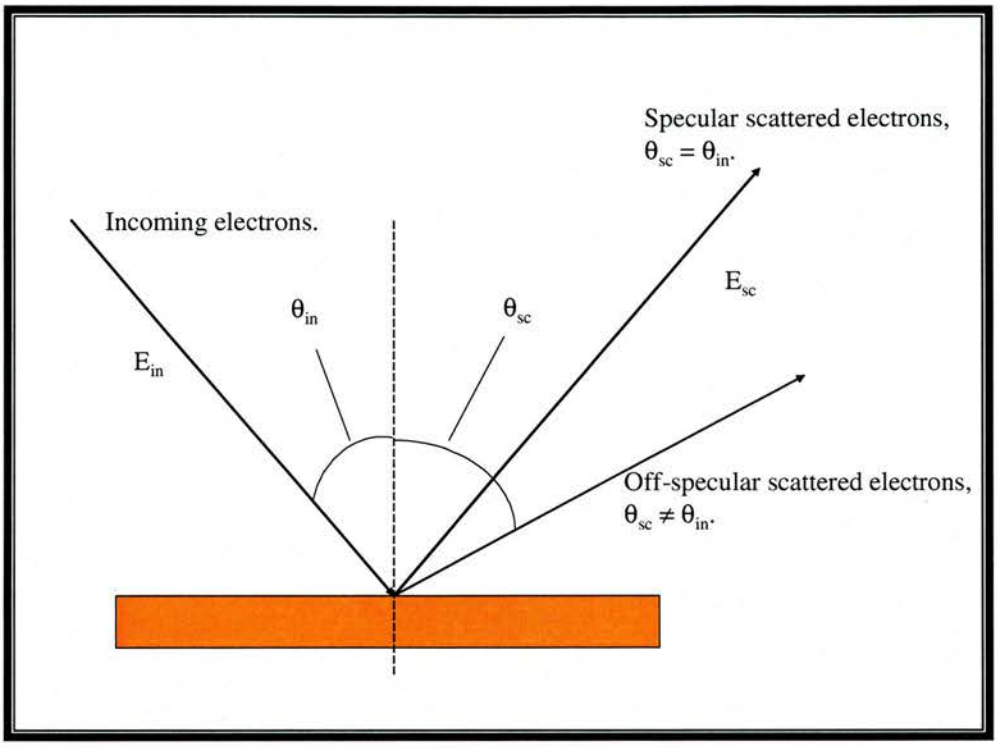

Figure 2-10. The incoming beam and scattered electrons at HREELS.

A considerable number of electrons are scattered elastically without any loss of energy, $E_{sc} = E_{in}$, which results in a strong peak in the spectrum called the elastic peak, and they are scattered in the specular direction, $\theta_{in} = \theta_{sc}$. The other electrons, which lose a fraction of energy to the vibrations, give rise to inelastic peaks in the spectrum.

Different types of scattering mechanisms are possible:

1) In dipole scattering the incoming electrons are scattered by the coulombic field of vibrating dipole of the molecule at the surface. The electron momentum parallel to the surface is conserved and the component perpendicular to the surface contributes to the energy loss. Because of this, the same surface selection rule (image charge effect) applies [7] as for RAIRS. Even the inelastic

electrons (which lose some energy to the vibrations) are scattered very close to the specular direction. This can be shown by looking at the electron momentum. By using the equation for electron momentum (see the LEED section) of the component perpendicular to the surface, and the equations for the energy loss, we get:

$$p_{in\perp} = \sqrt{2m_e E_{in}} \cos\theta_{in}$$

and

$$p_{sc\perp} = \sqrt{2m_e(E_{in} - hc\bar{\nu})} \cos\theta_{sc}$$

Then $p_{in\perp} = p_{sc\perp}$ which gives

$$\cos\theta_{sc} = \frac{\cos\theta_{in}}{\sqrt{1 - \frac{hc\bar{\nu}}{E_{in}}}}$$

As the energy loss usually is much smaller than the energy of the incoming electron (usually by 20-50 fold), the second term in the square root can be neglected and $\theta_{in} \approx \theta_{sc}$.

2) For impact scattering, the electrons are scattered by atomic force potentials of the surface. The scattering occurs over a wide range of angles. Vibrations of dynamic dipoles can be recorded both parallel and perpendicular to the surface, but only in off-specular direction. In addition, modes which have no dynamic dipole can also be excited in EELS by impact scattering.

Figure 2-11 shows a common setup for HREELS where a pair of electrostatic deflectors for monochromator and analyzer are used.

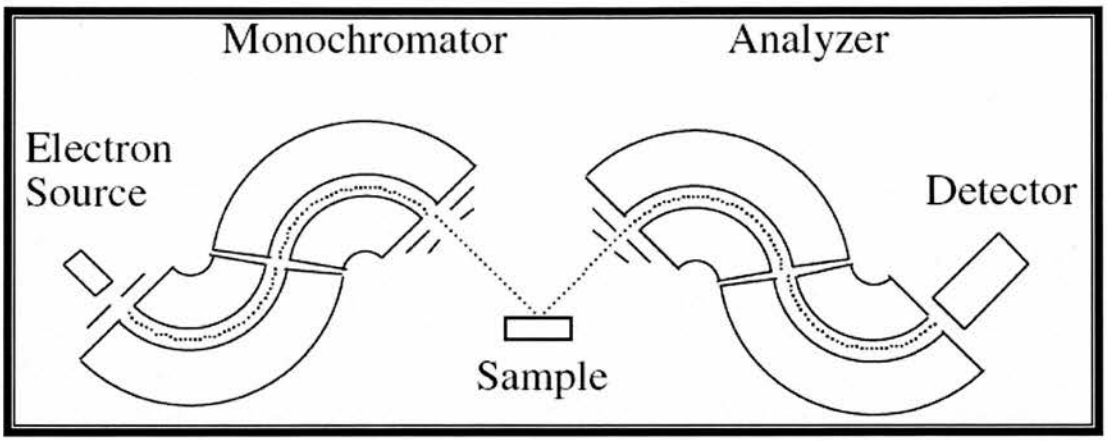

Figure 2-11. Simple description of a double set of monochromator and analyser for HREELS. Michigan State University web site [4].

By using a double set of each monochromators and analysers enhances the resolution. Optimisation of the beam is a quite complicated procedure and is controlled by computers. The analyser can be rotated to switch between specular orientation (dipole scattering) and off-specular orientation (impact scattering).

2.6 References

1. Queen Mary University of London, Dep. Of Chemistry, "An Introduction to Surface Chemistry", web site http://www.chem.qmw.ac.uk/surfaces/scc/ (accessed Sep 2005).
2. P. Atkins, J. De Paula, *Physical Chemistry, 7th ed.*, Oxford University Press 2002.
3. Binnig, G., Rohrer, H., Gerber, Ch., & Weibel, E. "Surface Studies by Scanning Tunneling Microscopy." ***Physical Review Letters*** 49, 1 (1982a): 57-60.
4. Michigan State University, Chemistry Department, Introduction to Surface Analysis, web site lecture notes, http://www.cem.msu.edu/~cem924sg/LectureNotes.html (accessed Sep 2005)
5. University of Guelph, Dep. Of Chemistry web site, http://www.chembio.uoguelph.ca/educmat/chm729/stmpage/stmdet.htm
6. R.G. Greenler, ***Journal of Chemical Physics*** 44 (1966) 310.
7. J.T. Yates, T.E. Madey, ***Vibrational Spectroscopy of Molecules on Surfaces.*** Plenum Press New York 1987.

Chapter 3: Experimental Procedures.

3.1 The ultra high vacuum (UHV) system.

Three separate UHV systems have been used for these experiments.

3.1.1 The STM-RAIRS system:

This consists of three separate stainless steel chambers. One is used for STM measurements and is equipped with the appropriate sample holder, tip and electronics by Omicron [1]. Another chamber is equipped with KBr windows for RAIRS measurements, as well as an Ar^+ sputtering device and resistive heater for cleaning the sample. It also has valves for vapour dosing chemicals, from either solid or liquid. Finally the largest chamber is the preparation chamber. It is equipped with an Ar^+ gun, resistive heater, LEED optics and fast entry lock for transferring samples to and from atmosphere. This is used most for cleaning the surfaces, adsorption of molecules prior to STM measurements, but also for cleaning substrates for RAIRS and using LEED to check the structure and cleanliness of the surface. The preparation chamber is connected to the STM and RAIRS chambers with valves and transfer arms are used to move the samples between them. Figure 3-1 shows a schematic setup of this system.

The STM device used was a VT-STM from Omicron and the softwares used for imaging were Scala Pro 5.0 [1] and WSxM Version 4.0 Develop 6.4 [2]. For RAIRS the Magna-IR 860 E.S.P. spectrometer and the software Omnic version 4.1b from Nicolet [3] were used.

The settings were:

No of scans 1024

Resolution 8 cm^{-1}

Data spacing 3.857 cm^{-1}

Final format – single beam

Velocity 0.6329 cm/s

Sample compartment MCT/A

Beam splitter and window material KBr

Source IR

Range 4000 – 500 cm^{-1}

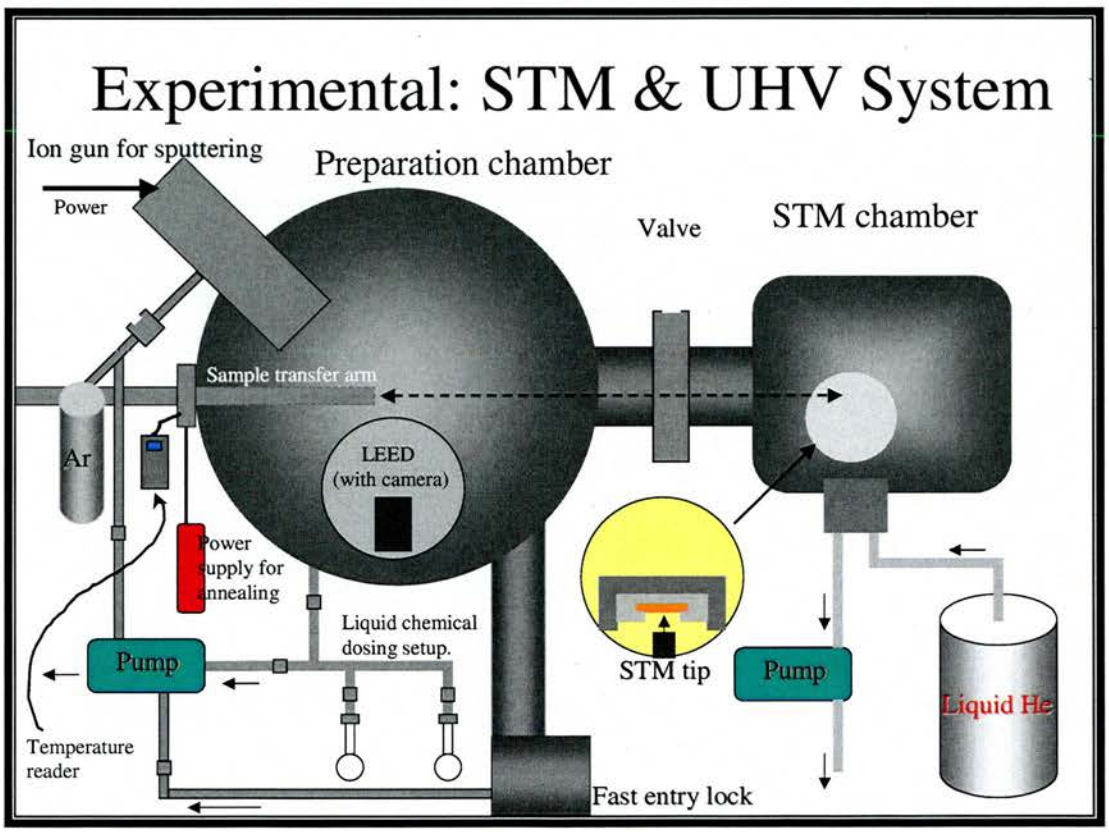

Figure 3-1. UHV vacuum system for STM (which is also linked to the RAIRS chamber).

3.1.2 HREELS system:

This contains two chambers. One is the preparation chamber, where the sample is cleaned and the surface reconstructed by cycles of Ar^+ sputtering and annealing with resistive heating. This chamber has also been used to evaporate gold on to silicon wafers. There is a fast entry lock for transferring the sample to and from atmosphere. The other chamber is used entirely for obtaining the HREEL spectra and is equipped with the appropriate spectrometer (HIB1000 Ibach EELS double pass spectrometer, VSW) [4] with a resolution better than 45 cm^{-1} at a beam current at the sample of 95 pA and a primary beam energy of 3eV.

3.1.3 Temperature Program Desorption (TPD) system:

This consists of a single chamber equipped with all necessary facilities for TPD including Ar^+ gun, resistive heater, programmed heating system and LEED. Although no useful results were obtained by TPD, this apparatus was used to provide very useful LEED information on the structure of benzyl mercaptan on Au(111).

3.2 Preparing and cleaning the substrate for UHV conditions.

For STM and RAIRS, the substrate, a rectangular piece (10mm x 8 mm) of Au(111) or Cu(110) with holes (diameter about 0.2 mm) in each corner, and a sample plate (a simple thin rectangular piece of stainless steel with a grip) are shown in figure 3-2. The substrate is mounted on the plate by placing a piece of tantalum wire through each hole, twisting the ends together and spot welding them onto the sample plate, as shown in figure 3-2.

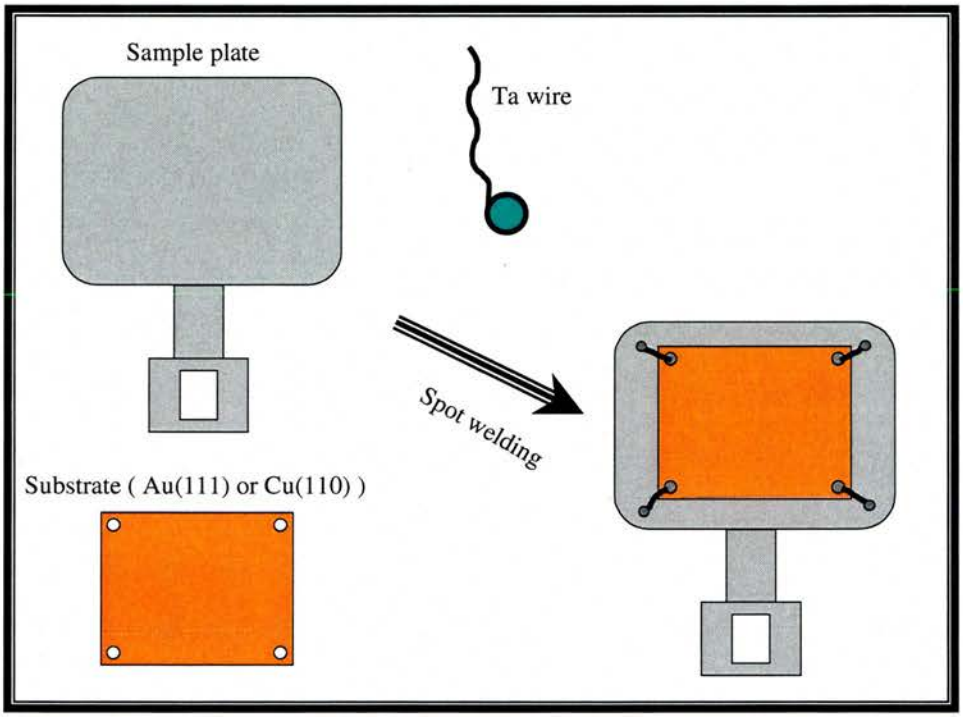

Figure 3-2. Mounting the substrate onto the sample plate.

The sample plate with the substrate was then cleaned in an ultrasonic bath with ethanol for a few minutes and blow dried with nitrogen gas on it. Once completed, it was ready for insertion in the UHV system via a manipulator transfer arm, which is equipped with a resistive heater for annealing and thermocouple for temperature monitoring.

For HREELS, the sample plate takes the form of a ring across which the substrate is mounted by screwing it tight at clamps on each side (see figure 3-

3). These clamps are also part of the resistive heating and the resistance through the substrate can be regulated depending how hard the screws are tightened (usually around 13-14 kΩ). The Au(111) substrate was prepared in two different ways.

1) A rectangular piece (16mm x 5.0 mm x 0.35 mm) of Si(111) was mounted across the plate. Then it was heated to 900°C followed by a slow (about 8°C/min) cool down to about 650°C. This should give the Si(111)(7x7) reconstruction, which could be observed by LEED as shown in figure 3-3.

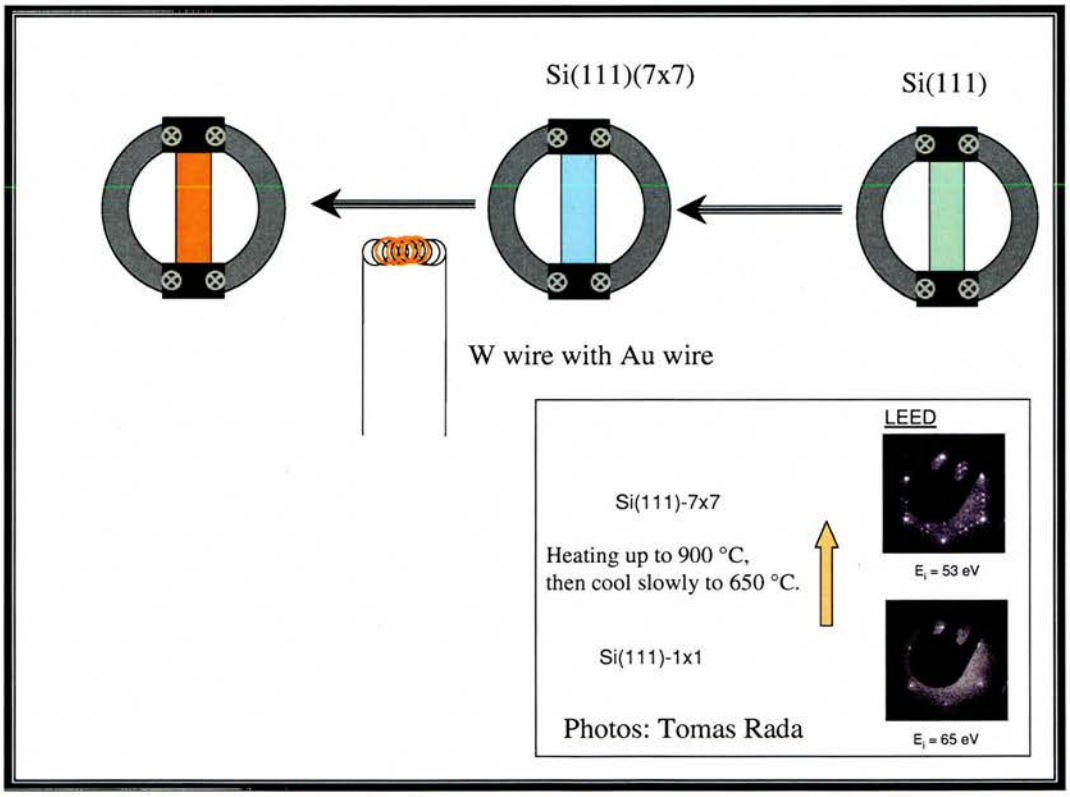

Figure 3-3: Preparation of a Si(111)7x7 surface and evaporating gold on to it.

If the Si(111)(7x7) LEED pattern did not appear, then the process was repeated but at a slightly lower cooling rate until the desired results were obtained. This reconstruction improves the adhesion properties for any gold

layer being subsequently deposited. Once this had been done successfully, gold could be deposited on the surface. A tungsten coil (made of a thread of 0.38 mm diameter) including pieces of Au wire (diameter 0.5 mm) was placed in the UHV chamber and connected to a power supply. By applying a current through the coil, the gold evaporates and gold atoms stick on the Si(111)(7x7). Using the same current through the W/Au wire during the same time for all experiment, the thickness of the applied gold layer should be consistent. In our case we used 4A for 10 minutes. After annealing the result is a Au(111) surface, which is energetically most stable.

2) A piece of ready cut Au(111) (of the same type as for STM and RAIRS above) was mounted directly onto the sample plate by twisting tantalum wires through the holes in the corners and attached to the "ring" (two on each side).

3.3 Gaseous adsorption of chemicals in UHV.

There are two different ways of dosing molecules onto a substrate in a UHV chamber, depending on whether the parent material is a solid or a liquid. Here only liquids have been used.

A specially made glass tubing connected via a glass-metal seal to a stainless steel pipe, which can be connected to the UHV system by either a Swagelock or metal knife-edge / copper gasket seal, is used here. It was cleaned in an ultrasonic bath for 10 minutes each with acetone and ethanol (in that order). It was then dried by connecting it to the UHV system and pumping out while heating it up. Once dry and clean, it was disconnected, filled with the

desired liquid and reconnected. The sample liquid was then purified from dissolved gases by a couple of cycles of the following procedure:

A) Freeze the liquid by dipping the glass tubing in a cup of liquid nitrogen.

B) Open the valve to the pump for about a minute, then close it again.

C) Thaw the frozen liquid by slow warming.

This was repeated until there was no more bubbling, usually 4-5 times.

3.4 Adsorption of chemicals from solution under ambient pressure.

Another way of creating an adsorbed monolayer is by immersing the substrate in a solution of the chemical. This was used for a number of thiols, in particular for experiments in atmosphere such as contact angle measurement and RAIRS. A solution of 1mM was prepared for each thiol. The thiol was measured with an accuracy of 0.01 mg and dissolved in ethanol (99%) in a 250 ml volumetric flask. Pieces of Au(111) evaporated on Si(110) wafers (usually 5 mm x 10 mm) were cut and placed in the solution. To allow enough time for a complete monolayer to form, it was left for 24 hours. After that it was taken out, rinsed with ethanol [99%] and dried in a flow of nitrogen gas. Then it was ready for analyses and was used for contact angle measurements, some RAIRS and HREELS (after UHV insertion via the fast entry lock).

3.5 Low Energy Electron Diffraction (LEED).

LEED was mainly used in this work to verify a clean and reconstructed Au(111) surface after it had been cleaned by sputtering and annealing. This was done prior to analyses by STM, RAIRS or HREELS, where the preparation chamber in each UHV system was equipped with a LEED device. A camera was fitted to the LEED screen in the STM-RAIRS UHV system. The UHV system used for TPD (temperature program desorption) also had a LEED device. Although no result were obtained with the TPD itself, it gave an excellent LEED pattern for high coverages of benzyl mercaptan on Au(111).

3.6 References

1. Omicron NanoTechnology GmbH, Limburger Straße 75, D-65232 Tanusstein, Germany. www.omicron.de (accessed Sep 2005).
2. Nanotec Electronica S.L., www.nanotec.es (accessed Sep 2005).
3. Thermo Electron Corporation (Nicolet), www.thermo.com or www.nicolet.com
4. VSW Ltd, www.vsw.co.uk (accessed Sep 2005)

Chapter 4: Benzyl Mercaptan on Au(111) and Cu(110).

4.1 Introduction

SAMs containing one or more aromatic rings are of importance because of their optoelectronic applications due to the aromatic chromophore as a functional group [1]. There has been several studies of aromatic thiols adsorbed on Au(111). Whelan et al. have found that the molecules of the simplest one, benzene thiol, adsorb with the aromatic ring parallel to the surface independent of coverage [2] but the monolayer is not very ordered. Dhirani et al. compared benzene thiol and two derivatives containing one or two phenylethynyl groups and found that longer chains [3] as well as more aromatic rings [4] increased the order. Comparison between aromatic and aliphatic thiols on Au(111) and Ag(111) were carried out by Zharnikov et al [5]. They concluded that the intermolecular interactions were stronger than the headgroup-substrate interaction for the aromatic thiols while the opposite were the case for the aliphatic ones. The molecules were bound to the substrate as thiolates, no dimers were present and, in aromatic SAMs, molecules were more tilted on Au(111) than Ag(111).

While it is hard to obtain a well ordered SAM of benzene thiol, things are much different with benzyl mercaptan, which has been investigated [1, 6, 7]. If a methylene group is inserted between the aromatic ring and the sulfur atom, the resulting benzyl mercaptan (and its derivatives) adsorb into well ordered

SAMs on Au(111) [1]. This is because that the methylene group could make the head group less rigid and lead to stronger intermolecular interaction. Also molecular dynamics simulations carried out by Jung et al. [8] show that BM forms a more ordered $(\sqrt{3}x\sqrt{3})R30^o$ structure than benzene thiol.

In this project, benzyl mercaptan has been used to produce a well defined hydrophobic surface on Au(111) (and to some extent also Cu(110)) in which the molecular orientation seems to be dependent on the coverage. LEED was used to obtain the structure for a high coverage of the thiol but was not capable of revealing any for structural details for low coverage. Further, HREELS was used to examine two different coverages and how the molecules were orientated in the two cases [9]. This was then verified with RAIRS which was also useful to estimate the critical exposure where the molecules change orientation between low and high coverage. In addition, STM was also used to obtain the pattern for both coverages. All methods were performed at room temperature, and cooling to low temperatures (down to 45K) using liquid helium were also done before some STM and RAIRS experiments.

4.2 LEED

For low coverage (20000L), no specific LEED pattern was observed, only the hexagonal spots for the Au(111) became less sharp as the coverage increased. However, rather suddenly, starting at a coverage of ca 50000L, a different LEED pattern appeared [9], which is shown in figure 4-1.

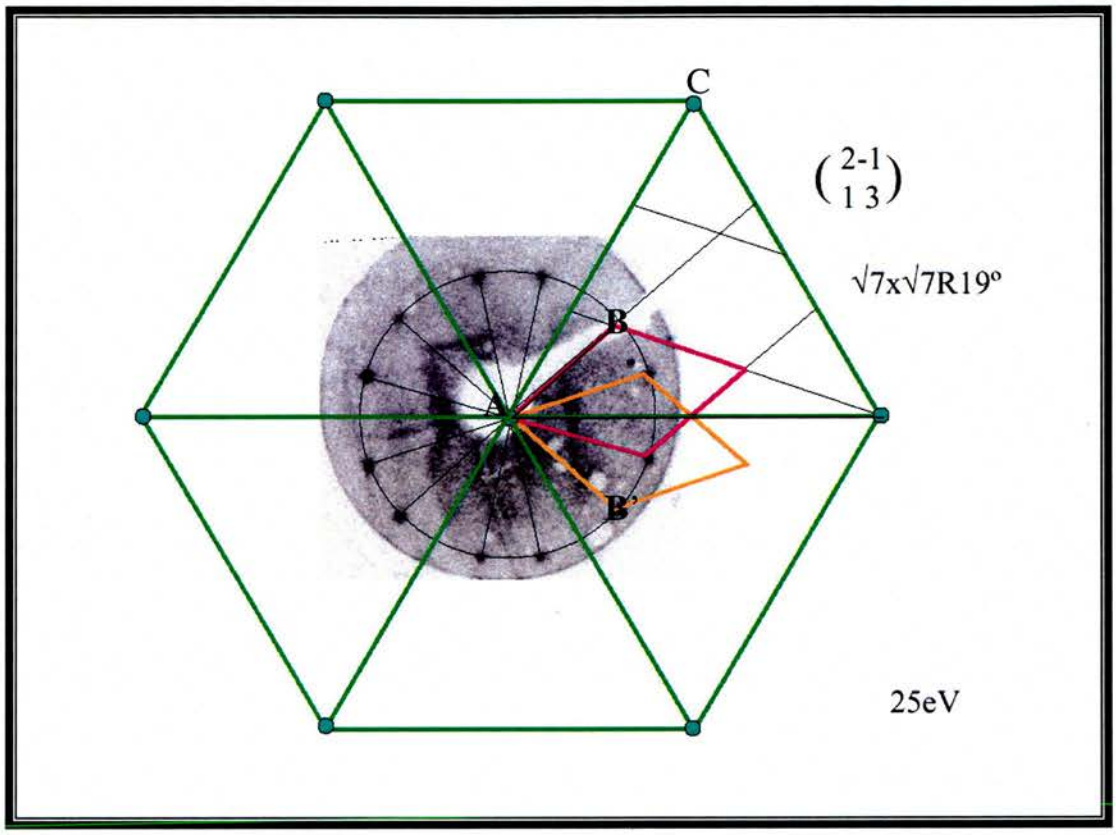

Figure 4-1: LEED pattern of high coverage BM adsorbed on Au(111). The outermost spots represent the Au(111) and the inner "ring" the two domains of BM. Sturrock et al [9].

In this LEED pattern, there are 6 pairs of spots situated in a ring. The first order spots of this pattern were obtained at 25eV beam energy. To prevent any damage to the overlayer, no higher order pattern at higher energies were taken. The spots forming the outer hexagon (green) correspond to the first order LEED pattern for the clean Au(111) surface. This was done by obtaining a LEED pattern after cleaning the surface. This pattern was obtained at a higher beam energy than the first order (as the spots were out of range for the camera) and then recalculated to 25eV to match with the overlayer LEED using the equations given in chapter 2. There are two reflectional domains of ordered benzyl mercaptan molecules on the surface and the unit cells for these are marked with orange and pink lines in figure 4-1. By comparing the length of one side of

the "diamond" (AB or AB' in figure 4-1, which corresponds to the unit cell of the overlayer), with the unit cell length for Au(111), (AC in the figure 4-1) it was noted that, AB and AB' are longer than AC by a factor $\sqrt{7}$. The LEED pattern is the reciprocal of the crystal lattice. So for the unit cell parameter, it is of the size $\sqrt{7}$ times larger than the one for the Au(111) unit cell. To check the relation between the real lattice and the LEED pattern, the program LEED-Pat [10] was used. Figure 4-2 show how it is used in this case.

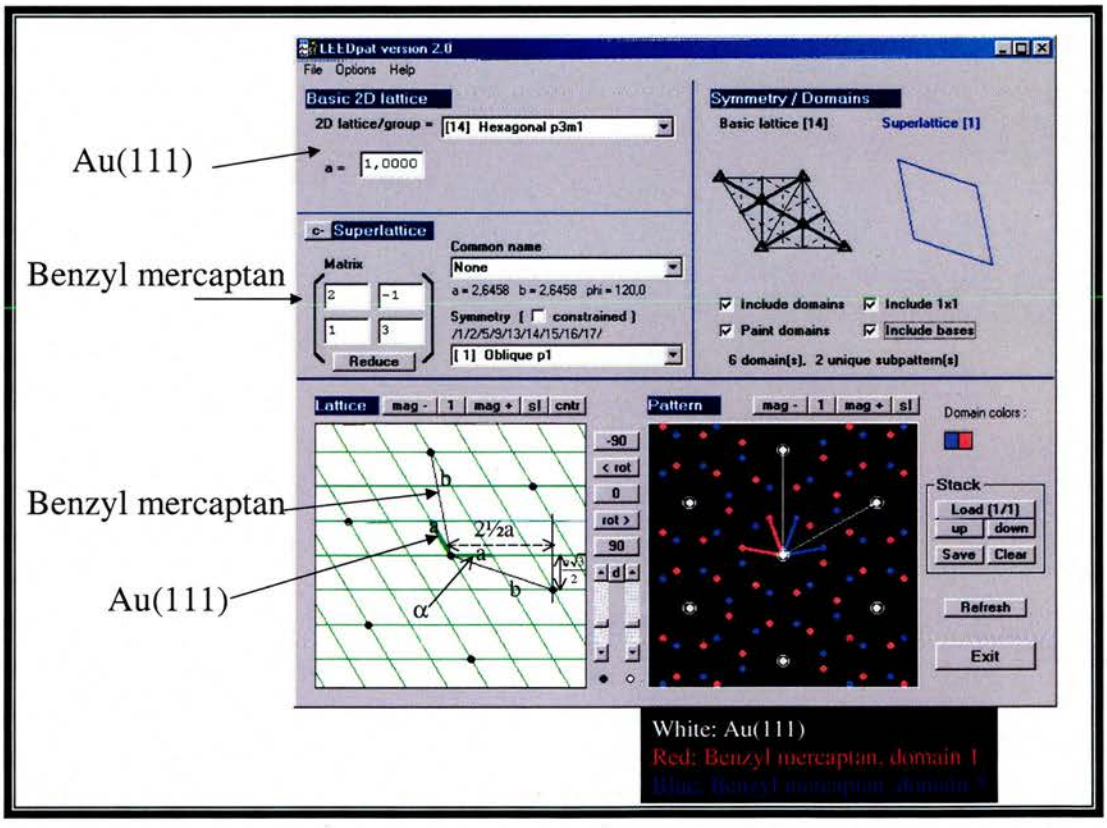

Figure 4-2. LEED-Pat program showing the relation between real and reciprocal pattern. Fritz-Haber Institut [10].

For convenience, the unit cell parameter for Au(111) = 1. For the overlayer, using matrix notation the unit cell will be $\begin{bmatrix} 2 & -1 \\ 1 & 3 \end{bmatrix}$. Alternatively, using Wood's notation the lattice parameter and the angle relative to the Au(111) can

be calculated as the following from figure 4-2: $b = \sqrt{\left(\frac{5a}{2}\right)^2 + \left(\frac{a\sqrt{3}}{2}\right)^2} = a\sqrt{7}$

$\sin\alpha = \frac{a\sqrt{3}/2}{\sqrt{7}} = 0.327 \Leftrightarrow \alpha = 19.1°$. So the result is ($\sqrt{7}$ x $\sqrt{7}$)R19.1º which is a common structure for molecular adsorption on Au(111) and other metals with the same crystal structure [11, 12, 13].

4.3 Electron Energy Loss Spectroscopy (HREELS)

4.3.1 Experimental

To provide additional characterisation of this adsorption system vibrational spectroscopy was employed to determine the molecular orientation as a function of coverage. HREEL spectra were obtained for both low and high coverages of benzyl mercaptan on Au(111), using exposure of 20000L and 50000L respectively. All spectra were resolution enhanced using Maximum likelihood methods [14] where the program "Cutting Edge" [15] was used.
In addition, DFT calculations of the geometry of the BM molecule and vibrational frequencies were carried out using Gaussian 98 [16]. The B3LYP functional and 6-31g set were used for the free BM molecule, while the Hartree Fock calculations were used for a thiolate on a initially planar hexagonal Au_7 cluster. As basis function, CEP-121G was used.

4.3.2 Results and discussion.

Figure 4-3 shows an HREEL spectrum for each coverage measured in the specular direction, ie where dipole scattering is dominant.

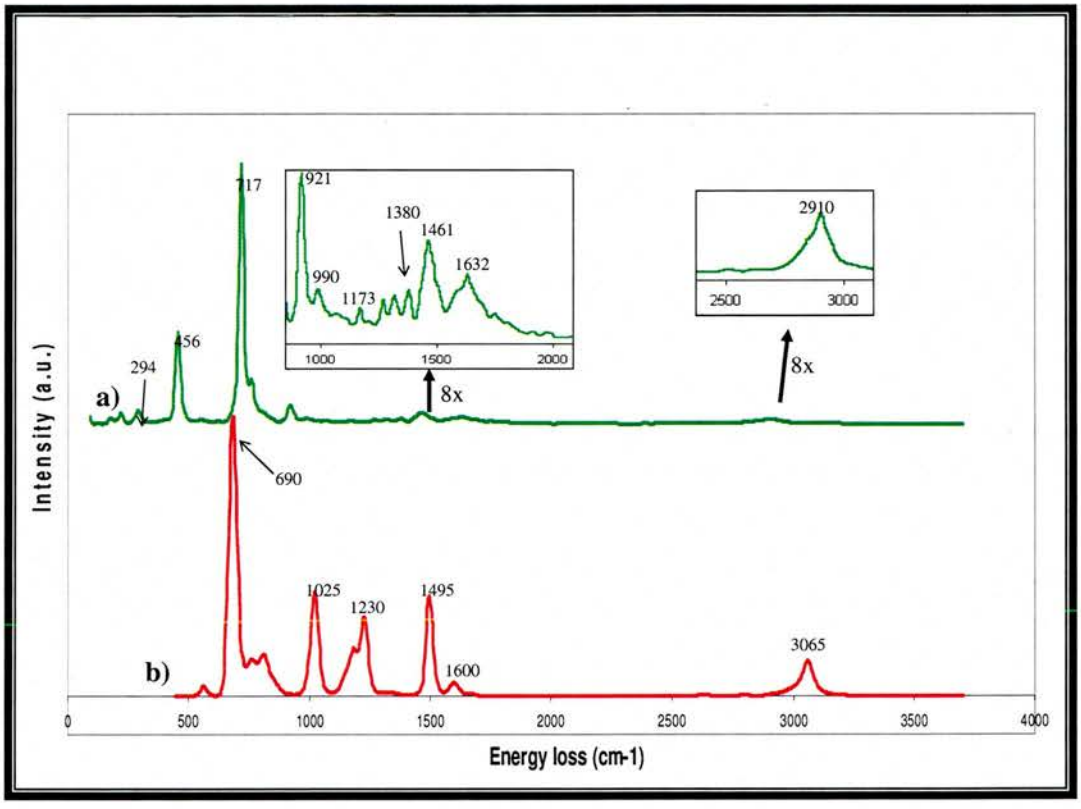

Figure 4-3. HREEL spectra for BM on Au(111) at a) low coverage and b) high coverage.

There are major differences between the two coverages. Table 4-1 indicates the assignments of the peaks found in the spectra and compared with the frequencies from a reference bulk spectrum [17] and the calculated frequencies for the free BM molecule and the corresponding thiolate on a Au_7 cluster.

Calculated frequencies for free BM Gaussean 98 [our own]	IR gas [NIST]	Assignment	Calculated frequencies for BM-Au_7 Gaussean 98 [our own]	HREELS (low coverage)	HREELS (high coverage)
45 (1.1)		C_6H5-CH_2SH torsion	215 (2.3)		
113 (0.2)		C_6H5-CH_2SH deformation	**302 (15.1)**	303	
196 (30.2)		CSH wag			
268 (2.0)		CCS bend or Au-S stretch	**392 (21.4)**		
343 (3.7)		C_6H5-CH_2SH out-of-plane bend			
424 (0.2)		out-of-plane ring deformation	459 (0.0)		
482 (0.7)	466	out-of-plane ring/CH_2 deformation	520 (8.5)	**459**	
575 (9.2)	556	in-plane ring deformation / CSH bend	605 (2.8)		
634 (37.0)	630	C-S stretch	**778 (27.2)**		**690**
654 (2.6)	650	in-plane ring deformation	678 (0.0)		
728 (36.8)	758	in-phase, out-of-plane C-H wag	**769 (10.2)**	**717**	
774 (4.0)		CH_2 rock / CSH bend			
797 (17.5)	799	out-of-plane ring def. / C_6H_5 out-of-plane wag	**825 (84.5)**		780
836 (3.9)	835	ring deformation / C_6H_5-CH_2SH stretch	866 (7.5)		820
878 (0.0)	678	out-of-phase, out-of-plane C-H wag	975 (0.1)		
946 (1.6)	949	out-of-phase, out-of-plane C-H wag / CH_2 rock	972 (7.8)		
984 (5.5)	982	$C_6H_5CH_2$-S-H in-plane bend / CH2 rock	1062 (4.7)		
1000 (0.0)		out-of-phase, out-of-plane C-H wag	1120 (0.1)		
1032 (0.1)	1027	out-of-phase, out-of-plane C-H wag	1136 (0.4)		
1037 (0.2)		C-C ring bend	1078 (0.2)		
1068 (0.2)	1069	C-C ring bend	**1116 (10.6)**	1044	**1025**
1123 (8.2)		aromatic C-H in-plane bend	1174 (8.8)		
1197 (3.0)	1201	CH_2 twist	1309 (0.3)	1179	1201
1223 (0.0)		aromatic C-H in-plane bend	1292 (1.6)		
1238 (0.2)		aromatic C-H in-plane bend	1305 (1.8)		
1254 (2.8)		C_6H_5-CH_2SH stretch	1344 (0.2)		1230
1298 (16.4)	1252	CH_2 wag	**1398 (65.9)**		
1372 (0.3)	1369	C-C ring stretch			
1396 (1.4)	1399	aromatic C-H in-plane bend	1474 (4.7)	1389	
1512 (7.5)	1498	aromatic C-H in-plane bend / C-C ring stretch	**1581 (15.1)**	1473	**1495**
1525 (8.4)	1449	CH_2 scissors	1417 (5.9)		
1556 (8.7)	1603	aromatic C-H in-plane bend / C-C ring stretch	**1641 (39.8)**	1617	1605
1643 (0.7)	1655	C-C ring stretch /aromatic	1747 (7.2)		
1663 (1.2)	1675	aromatic C-H in-plane bend / C-C ring stretch	**1777 (40.3)**		
2509 (41.7)	2592	S-H stretch			
3106 (17.1)	2945	CH_2 symmetric stretch	**3191 (16.6)**	2939	
3166 (4.3)		CH_2 asymmetric stretch	**3251 (11.5)**	2982	
3185 (8.9)	3030	C-H ring stretch	**3306 (12.8)**		3065
3193 (1.1)		C-H ring stretch	3321 (1.7)		
3203 (11.8)		C-H ring stretch	**3335 (58.3)**		
3212 (39.8)	3076	C-H ring stretch	**3354 (73.2)**		
3225 (19.5)	3160	C-H ring stretch	3380 (3.8)		

Table 4-1: Assignments for peaks found in HREELS spectra of BM adsorbed on Au(111) and compared with the frequencies for the gas phase BM [17] and the calculated frequencies using Gaussean 98 [16]. More intense peaks are shown in bold type.

The reference spectrum for the free BM molecule (gas phase) is shown in figure 4-4.

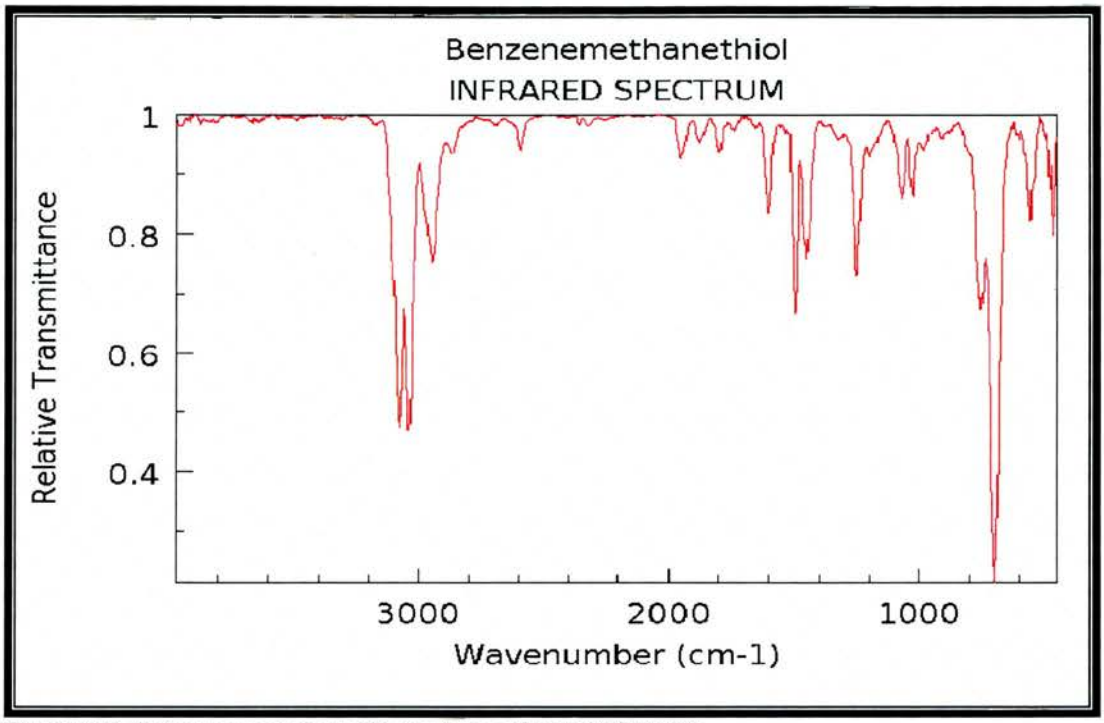

Figure 4-4. Reference gas phase IR spectrum of BM. NIST [17].

There is no peak around 2590 cm^{-1} for either coverage in the HREELS spectra in figure 4-3 while it is present for the free molecule in figure 4-4. As this is assigned to the S-H stretch of the free molecule, it is likely that the benzyl mercaptan loses the hydrogen and is bound to the surface as a thiolate. From the two spectra in figure 4-3, it is also possible to gain some information about the orientation of the molecule and, according to the dipole scattering selection rule, it can be concluded that the benzyl mercaptan molecule is lying flat with the aromatic ring parallel to the Au(111) surface at low coverage and is standing up with the ring perpendicular to the surface. The following findings are the key observations leading to these conclusions:

- For low coverage, there is a peak at 456 cm^{-1} while it is absent in the high coverage spectrum. For the free molecule, there is a peak at 466 cm^{-1}, which is assigned to an out-of-plane ring deformation, with its dynamic dipole

perpendicular to the plane of the aromatic ring. The selection rule for dipole scattering requires that only vibrations, whose dynamic dipole has a component perpendicular to the surface, are visible: Observation of this mode, therefore, indicates that the molecule is orientated with the ring flat lying on the Au(111) surface at low coverage.

- Similarly the strong peak at 717 cm^{-1}, assigned to the in-phase, out-of-plane C-H wag also with its dynamic dipole perpendicular to the ring, confirms this orientation. The shift to a lower wave number compared to the free molecule (758 cm^{-1}) is probably due to the influence of the nearby gold atoms in the surface. This was also found by Whelan et al. [2].

In contrast, molecules for which the main bonding interaction is through the aromatic ring, e.g. benzene on Pt, Pd or Ni, usually show an increase in frequency of the corresponding mode [18]. This should be due to the more repulsive H-Au interaction for the Ar-H out of plane bend as the benzene molecule situated closer to the surface than the aromatic ring of BM.

- Although not so intense (enlarged in figure 4-3), in the low coverage spectrum, there is a broad band at 2910 cm^{-1} which is assigned to CH_2 stretch (symmetric and asymmetric). When the aromatic ring is orientated parallel to the substrate, both aliphatic C-H bonds are forced to a more perpendicular direction.

- In contrast in the high coverage spectrum, the band for CH_2 stretches is absent, but instead there is a peak at 3065 cm^{-1} which corresponds to the C-H stretches in the aromatic ring. This would not be observed, if the ring were flat lying, suggesting that at the higher coverage the ring adopts a more upright orientation relative to the substrate surface plane.

- The large 690 cm^{-1} peak for the high coverage, assigned to the C-S bond stretch, is at a higher wavenumber than the corresponding band for the free molecule (630 cm^{-1}) [17]. It is most likely due to the negative charge of the sulfur atom in the thiolate form. In comparison, the calculated frequencies from Gaussian 98 [16] increases from 634 cm^{-1} for the free BM to 778 cm^{-1} for the adsorbed BM as shown in table 4-1. In contrast, DFT calculations using GAUSSIAN03 comparing the behaviour of $HOCH_2CH_2SH$ with the corresponding thiolate, $HOCH_2CH_2S^-$, indicate that the C-S stretching vibration is lowered from 711cm^{-1} to 630cm^{-1} on deprotonation.
- The ring stretch peak at 1495 cm^{-1} for the high coverage is much closer the same for the free molecule (1498 cm^{-1}) than it is in the low coverage case (1461 cm^{-1}). A reason for this is probably the influence the gold atoms have on the aromatic ring when it is lying flat close to the surface at low coverage. This agrees with Tao et al. [1]. As this mode is also seen in the low coverage case (however much less intense) we suggest that the ring is orientated not 100% parallel to the surface but very close to it.

Finally we need to be sure that it is really dipole scattering that gives us this information from the specular spectra above. To confirm this, a 5º off-specular HREEL spectrum was measured for the high coverage case. Figure 4-5 shows the comparison between the specular and off-specular spectra.

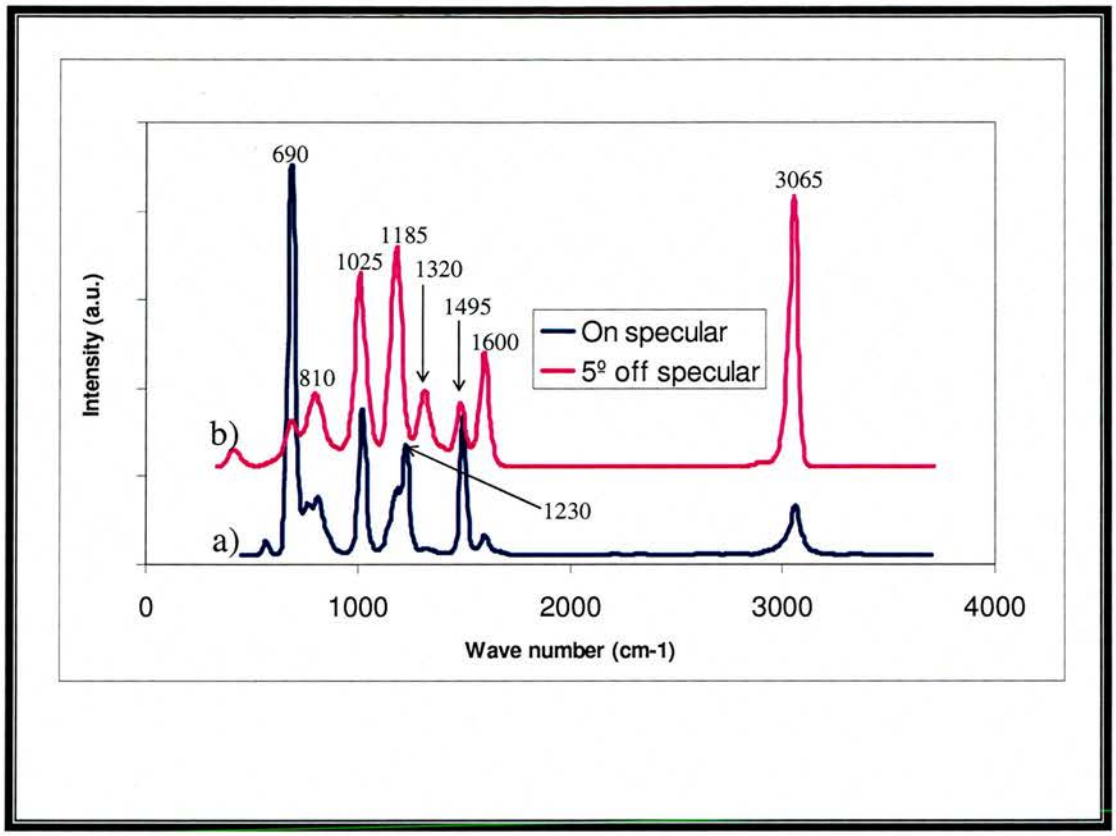

Figure 4-5. a) Specular and b) 5° off-specular HREEL spectra for high coverage BM on Au(111).

There is an obvious difference in relative intensity of the corresponding peaks between the spectra in specular and off-specular modes. The C-S stretch at 690 cm^{-1} and the aromatic ring stretch at 1495 cm^{-1} have decreased considerably, relative to other modes, as a result of their dipole scattering behaviour. On the other hand, the aromatic C-H stretch and the CH_2 twisting modes appear more strongly in the impact mode, and these are shown as the increase of the peak at 3065 cm^{-1} and the peaks in the region 1180-1320 cm^{-1}. It is possible that there is a negative ion resonance contribution to the intensity of at least some of these modes.

4.4 Infrared Reflection Absorption Spectroscopy (RAIRS).

4.4.1 Measurements for BM adsorbed on Au(111) at room temperature..

FTIR measurements of the benzyl mercaptan/Au(111) system were performed to verify the results from the HREELS. It was also useful to find more precisely the critical exposure at which the orientation of the benzyl mercaptan molecule changes orientation from the low coverage to high coverage profile. The experiment involved addition of gaseous benzyl mercaptan to the metal crystal surface alternating with collection of the IR spectrum. This was possible as dosing and analyzing were performed in the same UHV chamber without moving the substrate and therefore no need to optimize the beam to the detector after every dosing. On the other hand, however, the sensitivity for RAIRS is lower than for HREELS, particularly at low frequencies, so only a few of the characteristic peaks were observed.

First, the Au(111) substrate was cleaned by Ar^+ sputtering (ion energy 0.7-0.8 kV, Ar pressure at $3x10^{-5}$ mbar which gave a sample current of 30-40 μA) and annealing (resistive heating up to 800K). Cleaning was done in two different ways. Either by one long sputter of 1 hour followed by annealing at the desired temperature for 10 minutes, or by several cycles (usually around five) with sputtering for 10 minutes and annealing by heating just up to 800K and then allowing to cool (except the last cycle where it was kept at 800K for 10 minutes). This choice of method did not appreciably change the results LEED was used to check the cleanliness afterwards, which is shown in figure 4-6.

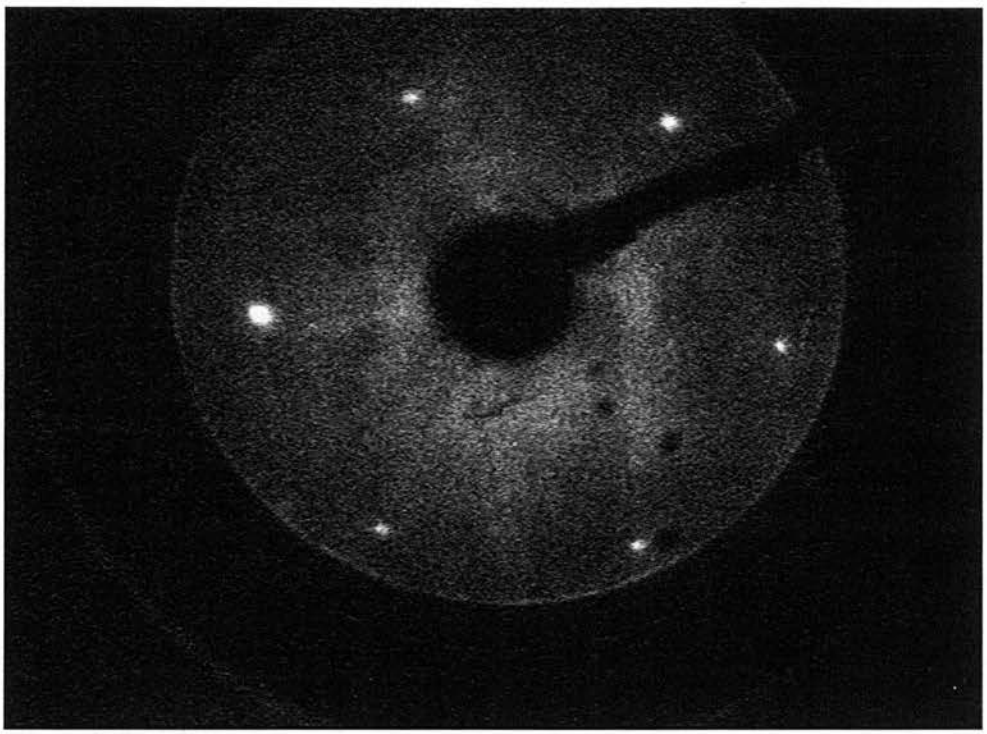

Figure 4-6. LEED pattern for a clean surface of Au(111).

Several spectra from the clean metal crystal surface were taken and reprocessed against the previous one until there were minimal changes. The last one is then used as a background and for reprocessing subsequent spectra with the adsorbate present. There are, however, some peaks that still interfere with the results. A slowly increasing broad band at 3100-3400 cm^{-1} comes from the ice in the detector formed by the liquid nitrogen cooling. Two other peaks (a doublet), around 2300-2400 cm^{-1}, comes from carbon dioxide.

Influence of water vapour should be brought down to a minimum (by purging the system with nitrogen for some hours), but can still be present. If this is too big, each sample spectrum is processed by subtraction of a water spectrum. This water spectrum was obtained by obtaining a spectrum from a clean substrate when the system has been recently well purged, then opening and closing the detector box before collecting a second spectrum in the

presence of increased water vapour, but otherwise identical sample conditions. The latter are then processed against the former. Figure 4-7 shows spectra of BM adsorbed on Au(111) for dosings up to 80000L in the range 3100 to 1100 cm^{-1}.

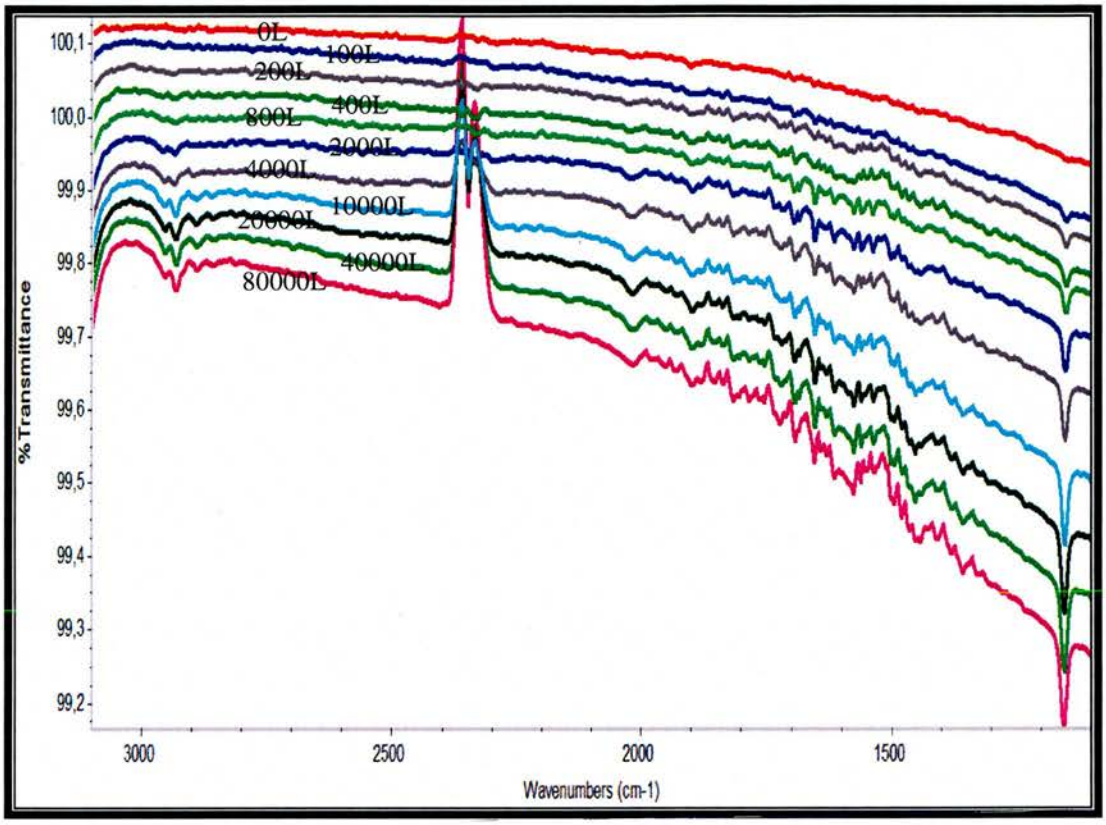

Figure 4-7: IRAS spectra in the range 3100 to 1100 cm^{-1} for benzyl mercaptan on Au(111) for different total exposures.

There are two regions that show characteristic bands of BM which give an indication as to how the molecules change orientation with the exposure (coverage) of the molecule. Figure 4-8 shows the FTIR spectrum in the region where the aliphatic C-H stretch occur.

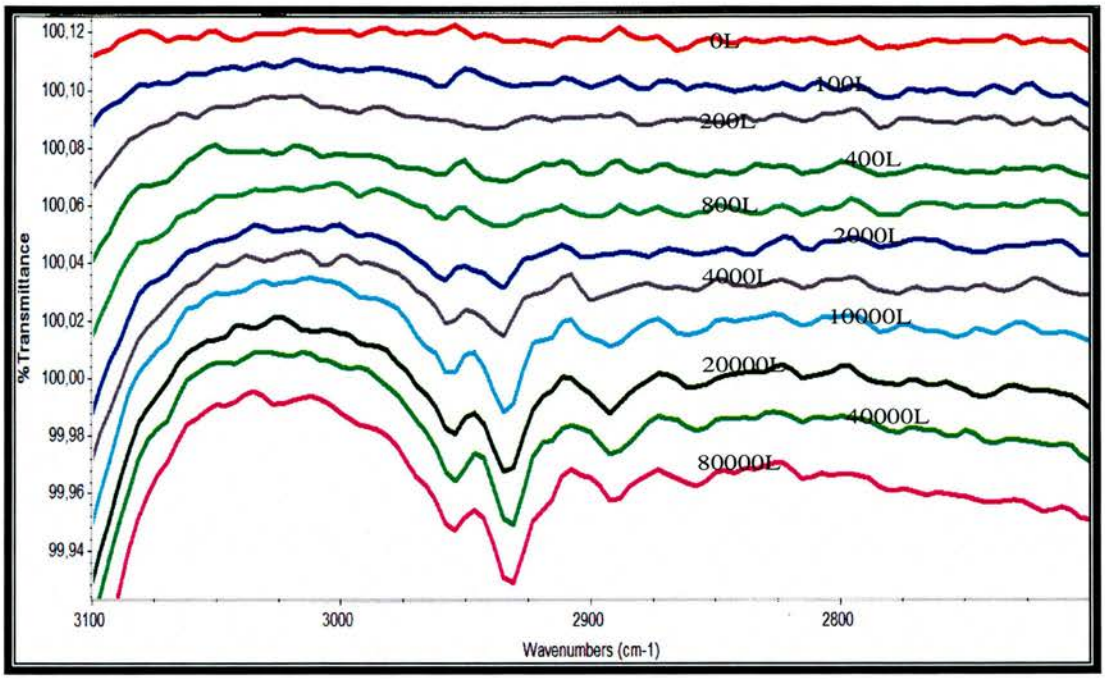

Figure 4-8: IRAS spectra in the range 3100 to 2700 cm^{-1} for benzyl mercaptan on Au(111) for different total exposures.

Here, it is obvious that the aliphatic CH_2 stretches (asymmetric and symmetric) peaks increase by exposures for the lower dosings, but level out and slightly decrease for the higher doses. Using the integrating function of the software (Nicolet) their areas were calculated. By plotting the area vs total exposure, we get this profile for the aliphatic C-H stretches shown in figure 4-9.

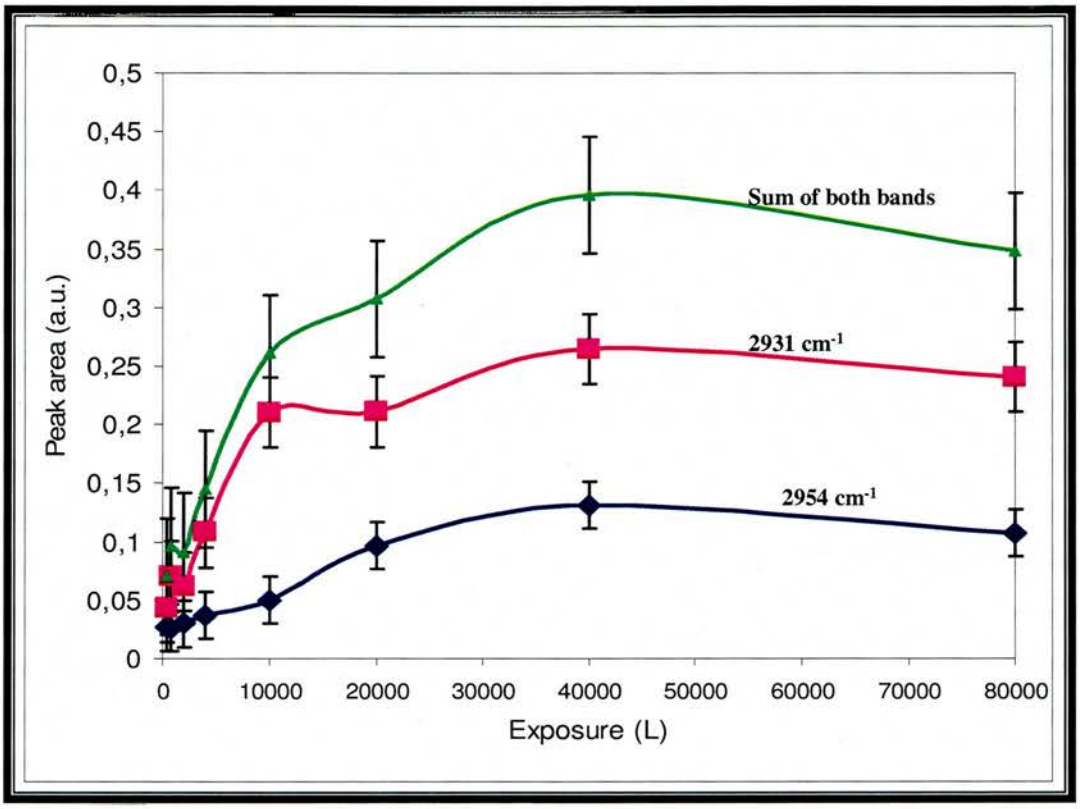

Figure 4-9: Peak areas for the aliphatic C-H stretches bands versus exposure.

Both peak areas (and hence the sum of them) rise to a maximum at an exposure of about 40000L where they start to decline. This is consistent with the HREELS data, since the surface selection rule also applies to RAIRS. As the coverage increases and the molecule changes orientation from an aromatic ring parallel to the surface to one with a more upright position, the aliphatic C-H bonds turns towards more of a parallel direction making them IR inactive. The peaks expected for the aromatic C-H stretching modes were not visible here, even for the higher exposures. They are probably "drowned" in the broad band caused by the growing detector ice.

The only other peak that changes through with the increasing exposure is one at 1153 cm^{-1}. Figure 4-10 show that part of the spectra around this peak.

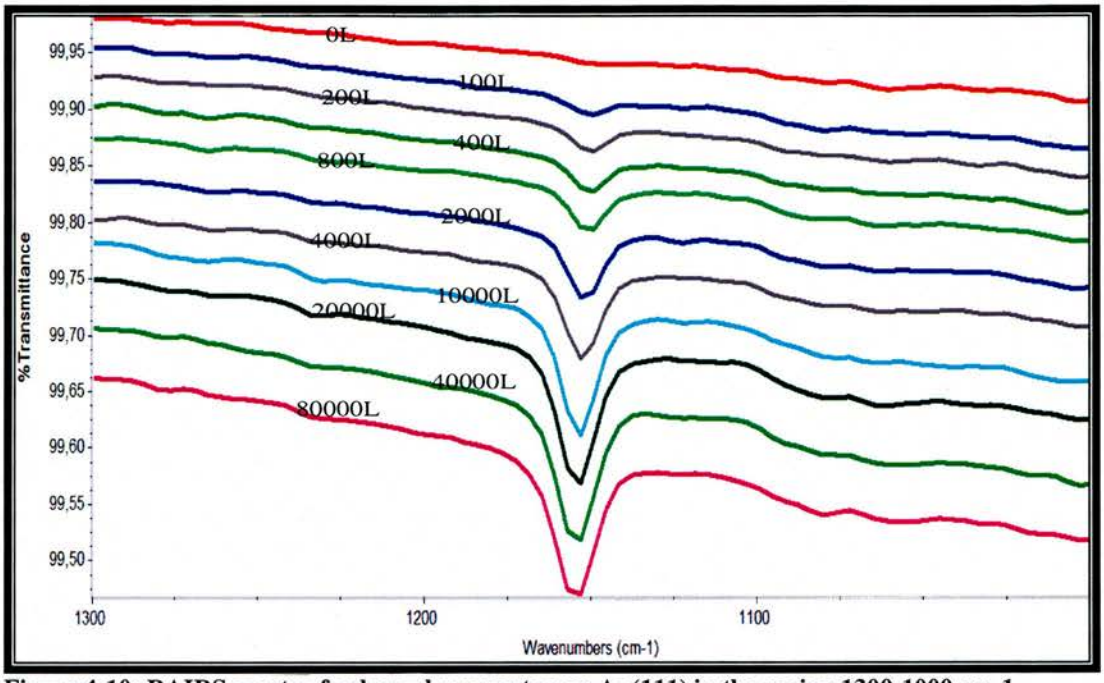

Figure 4-10: RAIRS spectra for benzyl mercaptan on Au(111) in the region 1300-1000 cm-1.

By integrating the peak areas and plotting them against exposure, we obtain the following profile shown in figure 4-11.

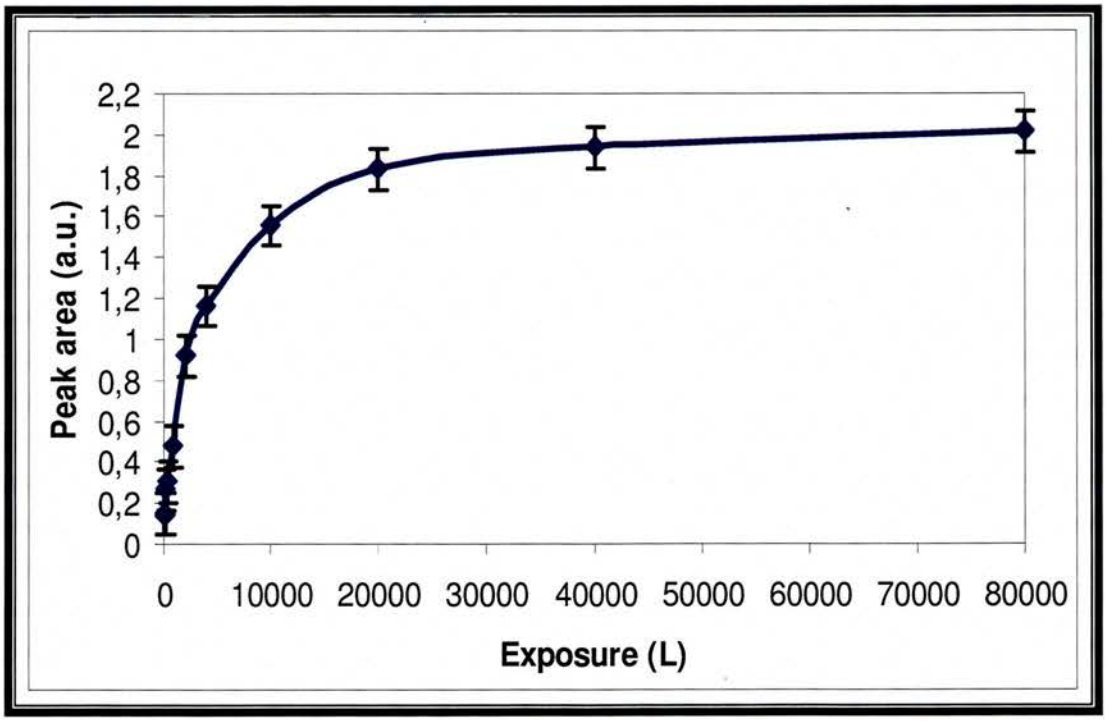

Figure 4-11: Peak area versus exposure for the band at 1153 cm^{-1} assigned for C-H in-plane bend.

This may be assigned to the C-H in-plane bend. At low coverage (when the BM molecule is lying flat on the surface) this mode is parallel to the surface. When the coverage increases the molecules change direction towards standing up position and the mode becomes more perpendicular which contributes to a more intense peak. Finally the monolayer becomes saturated and the intensity levels out.

4.4.2 Measurements for BM adsorbed on Cu(110) at room temperature.

Benzyl mercaptan was also adsorbed on Cu(110) and studied by RAIRS. The substrate was cleaned in the same way and checked with LEED as shown in figure 4-12.

Figure 4-12. LEED pattern of a clean Cu(110) surface.

This system show a similar behaviour for adsorption of BM on Cu(110) as for adsorption on Au(111) except that the turnover to the high coverage structure

occurs at a much lower exposure, probably because copper is more reactive than gold giving rise to a higher sticking probability on Cu(110).

Figure 4-13 shows a spectra for the region 3100 to 1100 cm^{-1}.

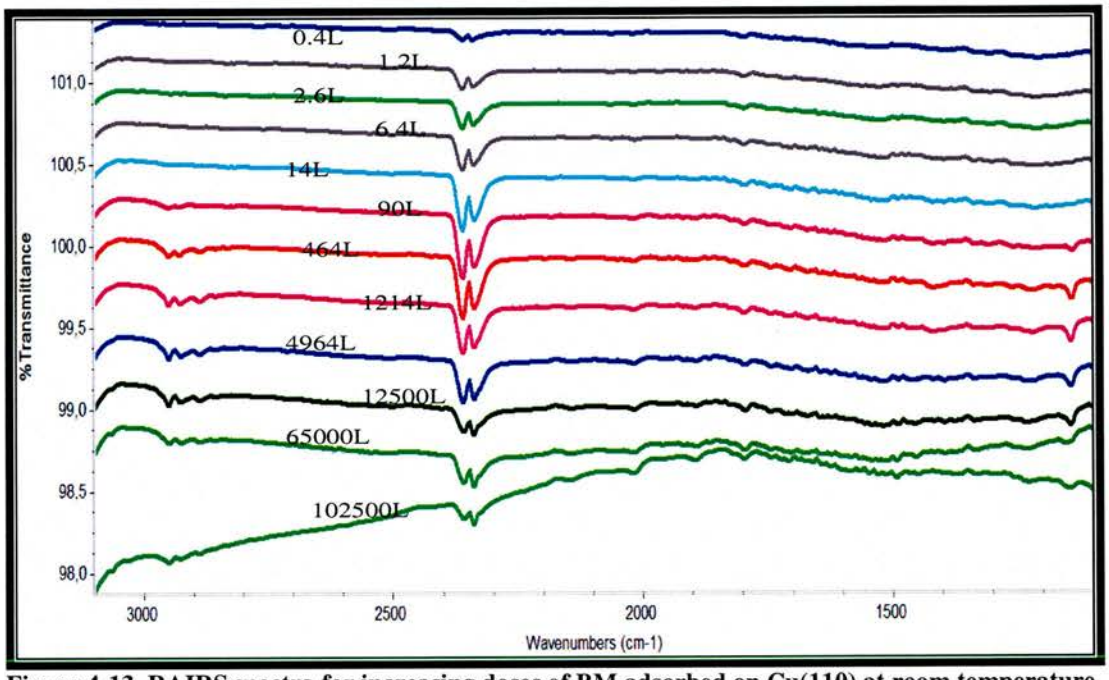

Figure 4-13. RAIRS spectra for increasing doses of BM adsorbed on Cu(110) at room temperature in the region 3100-1100 cm^{-1}.

The most interesting change of peak areas versus exposure are found for the aliphatic C-H and aromatic C-H stretches. Figure 4-14 shows the spectra for increasing total exposure in the range 2550-3150 cm^{-1}.

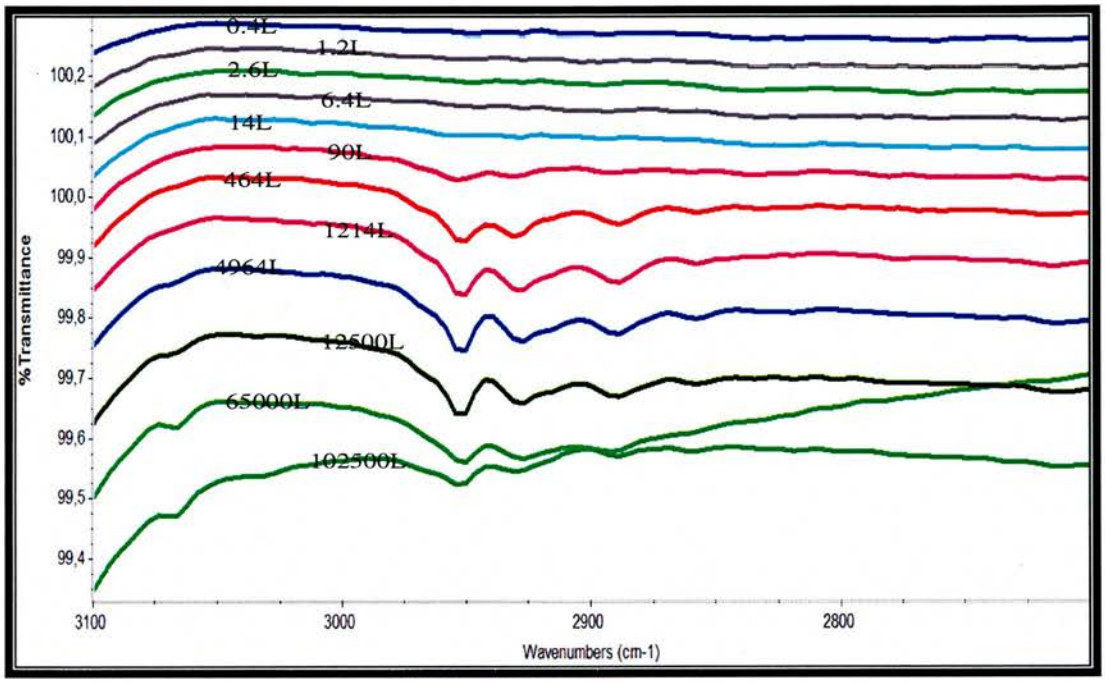

Figure 4-14. RAIRS spectra in the region 3100-2700 cm^{-1} for increasing doses of BM adsorbed on Cu(110).

Again, there is a rise in the CH_2 stretches (symmetric and asymmetric, 2930 cm^{-1} and 2950 cm^{-1} respectively) at low coverage as the total exposure increases, but the decrease at higher coverage is more obvious here and starts at a lower exposure than for Au(111). In addition, also the peak for the aromatic C-H stretch is visible on the slope of the large "detector ice band" for the higher exposures. By plotting the peak areas vs exposure, an interesting profile appears in figure 4-15.

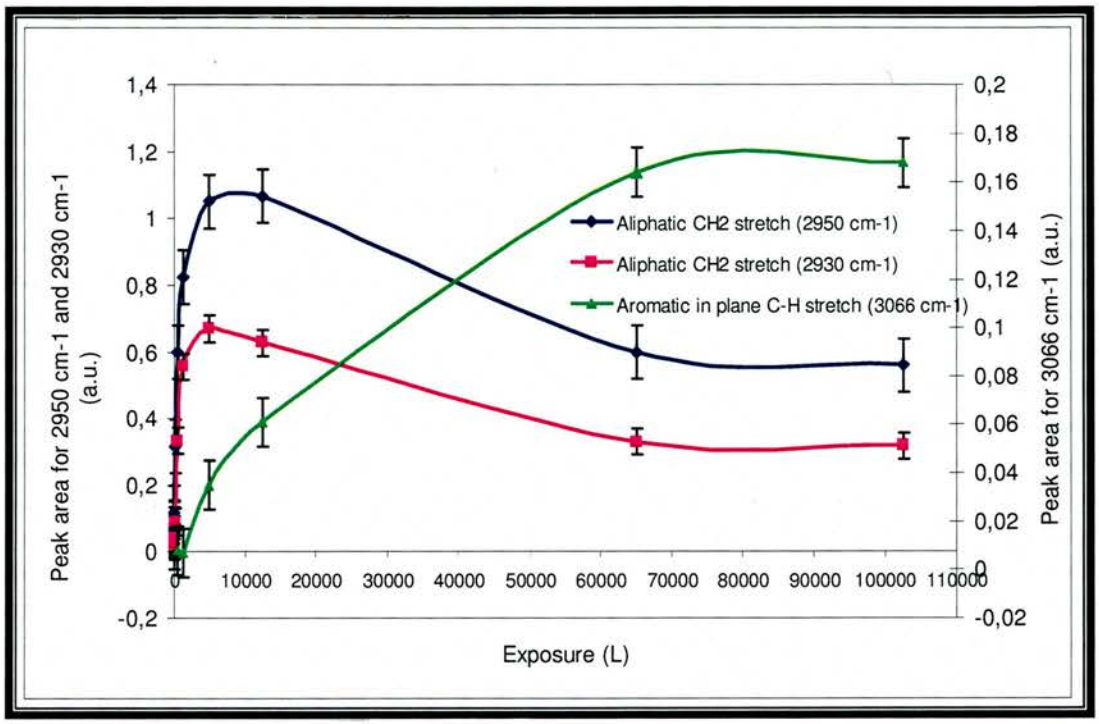

Figure 4-15: Peak area versus exposure for the aromatic and aliphatic C-H stretching modes.

This suggests that also on the Cu(110) surface, the molecules are lying flat with the aromatic ring parallel to the surface at low coverage and that they adopt a more upright orientation at high coverage. In this case the flat-lying molecules reach a maximum coverage at around 10000L exposure while final monolayer saturation occurs near 70000L exposure.

There was only one other band that changed intensity with increasing exposure, that at 1145 cm^{-1}. The RAIRS spectrum in that region is shown in figure 4-16, and the peak area of this band versus exposure of BM is shown in figure 4-17. This increases rapidly to a maximum at around 1200L and decrease slowly. This behaviour can be a result of that the aromatic out-of-plane C-H wag and the in-plane C-H bend are both contributing to this and not separated from each other.

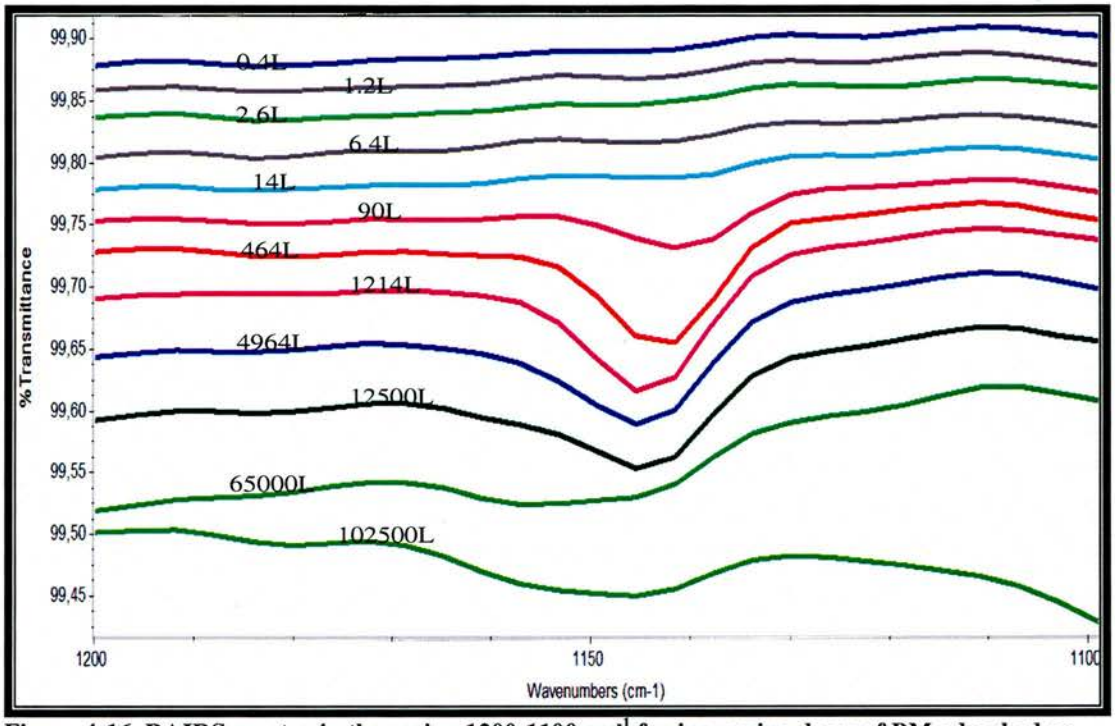

Figure 4-16. RAIRS spectra in the region 1200-1100 cm^{-1} for increasing doses of BM adsorbed on Cu(110).

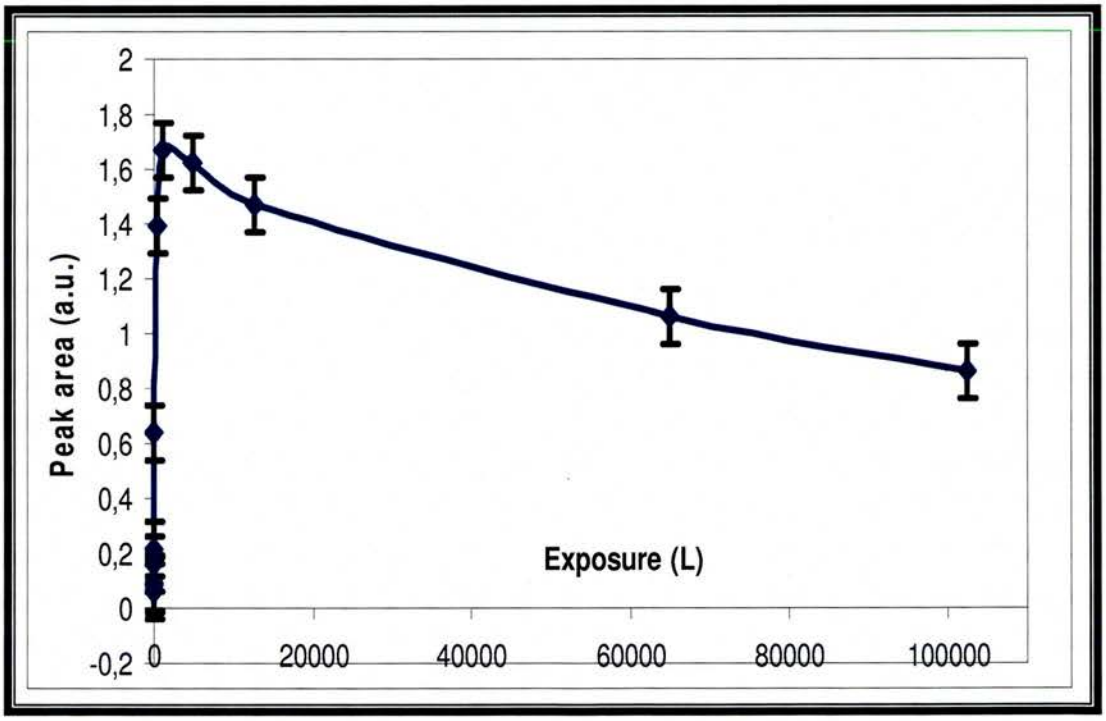

Figure 4-17: Peak area versus exposure for the band at 1145 cm-1.

So it seems that there is a similar coverage dependence profile for Cu(110) as for Au(111) but the turn to vertical orientation of the BM molecules occurs at a lower exposure, i.e. larger sticking probability on Cu(110).

4.4.3 Measurements for BM adsorbed on Au(111) at reduced temperatures.

Several different methods were employed to obtain a layer of BM molecules on the Au(111) surface at low temperature (around 45-50K), but only one of them were used for the adsorption of BM only.

First the substrate were cooled by sucking liquid helium through a cooling plate connected to the sample holder. Once the temperature has stabilized, BM was dosed stepwise followed by obtaining a spectrum after each dose. The accumulated exposure in Langmuirs were used as a measure of the growth. This was done for the build up of BM up to the saturated monolayer and then continuing towards the formation of a multilayer.

Figure 4-18 shows the spectra for the growth of a BM monolayer in the temperature range of 43-48K.

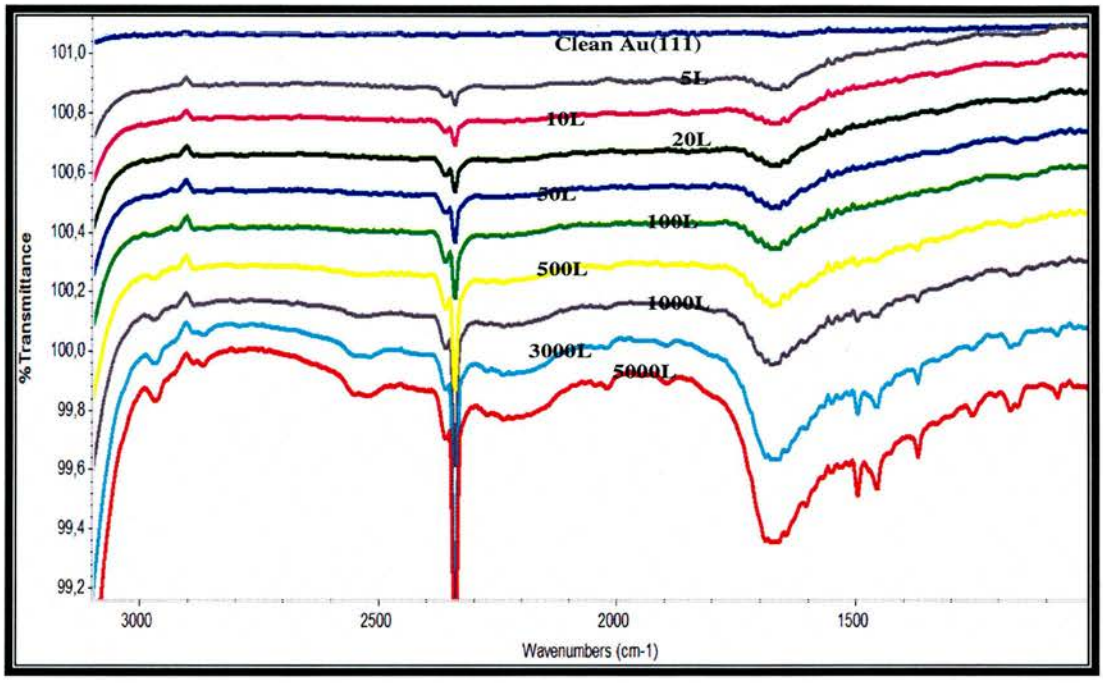

Figure 4-18. RAIRS spectra of BM dosed on Au(111) at 43K to 48K.

Here it is obvious that a multilayer starts to form at higher exposures (over 500L).

One sign is the absence of a band between 2500-2600 cm^{-1}, which is assigned for the S-H stretch, at exposures lower than 500L which means that the molecule loses the proton also at this low temperature when the monolayer builds up. However, for exposures from 500L and above several peaks appear and grow proportionally with increasing exposures. These are a sign of the formation of multilayers. The most important peak is the one around 2520 cm^{-1} which is assigned to the S-H stretch. As the molecules in the second layer do not bind to the gold atoms they do not lose their hydrogen in the mercapto group. A possible explanation for the other characteristic peaks which appear in the range 1000-1500 cm^{-1} (see table 4-1 in the HREELS section) is that the molecules in the second and higher layers are not ordered or orientated in the

same way as the first layer bound to the gold surface and hence increase proportionally as they would for the gas phase.

4.5 Scanning Tunnelling Microscopy (STM)

Two studies of adsorption of BM on Au(111) at room temperature were performed, one with low coverage, corresponding to an incomplete monolayer, and the other with a high coverage towards one monolayer [23].

4.5.1 Low coverage of BM on Au(111).

At an exposure of about 18000L a low coverage of BM molecules was found. At this coverage hexamer rings are formed on terraces of the Au(111) surface. Figure 4-19 show two such hexamers. The line profile showing the thickness of this hexagonal ring matches well with the width of the aromatic ring of the BM molecule (4.0Å).

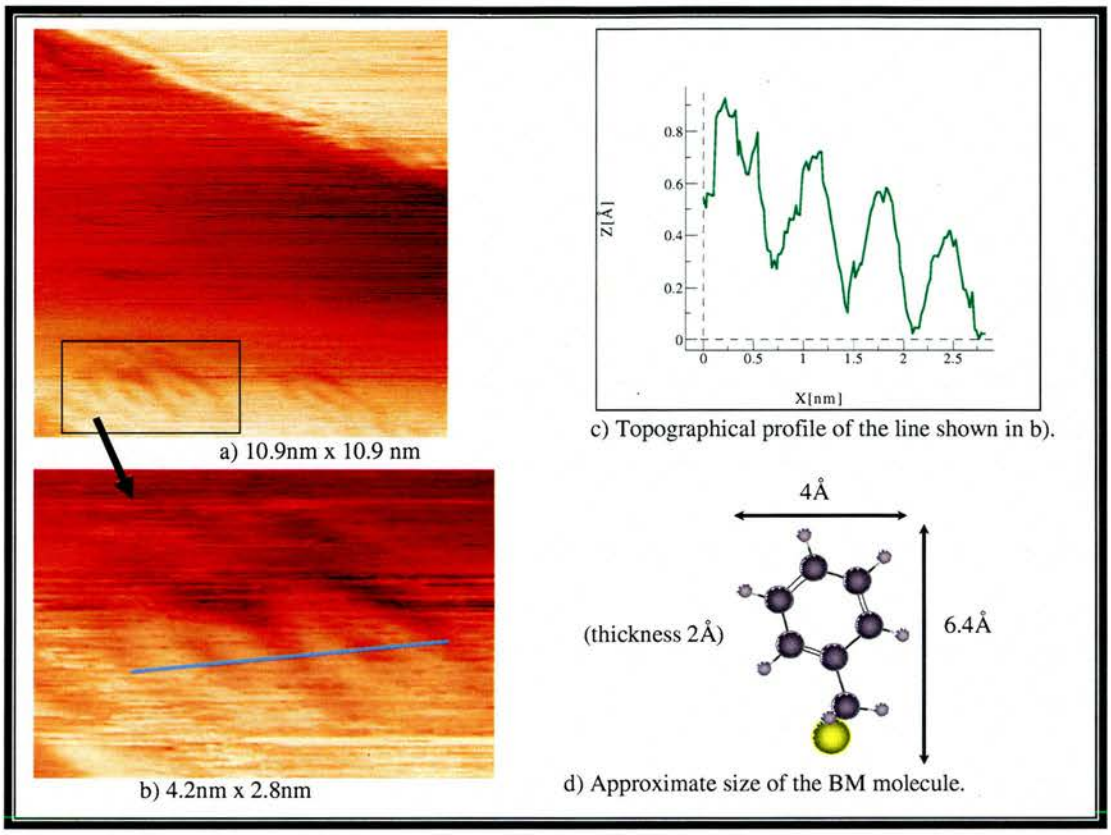

Figure 4-19. Hexagonal rings of BM molecule at low coverage (a), zoomed in at (b) with a line profile (c) corresponding to the line in (b). Tip conditions 47mV and 0.1nA.

The strong van der Waals interactions between the aromatic rings and the surface, as well as electrostatic interactions between the ring and the sulfur atom of a neighboring molecule are probably the reason for this orientation. Since there is plenty of space for the molecules to lie flat on the substrate surface, it is also possible that the aromatic rings are interacting with the gold atoms which has been shown elsewhere [1]. This also agree with our experiments with HREELS and RAIRS described above, where the vibrational modes with dipole change perpendicular to the surface are observed indicated flat lying molecules at low coverage [9].

Figure 4-20 shows a model of the hexagonal pattern of benzyl mercaptan molecules at low coverage.

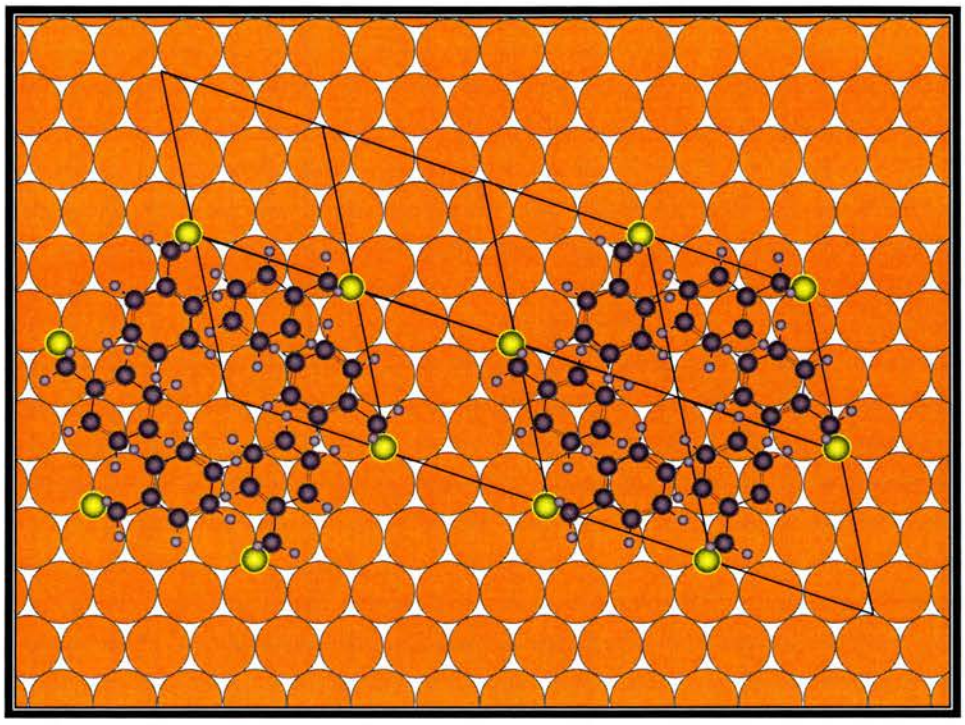

Figure 4-20: Schematic illustration of the hexagonal orientation of benzyl mercaptan molecules at low coverage on Au(111), including the $(\sqrt{7}x\sqrt{7})R19.1^{o}$ unit cell.

From the STM data, the diameter of the ring is about 8-9 Å which is equivalent to about 3 Au atoms, and the distance between the two rings is slightly less than that. This model allows the aromatic rings to interact with each other and the gold atoms. Also, this suggests that the sulfur atoms adsorb at some of the $(\sqrt{7}x\sqrt{7})R19.1^{o}$ sites which on further exposure gives this ordered structure (but with the molecules orientated upright) at saturation coverage as described next in section 4.5.2.

For adsorption of mercaptopyridine [19] and some purines and pyrimidines [20] on Au(111) at room temperature it has been shown that the first molecules adsorbs at certain sites. In the latter case it is proposed that the adsorption occurs in three stages. First a random adsorption in clusters, then the clusters adsorbs at the herringbone reconstruction site and finally an ordered monolayer is formed. It was not so clear in this case, but figure 4-21

shows an example for the initial stage of adsorption of BM at low temperature (15K as read by the thermocouple).

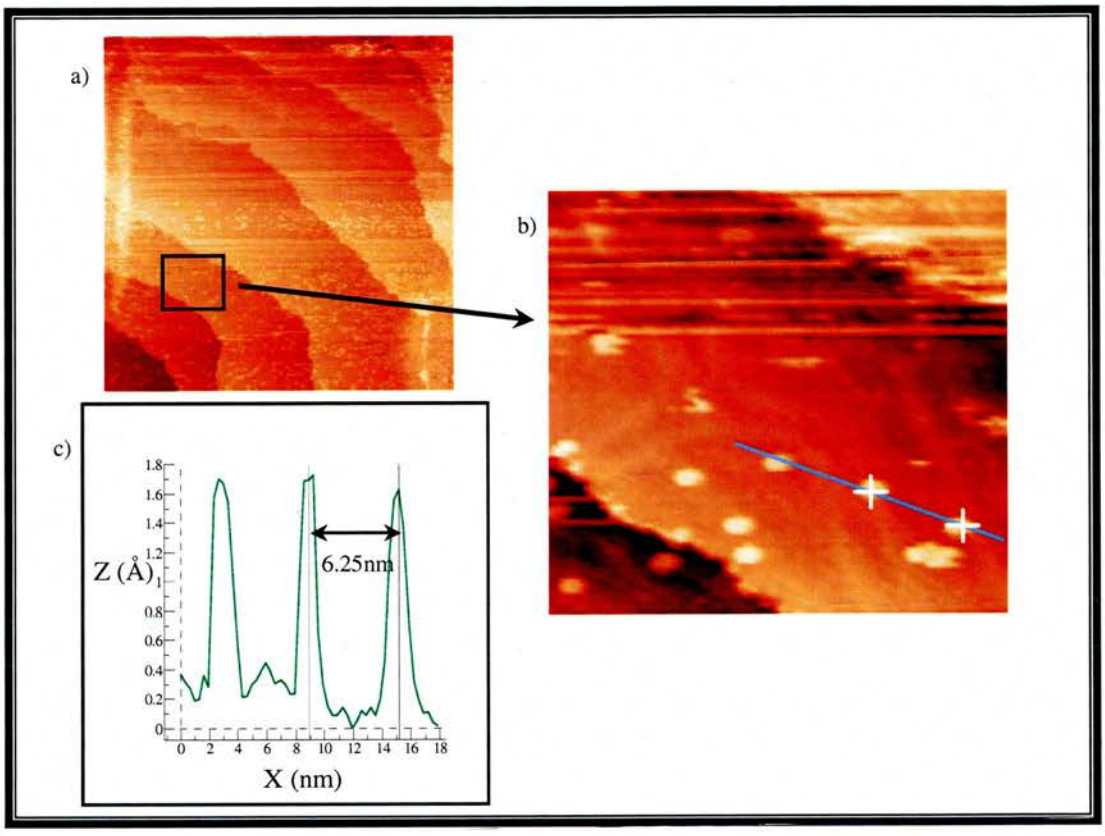

Figure 4-21. STM image of clusters of BM molecules at low coverage on Au(111) at 15K. a) Original image, 159nm x 159nm. Tip conditions -0.37A, 0.16nA. b) Zoomed in area with line profile, 29nm x 27nm. c) Plot of the line profile.

The distance between the two clusters in Figure 4-21 b) is 6.25nm as shown in c). Although this matches well with one spacing of the herringbone zig-zag pattern, 62.5Å/2.88Å = 22 Au Atoms, there were no nucleation repeatedly over a wide range of the periodicity of the herringbone which has an ideal monodomain of 7.3nm x 14nm [21].

4.5.2 High coverage of BM on Au(111).

When the clusters merge together a monolayer of flat-lying molecules is formed. Figure 4-22 shows an image of such a domain.

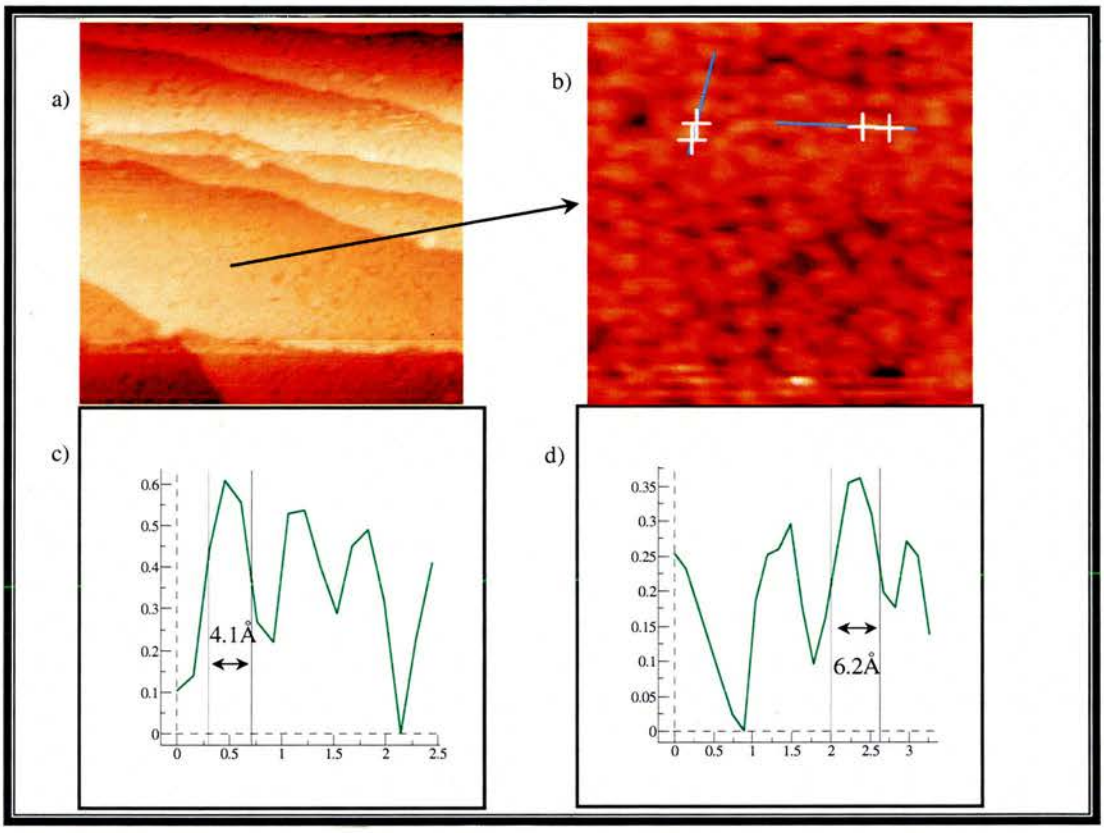

Figure 4-22. Monolayer formed by clusters at low coverage (exposure 10000L) of BM on Au(111) at 15K (read by the thermocouple). a) Original image, 76nm x 76 nm, tip voltage –380mV, tunnelling current 0.158nA. b) Zoomed in area, 9.2nM x 9.2 nm. c) and d) Line profiles of the left and right ones respectively in b), X in nm and Z in Å.

The line profiles in figure 4-22 are measured to be 4.1Å and 6.4Å respectively. These are in good agreement with the size of the molecule mentioned earlier and is a good indication that the molecule is flat lying.

For higher exposure, around 45000L, this higher coverage resulted in a full monolayer and is shown in figure 4-23 at 15K (read by the thermocouple). Here the STM images and the illustration show that the molecules are ordered

in a $(\sqrt{7}x\sqrt{7})R19.1^{o}$ structure relative to the Au(111) surface. The line profile drawn through a possible image shows a length of 6.23Å, which matches well with the distance over the diameter of the benzene ring and the attached sulfur atom. The distance between two adjacent molecules is also measured as 7.4Å and agrees well with the unit cell of the overlayer ($\sqrt{7}x2.88\mathring{A} = 7.7\mathring{A}$).

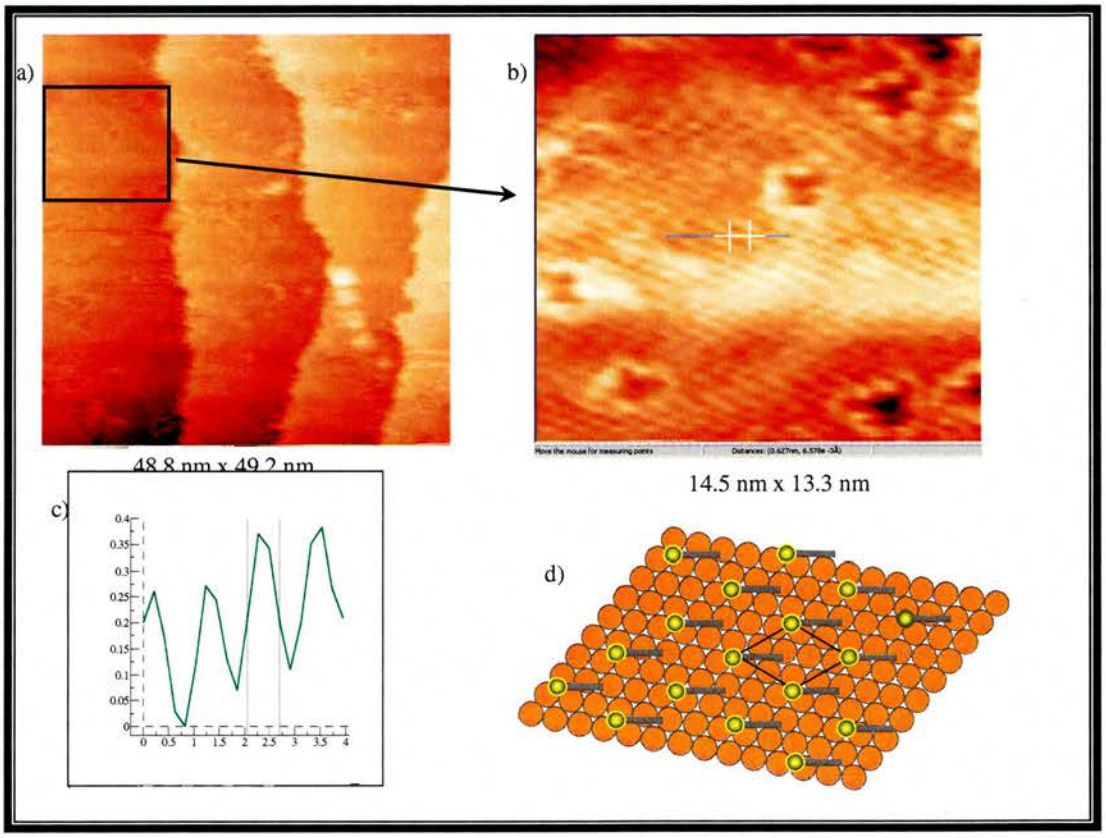

Figure 4-23: STM images at 15K (according to the thermocouple) for high coverage of benzyl mercaptan (exposure of 45000L at room temperature before cooling) on Au(111). a) Original image 49nm x 49nm with tip conditions of –456mV bias and 0.155nA tunnelling current. b) Selected zoomed in area, 14 nm x 13 nm. c) Line profile with markers along the length of the BM molecule measuring 6.3Å. d) Schematic illustration for the over layer of the standing up BM molecules.

This structure is also supported with the results from LEED, HREELS and RAIRS as described earlier in this chapter. The sulfur atom is also thought to occupy the three-fold hollow site rather than than the atop site which was predicted by the DFT calculation of BM-Au_7 [9].

The same structure has been found for other thiols, sulfides and disulfides (both organic and inorganic) adsorbed on similar crystal metal surfaces, for example Na_2S, H_2S and alkane thiols on Ag(111) [11] and H_2S on Cu(111) [13]. On the other hand, other structures for benzyl mercaptan adsorbed on Au(111) were found by other researchers using STM imaging during different adsorption conditions. Baunach et al obtained two ordered structures, $c(15x\sqrt{3})$-rect and $(2x\sqrt{3})$-rect respectively, when the molecules were adsorbed in liquid phase [7]. Tao et al studied substituted benzene and biphenyl mercaptans with and without a methylene group between the sulfur atom and aromatic ring. They were all deposited by immersing the Au(111) substrate in ethanol solution. A $(\sqrt{3}x\sqrt{3})R30^o$ structure was found for the methylene group containing ones, including benzyl mercaptan [1]. However, they reported no coverage dependence. Azzam et al. studied ω-(4'-methylbiphenyl-4-yl) alkanethiols, $CH_3(C_6H_4)_2(CH_2)_nSH$ (called BPn, where n = 3 and 4), on Au(111) which resulted in a commensurate $(2\sqrt{3}x\sqrt{3})R30^o$ structure for BP3 and a $(5\sqrt{3}x3)-rect$ structure for BP4 [22].

4.6 Conclusions

Adsorption of benzyl mercaptan onto Au(111) show many interesting features. Upon adsorption the molecule becomes deprotonated and the thiolate binds to the surface at all coverages at room temperature. HREELS and RAIRS show, according to the selection rule, that the orientation of the molecules is coverage dependent, with the aromatic ring parallel to the surface at low coverage and more perpendicular at high coverage. For high coverage, the

molecules adsorb in a well ordered $(\sqrt{7}x\sqrt{7})R19.1^{o}$ structure as seen in the LEED pattern and STM images, and at low coverage, the flat lying BM molecules form hexamers on the Au(111) surface. Similar orientation of the molecules seems to be the case also on Cu(110) however no structure were obtained. At low temperature (around 50K) multilayers are formed and high exposures while at room temperature only monolayers are formed.

4.7 References

1. Y.T. Tao, C.C. Wu, J.Y. Eu, W.L. Lin, ***Langmuir*** 13 (1997) 4018.
2. C.M. Whelan, C.J. Barnes, C.G.H. Walker, N.M.D. Brown, ***Surface Science*** 425 (1999) 195.
3. A.A. Dhirani, R.W. Zehner, R.P. Hsung, P. Guyot-Sionnest, L.R Sita, ***Journal of the American Chemical Society*** 118 (1996) 3319.
4. E. Sabatani, J. Cohen-Boulakia, M. Bruening, I. Rubinstein, ***Langmuir*** 9 (1993) 2974.
5. M. Zharnikov, M. Grunze, ***Journal of Physics: Condensed Matter*** 13 (2001) 11333.
6. J.Y. Gui, D.A Stern, D.G. Frank, D.C. Zapien, A.T. Hubbard, ***Langmuir*** 7 (1991) 955.
7. T. Baunach, D.M. Kolb, ***Analytical and Bioanalytical chemistry*** 373 (2002) 743.
8. H.H. Jung, Y.D. Won, S. Shin, K. Kim, ***Langmuir*** 15 (1999) 1147.
9. E.J. Sturrock, Q. Chen, P.H. Borchardt, N.V. Richardson, ***Journal of Electron Spectroscopy And Related Phenomena*** 135 (2004) 127.

10. LEED Pat 2, version 2.0 (2002), Fritz-Haber Institut, Berlin http://w3.rz-berlin.mpg.de/~hermann/LEEDpat (accessed Sep 2005).
11. R. Heinz, J.P. Rabe, ***Langmuir*** 11 (1995) 506.
12. T. Müller, D. Heuer, H. Pfnür, U. Köhler, ***Surface Science*** 347 (1996) 80.
13. G.J. Jackson, S.M. Driver, D.P. Woodruff, B.C.C. Cowie, R.G. Jones, ***Surface Science*** 453 (2000) 183.
14. B. G. Frederick, G. L. Nyberg1 and N. V. Richardson, ***Journal of Electronic Spectroscopy and Related Phenomena*** 64/65 (1993) 825.
15. Cutting Edge, version 2.0 Software (1997).
16. Gaussian 98 Software, Gaussian Inc., Carnegie Office Park, Bldg. 6, Pittsburgh, PA 15106, USA.
17. ***National Institute of Standards & Technology***, Standard Reference Database Number 69, July 2005 Release. http://webbook.nist.gov/chemistry (accessed Sep 2005).
18. S. Haq, D.A. King, ***Journal of Physical Chemistry*** 100 (1996) 16957.
19. M. Hara, H. Sasabe, W. Knoll, ***Thin Solid films*** 273 (1996) 66.
20. T. Boland, B.D. Ratner, ***Langmuir*** 10 (1994) 3845.
21. J.V. Barth, H. Brune, G. Ertl, ***Physical Review B*** 42 (1990) 9307.
22. W. Azzam, P. Cyganik, G. Witte, M. Buck, Ch. Wöll, ***Langmuir*** 19 (2003) 8262.
23. E.J. Sturrock, P.H. Borchardt, N.V. Richardson, "STM study of water and benzyl mercaptan on Au(111)" – unpublished work 2004.

Chapter 5 – Results: 2-mercaptoethanol on Au(111).

5.1 Introduction.

It is not only the interaction between the substrate and adsorbate that are important for the structure of a SAM. Also the adsorbate-adsorbate interactions play a big role in the formation of ordered SAMs [1]. Although the sulfur atoms in an aliphatic thiol themselves may adsorb in a $(\sqrt{3}x\sqrt{3})R30^0$ structure on hexagonal closed packed metal surfaces, eg Au(111), the van der Waals interactions between the alkyl chains can cause the structure of the SAM to be different [2-7]. In addition, the presence of a functional end group does not only show specific physical and chemical properties of the SAM, it can also further affect the structure of the adsorbed molecules. It is the balance between all these interactions (substrate-head, chain-chain, end-end and end-substrate) which determine the final structure of the SAM [8]. In particular, thiols containing the hydrophilic hydroxyl group, HS-$(CH)_n$-OH, are very useful as they can easily be mixed with the corresponding hydrophobic alkyl thiol, HS-$(CH)_n$-H in any ratio and hence fine-tune the hydrophilicity [9-11]

The intermolecular hydrogen bonding properties of the hydroxyl group within the pure SAM result in a different structure of the molecules compared to a pure SAM with its unhydroxylated analogue [12-15]. For example, Sprik et al. found that dodecanethiol molecules formed a clear $(\sqrt{3}x\sqrt{3})R30^0$ structure on Au(111), while the structure of 1-mercaptoundecanol was more "striped" [13].

There have been studies of 2-mercaptoethanol (2ME), one of the simplest hydroxylated thiols [16-18]. Since the hydrocarbon backbone is very short, the intermolecular interactions between the hydroxyl endgroup should be dominating [18]. Kudelski studied 2ME adsorption from solution onto surfaces of Au, Ag and Cu and found that the structure of the SAM was dependent of pH but not on neutral salts in the solution [16], and that the surrounding conditions had more effect on the SAM on Ag and Cu than on Au. Hyun and Rhee used STM to investigate the structure of 2ME adsorbed from ethanol solution on Au(111) [18]. This resulted in striped structures of $\left(nx\sqrt{3}\right)R30^0$ where n = 4, 5 and 6.

In this work we will study the structure for the SAM formed by gaseous deposition of 2ME in UHV and find out how the molecules are orientated. Apart from obtaining a LEED pattern for an ordered monolayer, the same experiments as for benzyl mercaptan were made for 2-mercapto ethanol (2ME). In contrast to BM, 2ME has a more hydrophilic and reactive tail group. Two different exposures were examined by HREELS on a Au(111) to see if also 2ME changes orientation depending on the coverage. The spectra were improved by resolution enhancement with Maximum Likelihood methods [19]. Then RAIRS were performed with a wider range of exposures to find the critical exposure when the molecules change orientation. This was performed at both room temperature and at low temperature (57 to 62K) using liquid helium as coolant. Some limited STM imaging was also performed, both at room temperature and low temperature, in order to find any ordered structure of the monolayer.

5.2 HREELS

5.2.1 Experimental details.

The substrate used here was Au(111) made by evaporating gold on to a silicon wafer. The silicon had been reconstructed to Si(111)(7x7) prior to the evaporation (see Chapter 3).

Spectra were recorded at two different exposures of 2ME, one of 225L and another of 405L, which represented a low and high coverage respectively.

5.2.2 Results and discussion.

The spectra were improved by resolution enhancement with the program "Cutting Edge" [20], a Maximum Likelihood method [19] and the results are shown in figure 5-1.

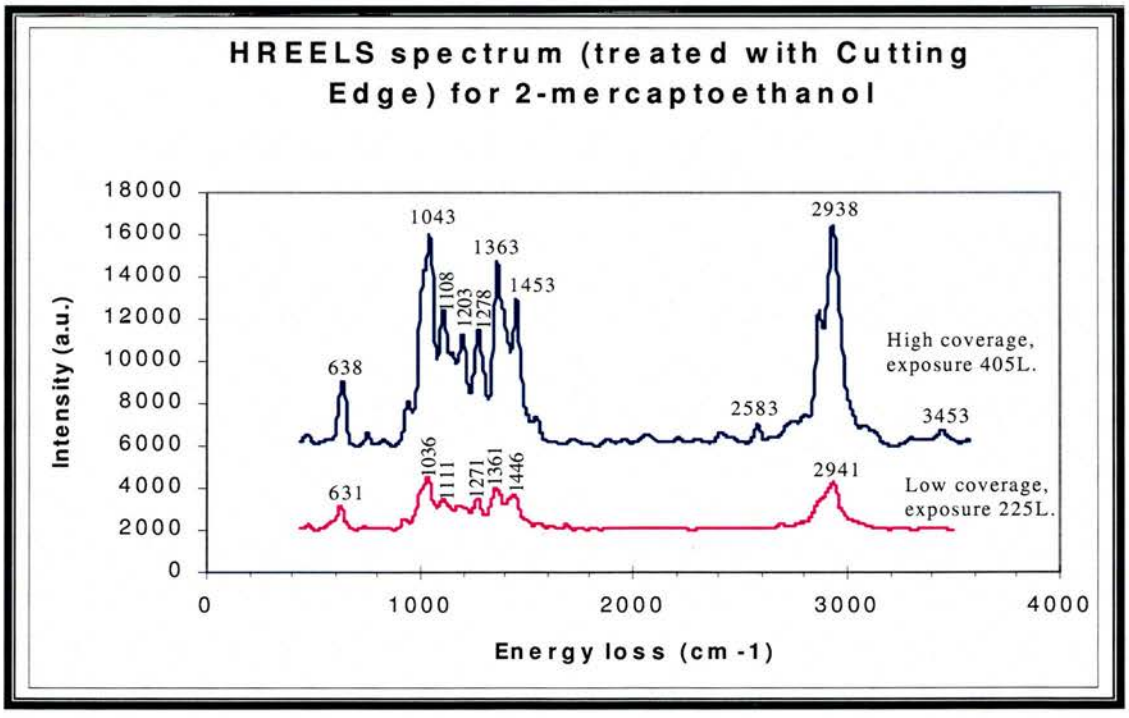

Figure 5-1: HREELS spectra for two exposures of 2-mercapto ethanol on Au(111), dosed at a pressure of $1x10^{-7}$ mbar in 50 and 90 minutes respectively, followed by resolution enhancement.

For comparison, the gas phase spectrum for 2ME [21] is shown in figure 5.2.

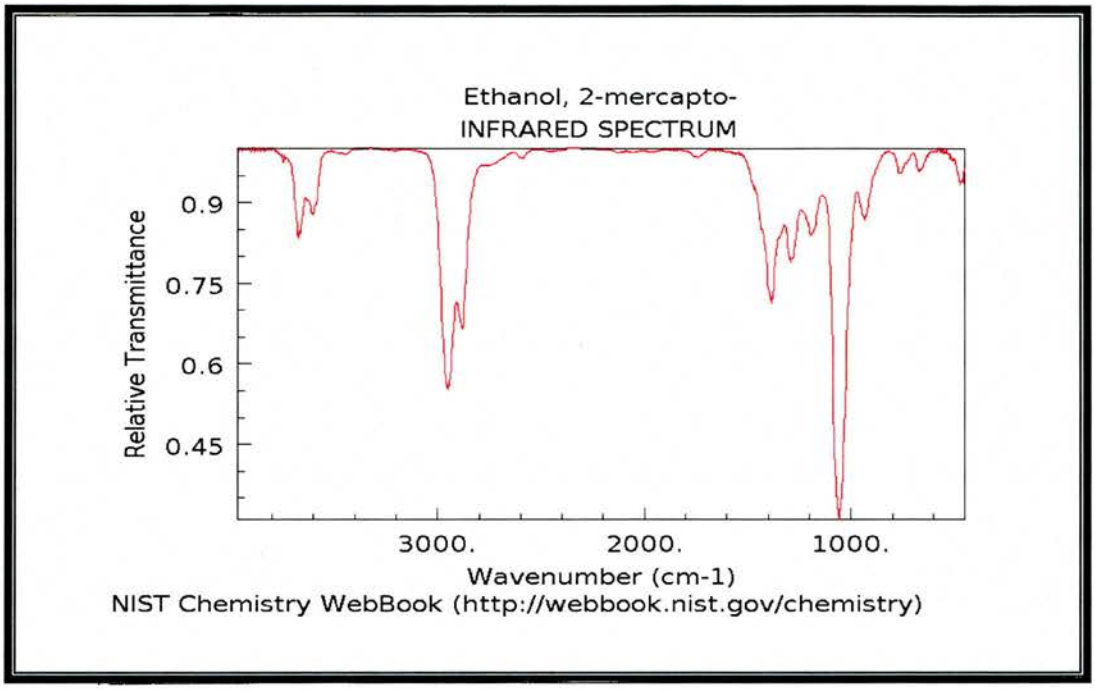

Figure 5.2. Reference gas phase spectrum for 2ME. NIST [21].

Table 5.1 lists the bands from these two spectra together with the ones from a gas phase reference [21] and the results from a calculation with the Gaussview 3.0 program [22] of which the spectrum is shown in figure 5-3.

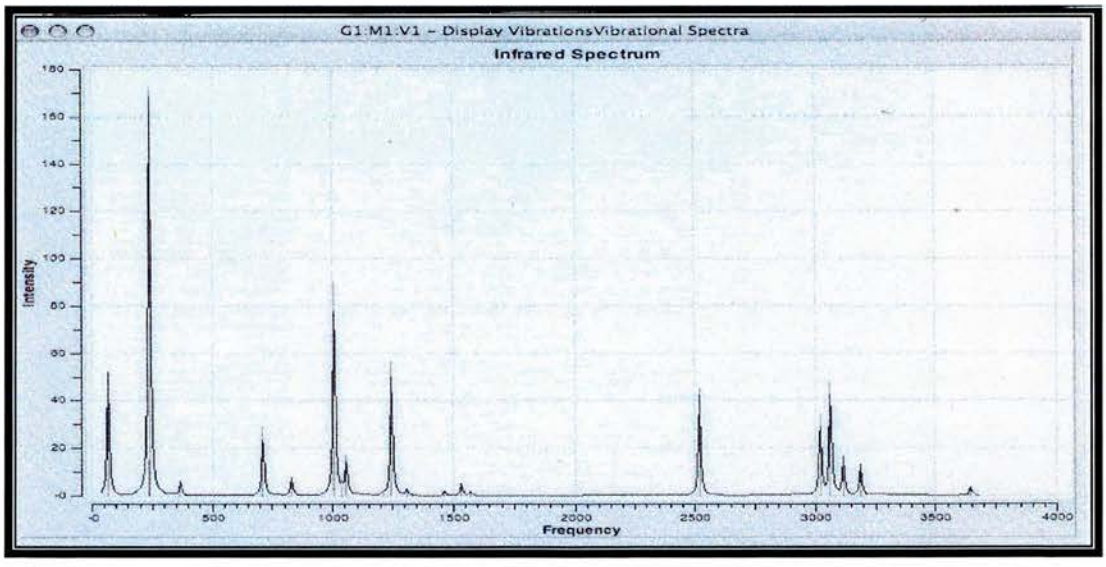

Figure 5.3. Vibrational spectrum for 2ME from DFT calculations using Gaussview 3.0 [22].

GaussView 3.0, free 2ME [22]	IR free 2ME gas [21]	Assignment	HREELS low (225L)	HREELS high (405L)
66 (52.4)		S-H out-of-plane bend		
122 (0.1)		OCCS deformation		
232 (15.0)		CCS bend		
239 (172.8)		OH out-of-plane bend		
367 (6.3)		CCO bend		
712 (28.8)	670	C-S stretch	626	637
829 (6.8)		SH in-plane bend		
830 (0.9)	754	CH_2 rock (both)		
1006 (89.8)	935	C-O stretch	931	978
1037 (3.3)		CH_2 twist adjacent O / CH_2 rock adjacent S		
1056 (16.5)	1058	C-C stretch	1036	1043
1211 (0.7)		CH_2 twist out-of-phase / little of CH_2 rock adjacent O		
1246 (56.4)	1189	COH in-plane bend		
1308 (2.8)		CH_2 wag adjacent S		
1329 (0.3)	1294	CH_2 bend (both)		
1464 (2.1)	1382	CH_2 wag adjacent O	1446	1453
1534 (5.1)		CH_2 scissors adjacent S		
1570 (1.8)		CH_2 scissors adjacent O		
2520 (44.9)	2590	S-H stretch		2588
3021 (34.1)	2878	Symm. CH_2 stretch adj. O	2890	2873
3063 (47.9)	2950	Asymm. CH_2 stretch adj. O	2941	2933
3116 (16.2)		Symm. CH_2 stretch adj. S		
3186 (13.1)		Asymm. CH_2 stretch adj. S		
		O-H stretch (H-bonding)	3405	3458
3646 (3.4)	3670	O-H stretch (free)		

Table 5-1. Vibrational frequencies from the HREELS for two exposures of 2ME, the calculated ones for the free molecule from Gaussean 3.0 [22] and from the reference spectrum of gaseous 2ME (NIST [21]) with assignments. The intensities of the GaussView frequencies are shown in brackets.

There are increases in intensity for the high coverage spectrum compared to the low coverage one but no major changes in relative band intensity. This immediately suggests that there are no substantial changes of orientation or conformation between these two coverage regimes. In the low coverage spectrum, there is no peak corresponding to the S-H stretch at around 2500-2600 cm^{-1}. This is because this bond breaks on adsorption and the covalent bond Au-S is formed [23]. On the other hand a weak feature appears at 2583cm^{-1} for the higher coverage, which might be explained by the formation

of a bilayer, although it might also be assigned to a combination band. The band for the Au-S stretch should appear at around 180-190 cm^{-1}, but this could not be resolved from the nearby elastic peak. Another weak peak at 3453 cm^{-1} appears for the high coverage, which can be assigned for the O-H stretch. In a gas phase spectrum of 2-mercaptoethanol [21], shown in figure 5-2, there is a peak at 3670 cm^{-1}, which is assigned for the stretch in the free O-H group. The shift to a lower wave number is most likely caused by hydrogen bonding between the O-H groups in the adjacent molecules in the adsorbed monolayer. This is obvious when comparing the spectra for the two regimes from the HREELS run in figure 5-1 and the reference gas phase in figure 5-2.

5.3 Reflection Absorption Infrared Spectroscopy

5.3.1 Adsorption of 2ME on Au(111) at room temperature.

As for the benzyl mercaptan, spectra for a number of exposures were more easily obtained for RAIRS than for HREELS, as the thiol could be dosed onto the gold surface directly in the same UHV chamber where the analyses were performed. So here the intensity of the bands and hence any molecular re-orientation could be followed in more detail

Figure 5-4 shows a series of exposure of 2ME on Au(111) at room temperature.

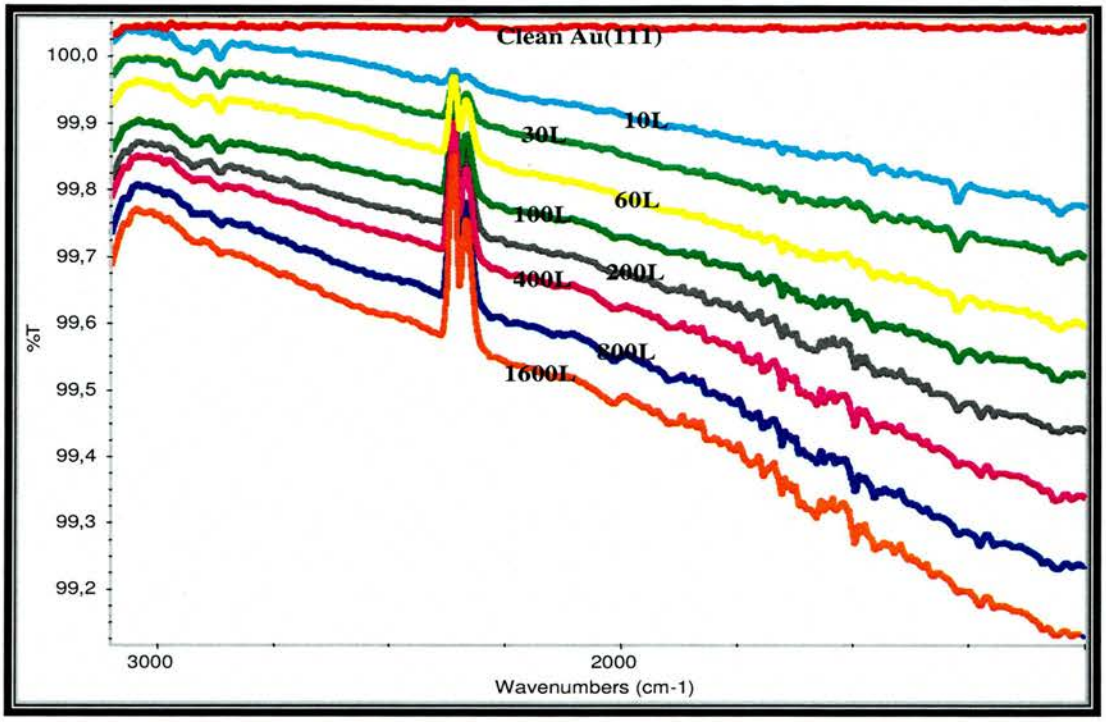

Figure 5-4: RAIRS spectra in the range 1000-3100 cm^{-1} for 2ME adsorbed on Au(111) at increasing exposure in Langmuirs.

There are some bands that vary with the exposure. These are summarized in table 5-2, together with their possible assignment and the theoretical and calculated frequencies from table 5-2. All the wavenumber for any band varies by not more than 3 cm^{-1} throughout the range of exposure.

GaussView 3.0, free 2ME [22]	IR free 2ME gas [21]	Assignment	RAIRS
1037 (3.3)		CH_2 twist adjacent O / CH_2 rock adjacent S	1057
1056 (16.5)	1058	C-C stretch	1195
1246 (56.4)	1189	COH in-plane bend	1224
1329 (0.3)	1294	CH_2 bend (both)	1273
1464 (2.1)	1382	CH_2 wag adjacent O	1495
3021 (34.1)	2878	Symm. CH_2 stretch adj. O	2867
3063 (47.9)	2950	Asymm. CH_2 stretch adj. O	2926

Table 5-2. Frequencies and possible assignments for 2ME adsorbed on Au(111) together with the reference [21] and calculated [22] wavenumbers.

The next two figures, 5-5 and 5-6, show two enlargements of the regions 3100-2700 cm^{-1} and 1550-1000 cm^{-1} respectively from the spectra in figure 5-3. There it is more easy to see how the some specific bands vary in intensity versus the exposure of 2ME.

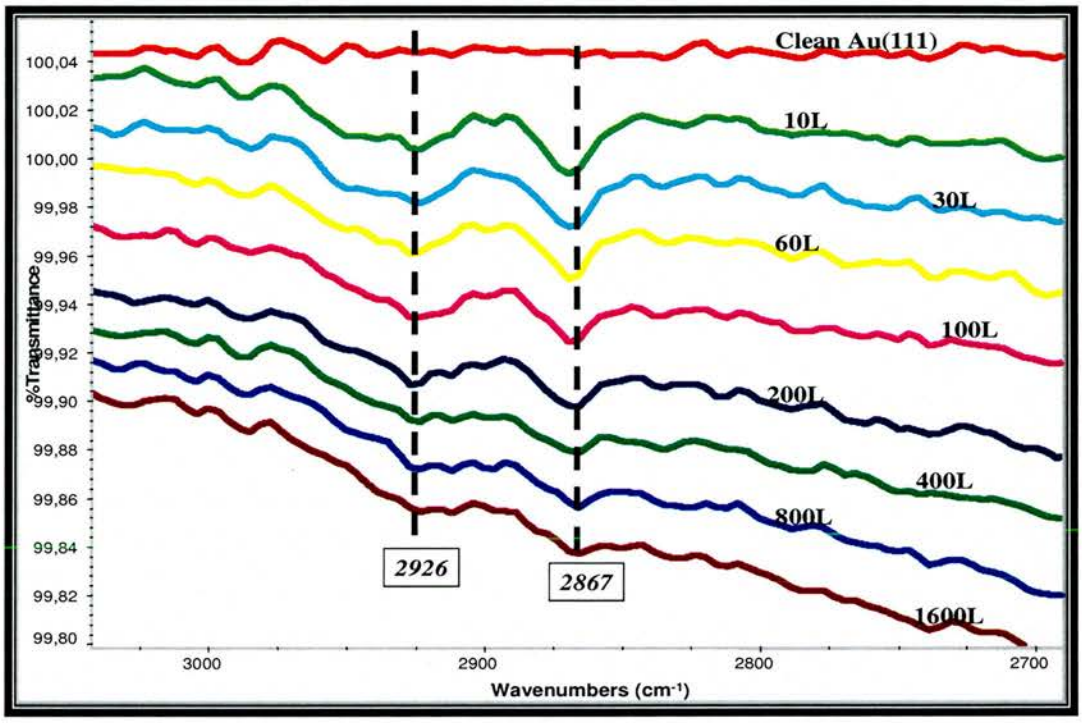

Figure 5-5: RAIRS spectra of 2ME adsorbed on Au(111) at increasing exposure in Langmuirs for the region 2700-3000 cm^{-1} including interesting bands frequencies in boxes.

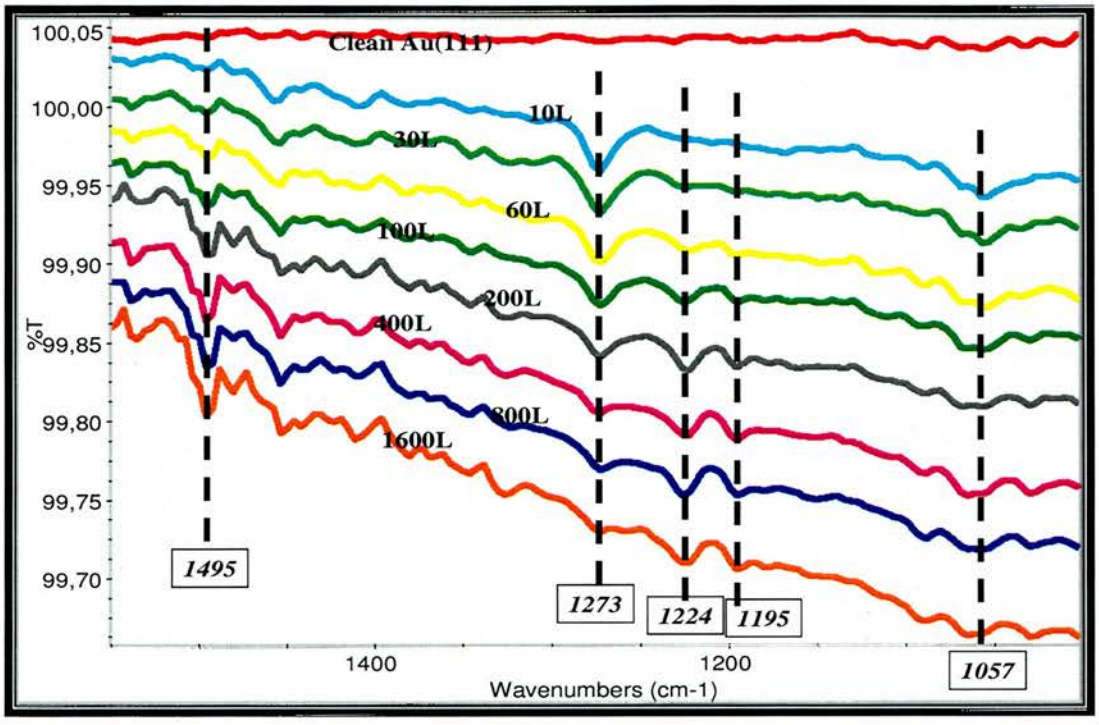

Figure 5-6: RAIRS spectra of 2ME adsorbed on Au(111) at increasing exposure in Langmuirs for the region 1000-1550 cm^{-1} including interesting bands frequencies in boxes.

These bands show an interesting profile along with the increased exposure. First, the intensity of the bands at 2868 cm^{-1} and 2925 cm^{-1}, which are assigned for the symmetric and asymmetric C-H stretches, are strongest for the lower exposures, around 10-30 L, then drops to a lower level at 60L and remain there up to about 200L. Finally they slowly decrease further for higher exposures, up to 800L where they level out. This is shown in figure 5-7.

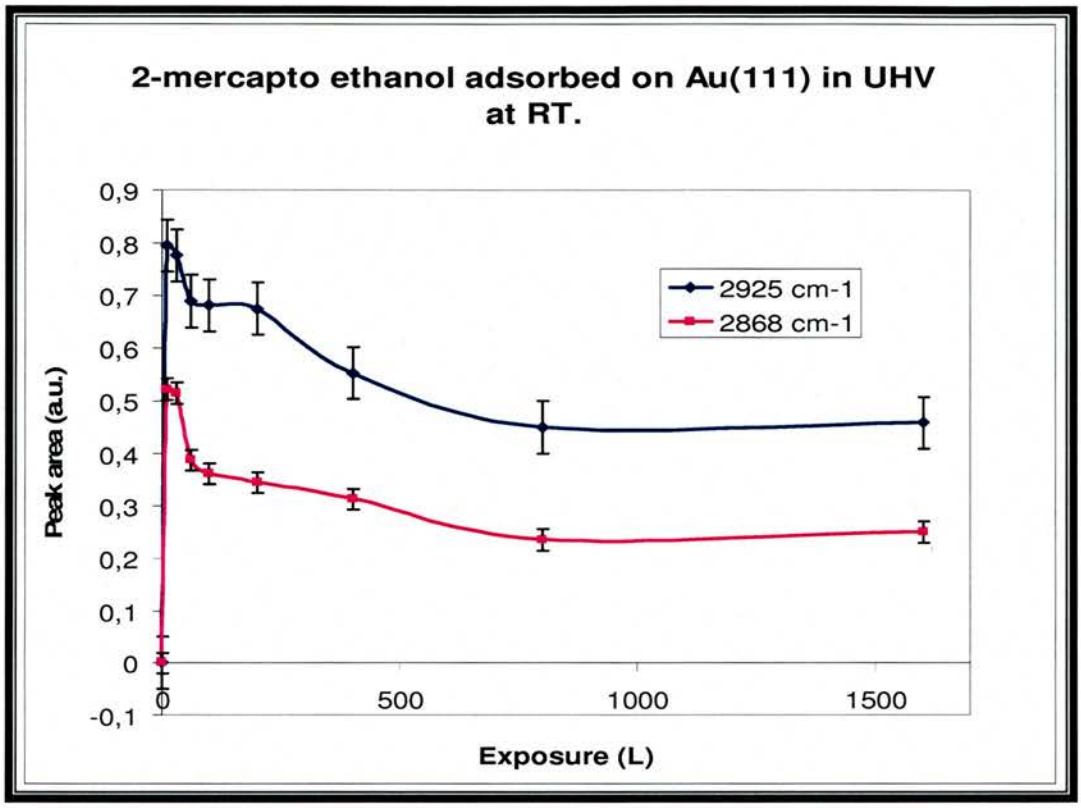

Figure 5-7: The peak areas for the aliphatic C-H stretches vs exposure of 2ME.

In fact it seems that the 2ME molecule has three different orientations when going from a very low coverage to a full monolayer. The possible reason for this is that the molecules are lying flat (parallel to the surface) at low coverage and then rise to a vertical orientation when the surface becomes more covered. But here it seems that the molecules have an intermediate orientation between the low and high coverage. A suggested turn over of the molecules in the monolayer is illustrated in figure 5-8.

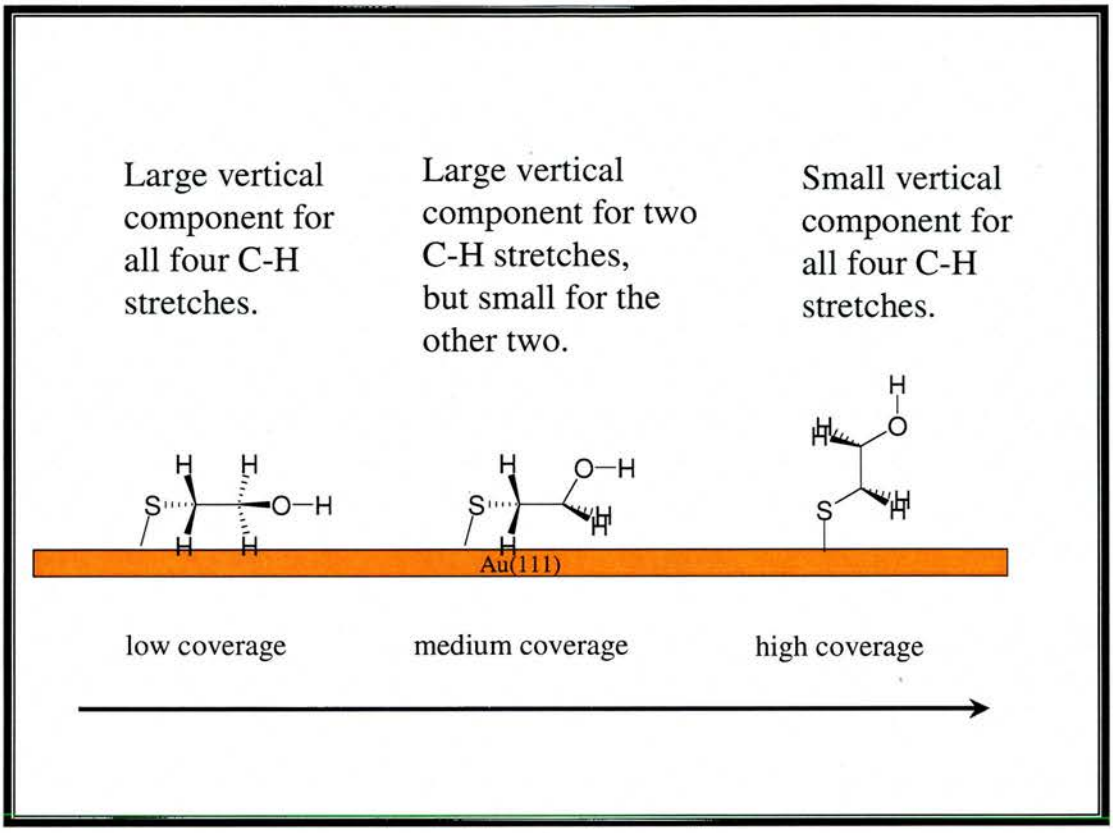

Figure 5-8: Possible orientations of the 2ME molecule at different coverages of the SAM on the Au(111) surface.

There are also other peaks in these spectra that support that the 2ME molecule rises with increasing coverage. Figure 5-9 shows three bands where the intensity (peak area) rise with the increased coverage (exposure). Possible assignments for these are C-C stretch for 1195 cm^{-1}, COH in-plane bend for 1224 cm^{-1} and CH_2 wag for 1495 cm^{-1}.

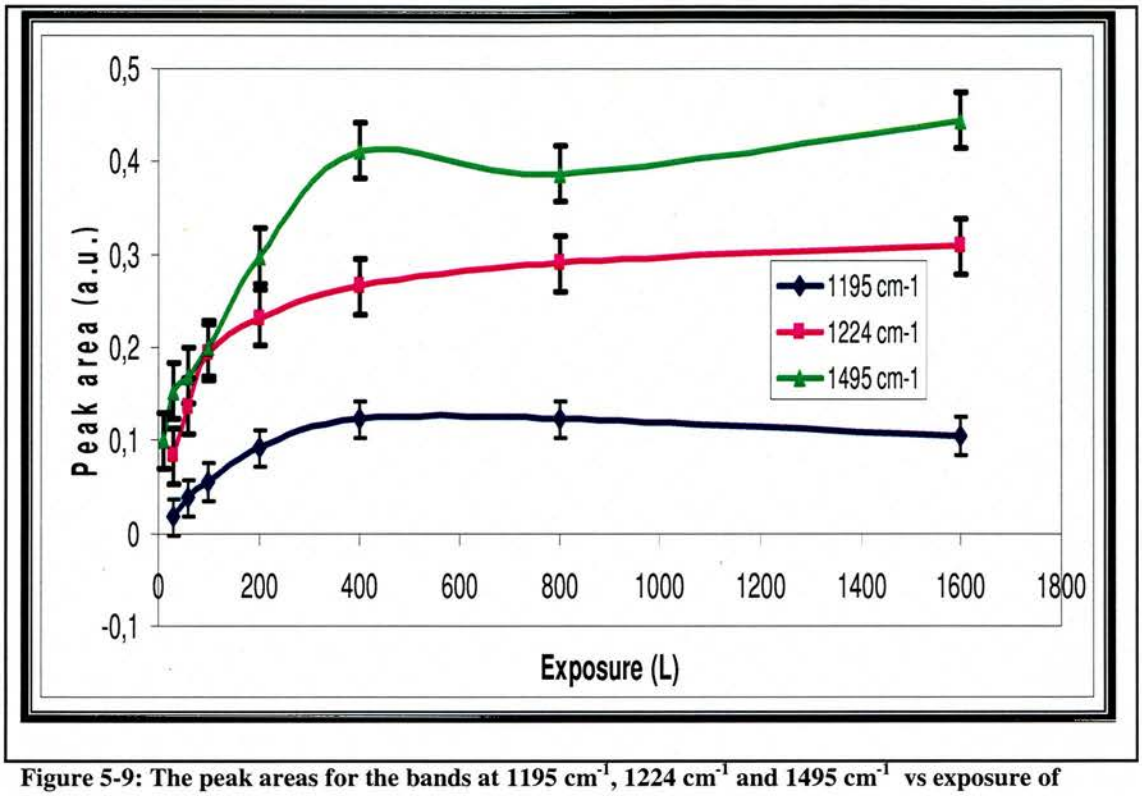

Figure 5-9: The peak areas for the bands at 1195 cm^{-1}, 1224 cm^{-1} and 1495 cm^{-1} vs exposure of 2ME.

First, the 1195 cm^{-1} band rises with exposure because that the C-C stretch becomes more vertical as the molecule turns to a more standing up orientation with the increased coverage. The curve then levels out when the C-C bond in the molecules are perpendicular to the surface. Similarly, the COH in-plane bend at 1224 cm^{-1} is more parallel to the surface at low coverage but gradually obtains a more vertical orientation as the coverage increases. Finally, the band at 1495 cm^{-1} increases rapidly at low coverage with increasing exposure and then levels out. This is because the CH_2 wag becomes more perpendicular to the surface for the vertical orientation at higher coverage. The slight decrease for the higher exposure may depend on weak contribution from the unseparated bands for CH_2 scissors (which becomes more parallel to the surface when the molecules stand up) at slightly higher wavenumbers, although it is within the error bars.

On the other hand, two other peaks instead decrease with increasing exposure and coverage, after a rapid jump to a maximum at very low coverage, as shown in figure 5-10. The band at 1057 cm^{-1} is assigned to both CH_2 twist (adjacent to S) and CH_2 rock (adjacent to O) according to the DFT calculations [22]. It is the rocking that contribute most to the band and are more perpendicular at low coverage when the molecules have the flat-lying orientation. Similarly the CH_2 bend at 1273 cm^{-1} contribute stronger when the mode is more perpendicular to the surface when the C-C backbone are orientated parallel to the surface at low coverage.

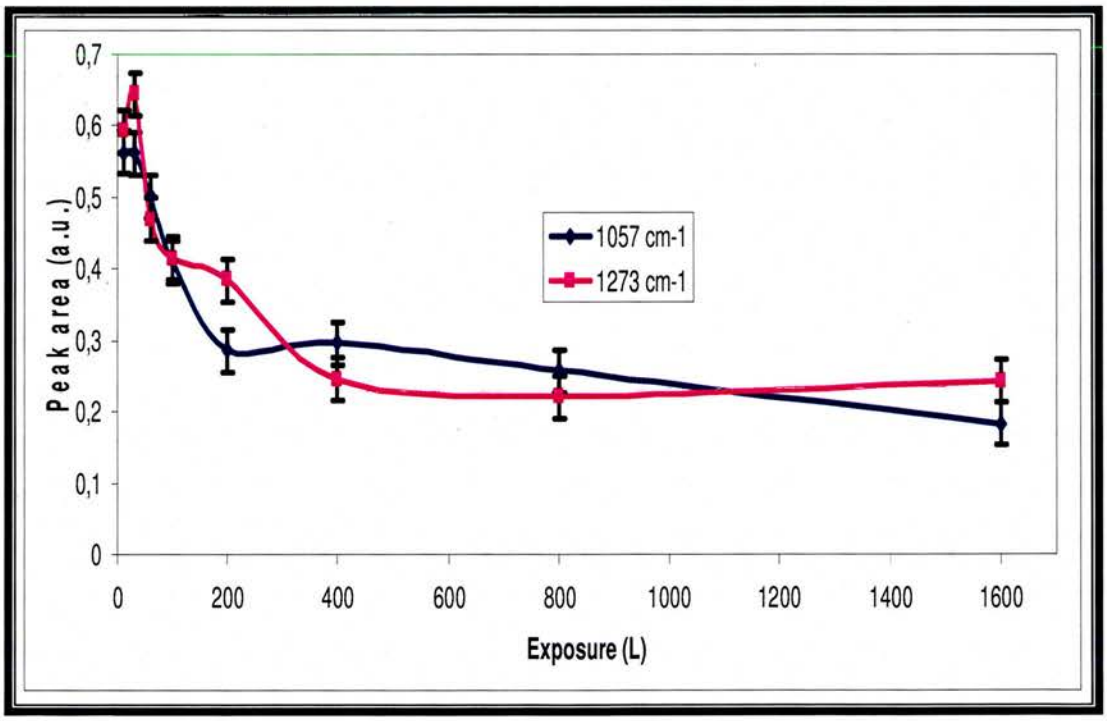

Figure 5-10: The peak areas for the vibrations around 1053 cm^{-1} and 1273 cm^{-1} (both for C-H bend) vs exposure of 2ME.

Finally, a band for the hydrogen bonding around 3450 cm^{-1} could be possible to see, especially for the higher coverage spectra. However this was not observed

because it could not be resolved from the very large band around 3000-3500 cm^{-1}, which arises from the growing ice film on the detector. Also the free O-H stretch at around 3600 cm^{-1} did not appear because it is also close to this large "interfering band".

5.3.2 Adsorption of 2ME on Au(111) at low temperature.

As for BM, the measurement of 2ME, at low temperature with liquid helium cooling, was also performed in these three different ways, however only one of them was useful for studying the onset of a multilayer of 2ME.
First, the substrate was cooled using liquid helium to below 70K. Then it was warmed up to room temperature again using resistive heating. After a few minutes it was cooled down again. Once the temperature has stabilized, stepwise dosing of 2ME was performed to follow the growth up to the saturated monolayer and then see how a multilayer started to form.
Figure 5-11 shows the results of stepwise addition of 2ME on to Au(111) after cooling to around 60K. At this temperature, the molecules seem to have a higher sticking probability than at room temperature. The bands found in the room temperature spectra appear already at the lower coverages, and at an exposure of 10L and over, additional bands start to appear. All bands are listed in table 5-3 with possible assignments and frequencies from the reference and calculated spectra. This is probably due to an onset of a multilayer as the band at around 2540 cm^{-1} appears because those molecules do not lose their hydrogen atom in the SH-group. Interestingly, deprotonation in the first monolayer does occur even at this low temperature. Also, the multilayer molecules do not seem to have a preferential orientation, unlike those in the first

layer, as the bands now seems to increase linearly with further exposure, which is shown in fugure 5-12.

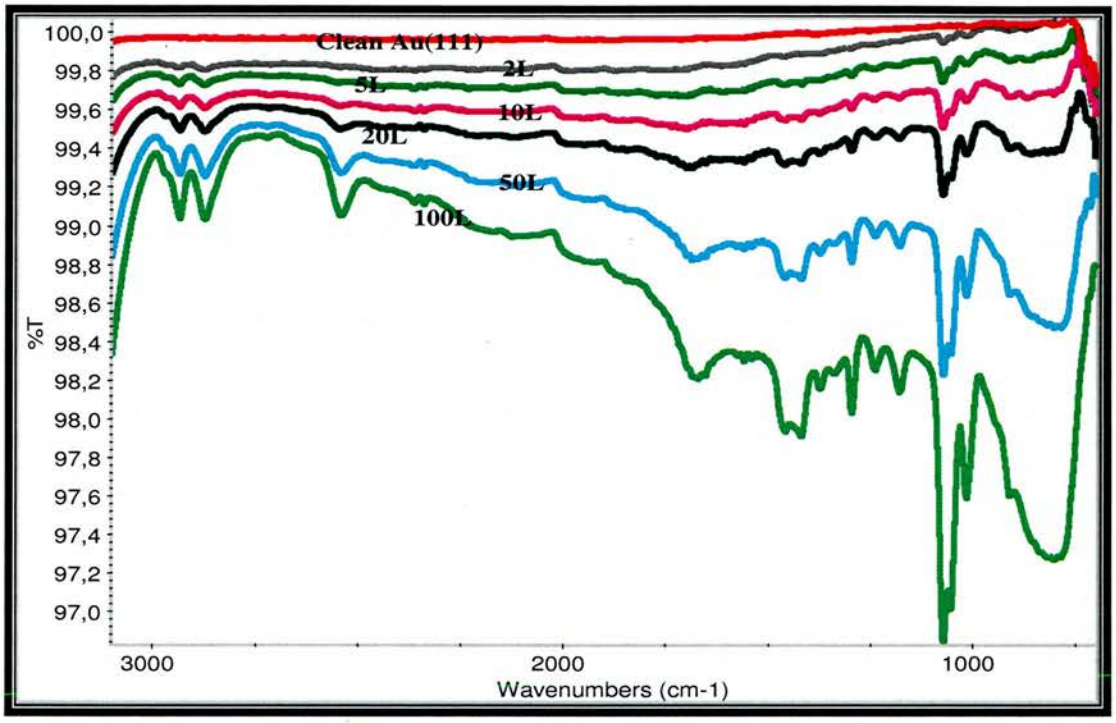

Figure 5-11. RAIRS spectra for the increase exposure of 2ME on Au(111) at reduced temperature (57K to 59K).

GaussView 3.0, free 2ME [22]	IR free 2ME gas [21]	Assignment	RAIRS (57-59K)
1006 (89.8)	935	C-O stretch	1014
1056 (16.5)	1058	C-C stretch	1069
1211 (0.7)		CH_2 twist out-of-phase / little of CH_2 rock adjacent O	1180
1246 (56.4)	1189	COH in-plane bend	1239
1308 (2.8)		CH_2 wag adjacent S	1296
1329 (0.3)	1294	CH_2 bend (both)	1373
1464 (2.1)	1382	CH_2 wag adjacent O	1420, 1451
2520 (44.9)	2590	S-H stretch	2545
3021 (34.1)	2878	Symm. CH_2 stretch adj. O	2873
3063 (47.9)	2950	Asymm. CH_2 stretch adj. O	2935

Table 5-2. Frequencies and possible assignments for 2ME adsorbed on Au(111) at low temperature (57-59K) together with the reference [21] and calculated [22] wavenumbers.

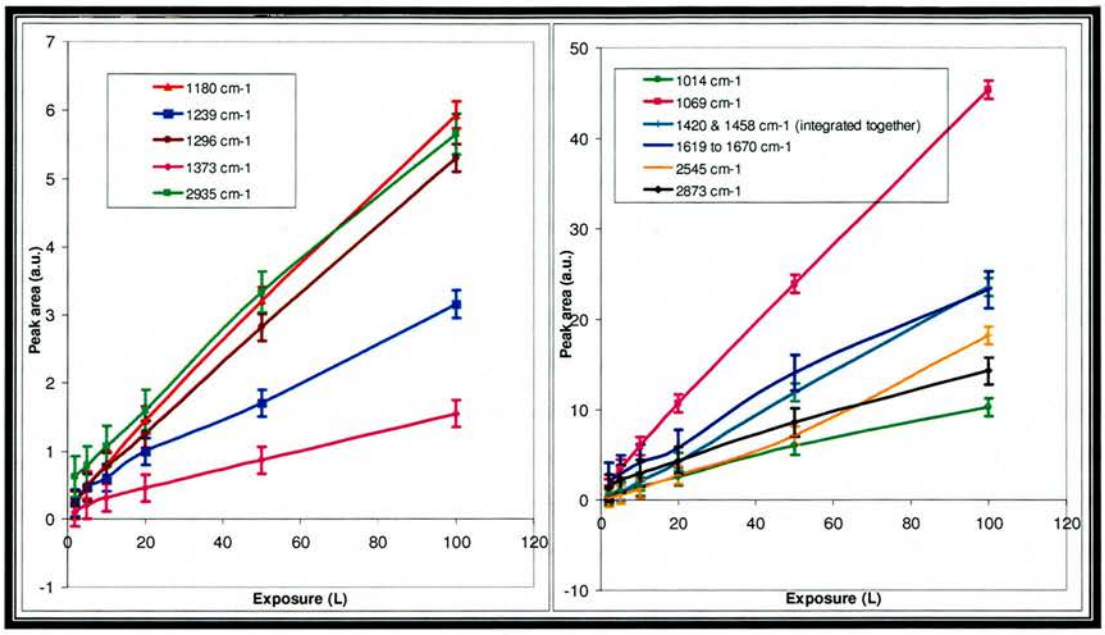

Figure 5-12. Peak areas vs exposure for bands found in RAIRS spectra for 2ME adsorbed on Au(111) at reduced temperature (57K to 59K).

This suggests that the multilayer just builds up quantitatively and the 2ME molecules are randomly ordered as they would be in the gas phase. Also, when comparing the spectra in figure 5-11 with the gas phase spectrum from NIST [21] there are many similarities.

5.4 Conclusions

The outcome of HREELS did not show coverage dependence for the structure of 2ME on Au(111) between the two different coverages performed. There was only an increase in intensity of all the bands for the higher coverage. This is probably because both exposures were within the same coverage dependent structure. However there were indications of hydrogen bonding between the OH-groups of the molecules.

On the other hand, the results from RAIRS showed an obvious coverage dependency of the orientation of the molecules. As in the case for BM, also the

2ME molecules seems to lie parallel to the surface at lower coverages and rise to a more standing up orientation at higher coverage. There also seemed to be an intermediate orientation at mid coverage with a suggested orientation of C-C backbone parallel to the surface and O-H more perpendicular.In particular the C-H stretches showed that, and most of the other band supported it.

5.5 References

1. G.E. Poirier, ***Chemical Review*** 97 (1997) 1117.
2. F. Balzer, R. Gerlach, G. Polanski, H.G, Rubahn, ***Chemical Physics Letters*** 274 (1997) 145.
3. N. Camillone, C.E. Chidsey G.-Y. Liu, G. Scoles, ***Journal of Chemical Physics*** 98 (1993) 3503.
4. P. Fenter, A. Eisenberger, K.S. Liang, ***Physical Review Letters*** 70 (1993) 2447.
5. J.-P. Bucher, L. Santensson, K. Kern, ***Applied Physics A*** 59 (1994) 135.
6. G.E. Poirier, M.J. Tarlov, ***Langmuir*** 10 (1994) 2853.
7. E. Delamarche et al., ***Langmuir*** 10 (1994) 2869.
8. T.Y.B. Leung, M. C. Gerstenberg, D.J. Lavrich, G. Scoles, ***Langmuir*** 16 (2000) 549.
9. I. Engquist, I. Lundström, B. Liedberg, A.N. Parikh, D.L. Allara, ***Journal of Chemical Physics*** 106 (1997) 3038.
10. C.D Bain, H.A. Biebuyck, G.M. Whitesides, ***Langmuir*** 5 (1989) 723.

11. D.J Olbris, A. Ulman, Y. Shnidman, ***Journal of Physical Chemistry*** 102 (1995) 6865.

12. G.E Poirier, E.D Pylant, J.M. White, ***Journal of Chemical Physics*** 104 (1996) 7325,

13. M. Sprik, E. Delamarche, B. Michel, U. Röthlisberger, M.L Klein, H. Wolf, H. Ringsdorf, Langmuir 10 (1994) 4116.

14. G.E. Poirier, E.D. Pylant, J.M. White, ***Journal of Chemical Physics*** 105 (1996) 2089.

15. L.H. Dubois, B.R. Zegarski, R.G. Nuzzo, ***Journal of Chemical Physics*** 98 (1993) 678.

16. A. Kudelski, ***Langmuir*** 19 (2003) 3805.

17. L. Supriya, R.O. Claus, ***Chemistry of Materials*** 17 (2005) 4325.

18. M. Hyun, C.K. Rhee, ***Bulletin of Korean Chemical Society*** 22(2) (2002) 213.

19. B.G. Frederick, G.L. Nyberg and N.V. Richardson, ***Journal of Electronic Spectroscopy and Related Phenomena*** 64/65 (1993) 825.

20. Cutting Edge, version 2.0 Software (1997).

21. ***National Institute of Standards & Technology***, Standard Reference Database Number 69, July 2005 Release. http://webbook.nist.gov/chemistry (accessed Sep 2005).

22. Gaussian, Inc., 340 Quinnipiac St Bldg 40, Wallingford, CT 06492 USA, http://www.gaussian.com (accessed Sep 2005).

23. A. Ulman, ***Chemical Reviews*** 96 (1996) 1533.

Chapter 6: Water adsorption on Au(111) and thiols.

6.1 Introduction.

Water, the most abundant liquid on earth and well known to everyone, plays many important roles in physics, chemistry and biology [1]. Despite the small and simple molecule, its properties are very extensive and complex [2]. As many reactions and other processes take place on interfaces, it is of great importance to study how the water molecules interact with surfaces [3], including biomaterials [4].

When a water molecules adsorbs, many things can happen depending on the nature of the surface [3]. It may just bind to the surface unaffected, dissociate, donate or accept a proton as an acid or a base, adsorb as individual molecules or hydrogen bond to other water molecules and form clusters.

The adsorption of water on crystal metal surfaces has been well studied on a wide range of metals, especially face centred cubic ones cut at the (111) plane, for example Pd(111) [5-6], Cu(111) [7], Ag(111) [8], Pt(111) [5,9-12] and Au(111) [13-23].

An STM study of water adsorbed on Pd(111) by Mitsui et al. has been performed at 40K [6]. They found that the water first adsorbs as single molecules and then upon collisions form dimers, trimers and so on up to hexamers which was found to be most stable. With higher coverage, these hexamers then form a $(\sqrt{3}x\sqrt{3})R30^{o}$ honeycomb structure.

Morgenstern et al. used an STM tip to form ice clusters from water monomers adsorbed on Cu(111) below 20K [7]. They showed that diffusion, formation, and structural changes of clusters are induced by electrons coupling to vibrational modes of the molecule, and this manipulation can induce stable two- and three-dimensional clusters which deviates from the favourable on top positions. In contrast, at 70K hexamers of water molecules adsorb on Ag(111) in on-top positions [8] at half a bilayer.

On Pt(111) the structure of the adsorbed water molecule is coverage dependent at 137K. For an incomplete monolayer the molecules form $(\sqrt{37}x\sqrt{37})R25.3^{o}$ islands and towards saturation the monolayer becomes more compressed to a $(\sqrt{39}x\sqrt{39})R16.1^{o}$ structure [9]. The latter then continue to grow as multilayers up to about 5 bilayers, and further growth results in a hexagonal R30º closed packed structure as in bulk ice [10] At 90K in the top half of the outermost bilayer on Pt(111), the molecules are undetected by LEED because the ice surface is terminated by strongly vibrating molecules [11]. At even lower temperatures, monomers (below 40K), dimers and trimers (above 40K) of water molecules are stable on Pt(111) [12].

Water adsorption on Au(111) has been investigated extensively. Ikemiya used STM to study water adsorption on Au(111) at 100K and found that the molecules first form an amorphous and planar film on the metal surface without reconstructing it [13]. Then water clusters grow on top of that film instead of directly on the Au(111) surface. The reason for this is probably the greater mobility of water on the bare surface and that the Au-H_2O interaction is weak. This was further verified by Kay et al who used TPD to study the hydrogen bonding between the molecules in the adsorbate at 85K [14]. They found that

the water molecules bind more strongly to each other than to the gold atoms and cluster into three dimensional units after adsorption due to the ability for each molecule to H-bond to four neighbours.

In general it has been found that the properties of ice films are substrate dependent and the wetting properties of water on Au(111) is much weaker than other crystal metal surfaces as for example Pt(111) [15-16].

Also the nucleation site for adsorption of atoms and molecules on Au(111) are of great importance. In particular the herringbone turns of the Au(111)-$\left(22x\sqrt{3}\right)$ surface reconstruction [20] have been found to induce nucleation of for example Ni atoms [21] and 4-mercaptopyridine [22]. For the latter, the growing SAM also induced the formation of a periodic herringbone structure of Au(111).

Engquist et.al. studied the ice structure of D_2O adsorbed on top of a mixture of SAMs containing one long chain alkane thiol (C_{15}) and its hydrophilic analogue with OH as head group using TPD and RAIRS. They found that the adsorbed ice is amorphous below 120K at all mixtures. At higher temperatures near desorption the ice becomes polycrystalline for the most hydrophobic SAMs only [24]

Here we will study how the water molecules adsorb on both bare Au(111) and after applying SAMs of the two thiols, BM and 2ME, as described in the previous two chapters. Depositions of water (as D_2O) and the thiols, and analyses by RAIRS and STM, will take place in UHV environment as before. In addition, the macroscopic wetting properties of mixed SAMs applied from solution in atmosphere will also be studied with contact angle measurements.

6.2 Contact angle measurements for self assembled monolayers containing mixtures of 2-mercaptoethanol and benzylmercaptan.

To assist in the interpretation of UHV nanoscale studies of water on gold supported thiols, macroscopic investigations of the contact angle of water on such surfaces was also carried out to determine the relative hydrophilicity of these surfaces. For mixtures of BM and 2ME, covering a wide range of molar ratios, contact angles were measured following adsorption from solution onto a gold surface previously evaporated on a silicon wafer. 7-8 drops of water (deionised) were applied on to each surface. Figure 6-1 shows the variation of contact angles against molar composition (of the solution).

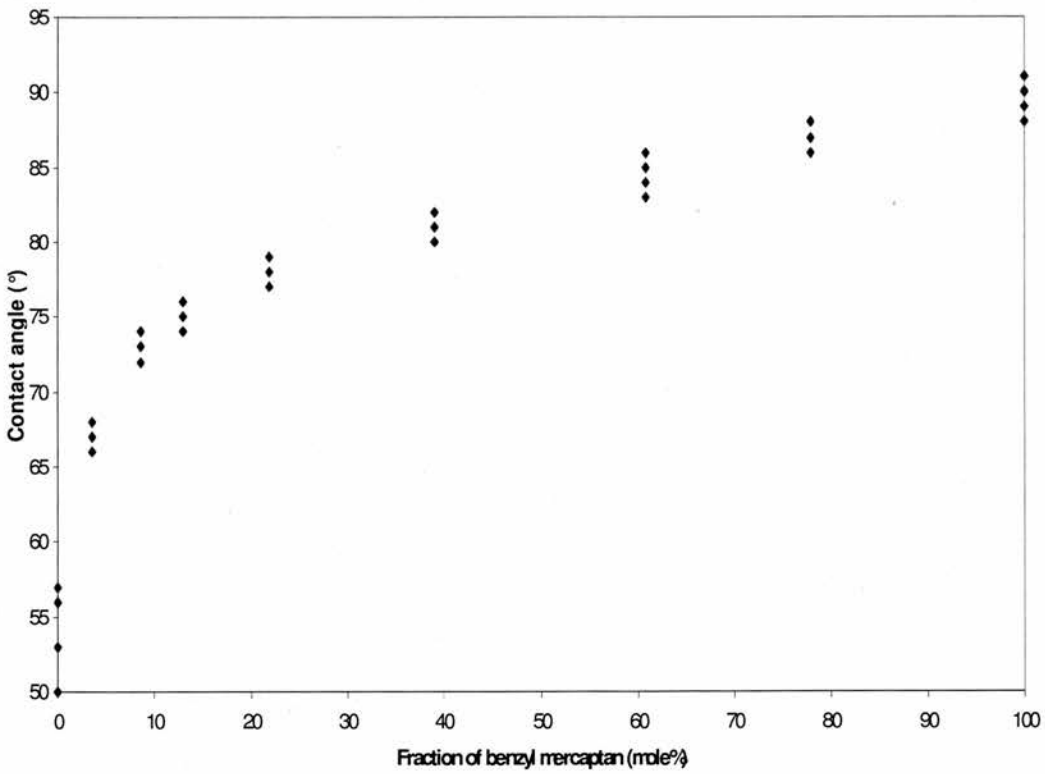

Figure 6-1. Contact angles versus the molar ratio between 2ME and BM (expressed in % of BM) in solution.

For the most hydrophilic case the angle is around 50º. Then it rises steeply the first 15 mol % of BM in solution to about 75º followed by a more gentle (and roughly linear) rise to around 90º for 100% BM. There could be two reasons for this profile. The most probable is that the BM molecules have a higher sticking probability in the solution and hence adsorb more quickly than the 2ME molecules. It may also depend on that the BM molecules take up more space and reach farther out from the surface and thus "hide" the shorter 2ME molecules.

In comparison, Engquist et al. obtained a nearly linear profile of the contact angle versus molar ratio for mixted SAMs of $HS(CH_2)_{15}OH$ and $HS(CH_2)_{14}CH_3$ along the whole range of hydrophilicity [25]. This is probably due to the fact that both types of molecules are very similar in length and shape.

6.3 General experimental information of the adsorption of water onto surfaces.

First water was adsorbed directly on a clean surface of Au(111). This was performed to get some idea of how the water molecules adsorb, how ordered they are and to compare this with further experiments when adsorbed as an overlayer on an existing adsorbed layer of thiol or other species. Since water exists only in gaseous form at room temperature in UHV, the substrate needs to be cooled. The desorption temperature of water in UHV is around 140K. Both for STM and RAIRS studies cooling was effected using liquid He cooling. This allowed stable imaging conditions for STM but there was some

slight day to day instability of final temperature in the RAIRS experiments but the sample temperature was well below the desorption temperature.

Also, while "normal" water (H_2O) was used for STM studies, the deuterated analogue, D_2O, was used in the RAIRS experiments. In the latter "normal" water interfered with the results in two ways. First, since the IR beam path is not restricted to UHV regions traces of water vapour in the path interfere with the spectra, although this could be minimized by purging the system with nitrogen gas. Secondly, as the detector is cooled with liquid nitrogen, ice builds up on it, which grows larger by time, and gives a large and broad band around 3000-3400 cm^{-1} which easily could "drown" any desired peaks in this region. It should also give rise to a peak around 1600 cm^{-1} however this was not observed here. Using D_2O instead, the bands are shifted by a factor of $\frac{1}{\sqrt{2}}$ to lower frequencies and appear at a cleaner part of the spectrum.

The interesting bands discussed here are the free O-D stretch around 2700 cm^{-1} and the hydrogen bonded O-D stretch around 2400-2500 cm^{-1}. The latter in particular is useful in trying to get an idea of the structure of the ice layer, whether it is amorphous or more ordered (polycrystalline). Several authors have studied the phases of ice layer on Au(111) and other substrates [24-28]. The large hydrogen bonded O-D stretch band is actually a mixture of more than one peak, in particular if there are several phases of the ice. More ordered ice has this band at lower wave number, around 2400 cm^{-1} while the amorphous ice gives rise to a band at just over 2500 cm^{-1} [28]

Here we could not resolve the individual bands, nor the separate frequencies. Although there were some shoulder peaks between 2300 and 2400 cm^{-1} in some spectra, these seems to be assigned for the CO_2 impurities in the

path for the IR beam in the spectrometer. Instead, the frequency for the maximum intensity is used here to roughly tell if the ice is mostly amorphous or ordered.

Finally, the third band assigned for D-O-D bending mode (around 1200 cm^{-1}) will not be discussed in detail as it only increased linearly with exposure for all experiments and the frequency did not change much (also hard to find due to low signal to noise ratio).

6.4 FTIR studies of D_2O ice film growth directly on Au(111).

6.4.1 Experimental details:

The cleanliness of the surface was first checked with LEED after it had been cleaned by Ar^+ sputtering and annealing cycles.

After the substrate was cooled for the first time, it was annealed at room temperature and held there for a few minutes and then cooled down again. This was to remove any possible traces of water that could have adsorbed onto the surface from the chamber in the slow initial cool down. The first cool down took just over an hour while the second one around 30 minutes to become stabile. Some spectra were recorded of the clean Au(111) after the temperature had stabilised, which in this case was around 43-48K. These were sequentially reprocessed with the previous one as background until a good baseline was obtained with only weak peaks from the growing detector ice and small traces of water and CO_2 that cannot be avoided completely due to slight fluctuations in the amount of these in the beam path. A layer of D_2O was then built up

gradually by step-wise dosing and collecting a spectrum after each addition. A spectrum of the clean Au(111) surface was used as background. The exposure in Langmuirs (L) was used as a measure of the amount of D_2O adsorbed on the surface.

6.4.2 Results and discussion:

Figure 6-2 show the spectra for ten different exposures.

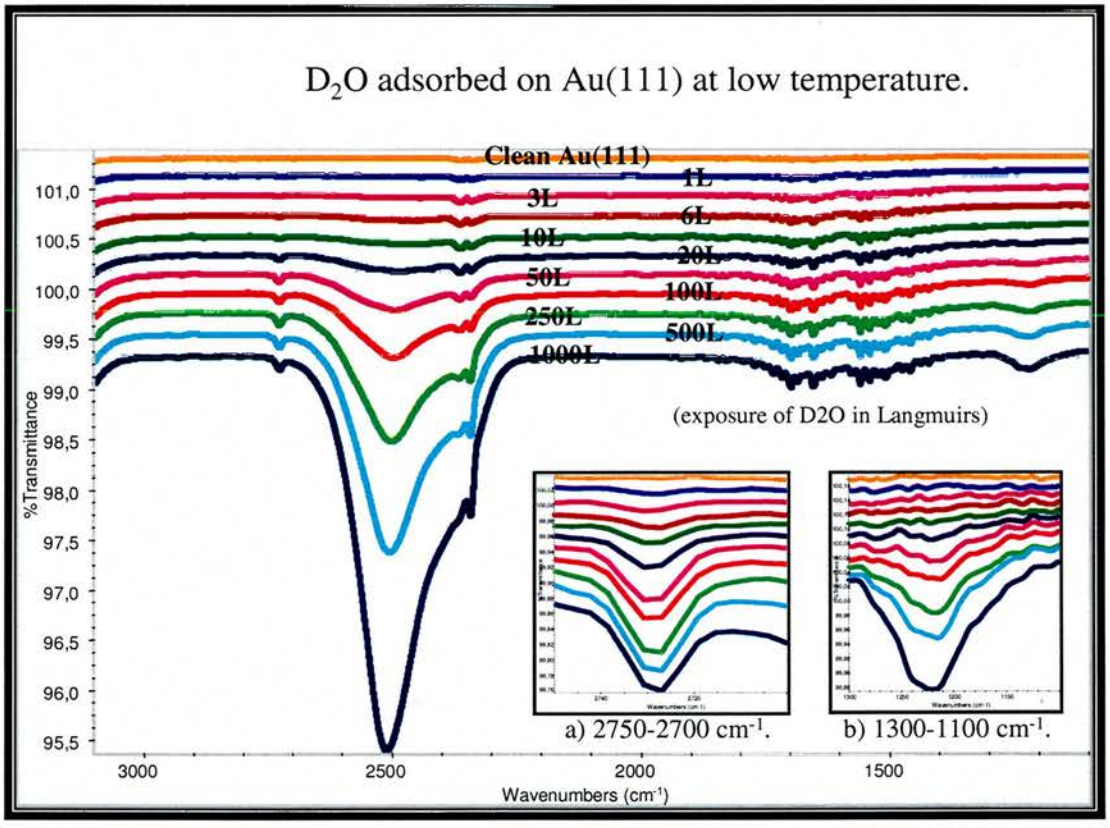

Figure 6-2. RAIRS spectra for increasing exposure of D_2O at low temperature (43-48K) directly on Au(111).

Three peaks appear on adsorption of the D_2O,which are related to the formation of the ice overlayer, a narrow band at 2725-2730 cm^{-1}, which corresponds to free, non-H-bonded O-D stretch at the surface, a broader band at 2480-2510 cm^{-1} which is the corresponding hydrogen bonded O-D stretch)

and around 1220 cm^{-1} the O-D bending mode. Figure 6-2 a-f show the frequencies and peak area versus the growth of the D_2O ice overlayer.

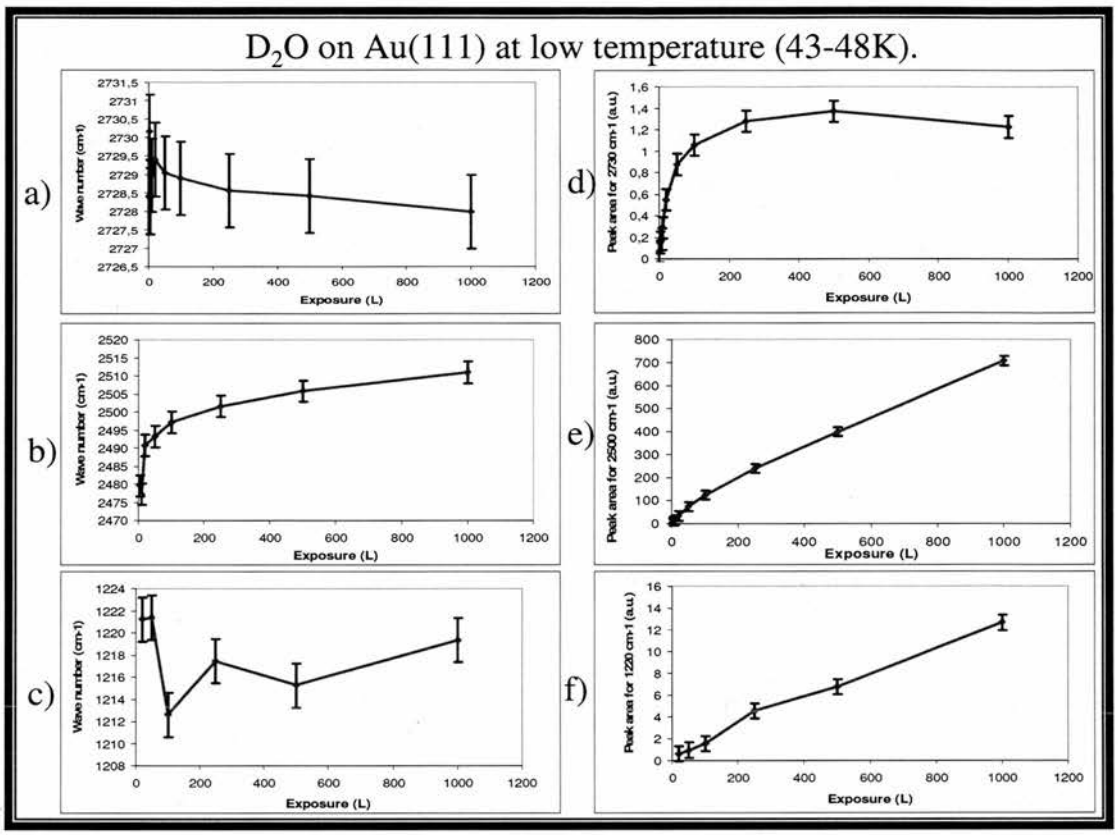

Figure 6-3. The wavenumbers of the bands around a) 2730 cm^{-1}, b) 2500 cm^{-1} and c) 1220 cm^{-1} and their peak areas at d), e) and f) respectively with the growth of the D_2O ice (expressed in exposure in langmuirs) on Au(111) at low temperature (43-48K).

The only band of these three that have any significant change in wave number with the growth of the D_2O ice is the one for the hydrogen bonded O-D stretch around 2500cm^{-1}. For very low coverage of D_2O the wave number is lower at 2475 cm^{-1} but rises as the ice layers build up, first rapidly and then levels out around 2510 cm^{-1}, which is shown in figure 6-3 b). The interaction between the D_2O molecules forming clusters at low coverage and building to the first layer and with the gold atoms probably causes this shift to a lower wave number. As the next layer builds up, the molecules are further from the gold

surface and are not affected as much. With further layers of D_2O there are more "pure" hydrogen bonding and hence the peak shifts up to that typical of ice films. Also, in figure 6-3 e) and f) the areas of the two peaks characteristic of bulk ice increase linearly with the exposure and this is an indication that the ice layer builds up proportionally with the exposure.

The band at 2730 cm^{-1} shows a different behaviour with increasing exposure of D_2O, as shown in figure 6-3 a). The only free O-D bonds are to be found at the edge of clusters or the surface of the growing film. All molecules in the layers underneath are involved in hydrogen bonding. The peak area increases steeply with exposure for low coverage and then levels out and becomes constant over 200L as shown in figure 6-3 d. This is because the first layer of D_2O on the Au(111) surface builds up and the density of free O-D stretches increases. When the next layer starts to form, there will not be any more such stretches, as the molecules in the first layer will become involved in hydrogen bonding instead, while the new molecules "take over" the free O-D stretches.

The O-D bending does not show any dependence in wave number against the exposure of D_2O and the peak area increases linearly as expected for constant sticking probability.

6.5 FTIR studies of D_2O ice film growth on a self-assembled monolayer of 2-mercaptoethanol on Au(111).

6.5.1 Experimental details.

Before the D_2O was added, the 2ME was dosed on the surface. This was done in different ways. First, the substrate was cooled down with liquid helium as above. Once the low temperature had stabilised, 2ME was dosed onto the surface before D_2O was added. This was done for each of low coverage (2L exposure), saturated monolayer (8L) and multilayer (100L). Second, 2ME was adsorbed at room temperature prior to cooling, one run each for low coverage and saturated monolayer, 80L and 1500L exposures respectively. Then the sample was cooled down and once the temperature had stabilised, D_2O was added. Finally, a multilayer was applied at reduced temperature followed by "flashing" the sample up to room temperature and then re-cooled again before adding D_2O.

6.5.2 Results and discussion.

When the D_2O molecules are adsorbed on a SAM of 2-mercaptoethanol, the wave numbers of the three characteristic bands for D_2O show a somewhat different dependence versus the exposure of D_2O than for the adsorption of the heavy water molecules on bare Au(111). This is most obvious at higher coverages beyond one monolayer. The increases of the peak areas with the exposure of D2O, however, are the same for the two adsorption systems.

First, the spectra for the cumulative addition of D_2O at low temperature (81-98 K) on low coverage 2ME (80L at RT, 2L at low temperature) adsorbed on Au(111) are shown in figure 6-4. In the case of Figure 6-4a, 2ME adsorption was carried out at low temperature (around 90K) while for the spectra in Figure 6-4b adsorption of 2ME took place at room temperature prior to cooling. Next the same spectra for high coverage (one monolayer) of 2ME are shown in figure 6-5. Finally figure 6-6 show two spectra for a multilayer of 2ME adsorbed at reduced temperature where in one case the sample was heated to room temperature and re-cooled to form a monolayer. All these spectra are the result of reprocessing the raw spectra with the first raw spectrum of the thiol adsorbed on the Au(111) when the temperature had stabilized after cooling with liquid helium. Then the effect of adding the D_2O is then seen directly.

In figure 6-4, the shape of the O-D stretching band for both low coverage cases of 2ME is somewhat different with a broader shape of the peak that the monolayer and multilayer runs in figures 6-5 and 6-6 respectively.

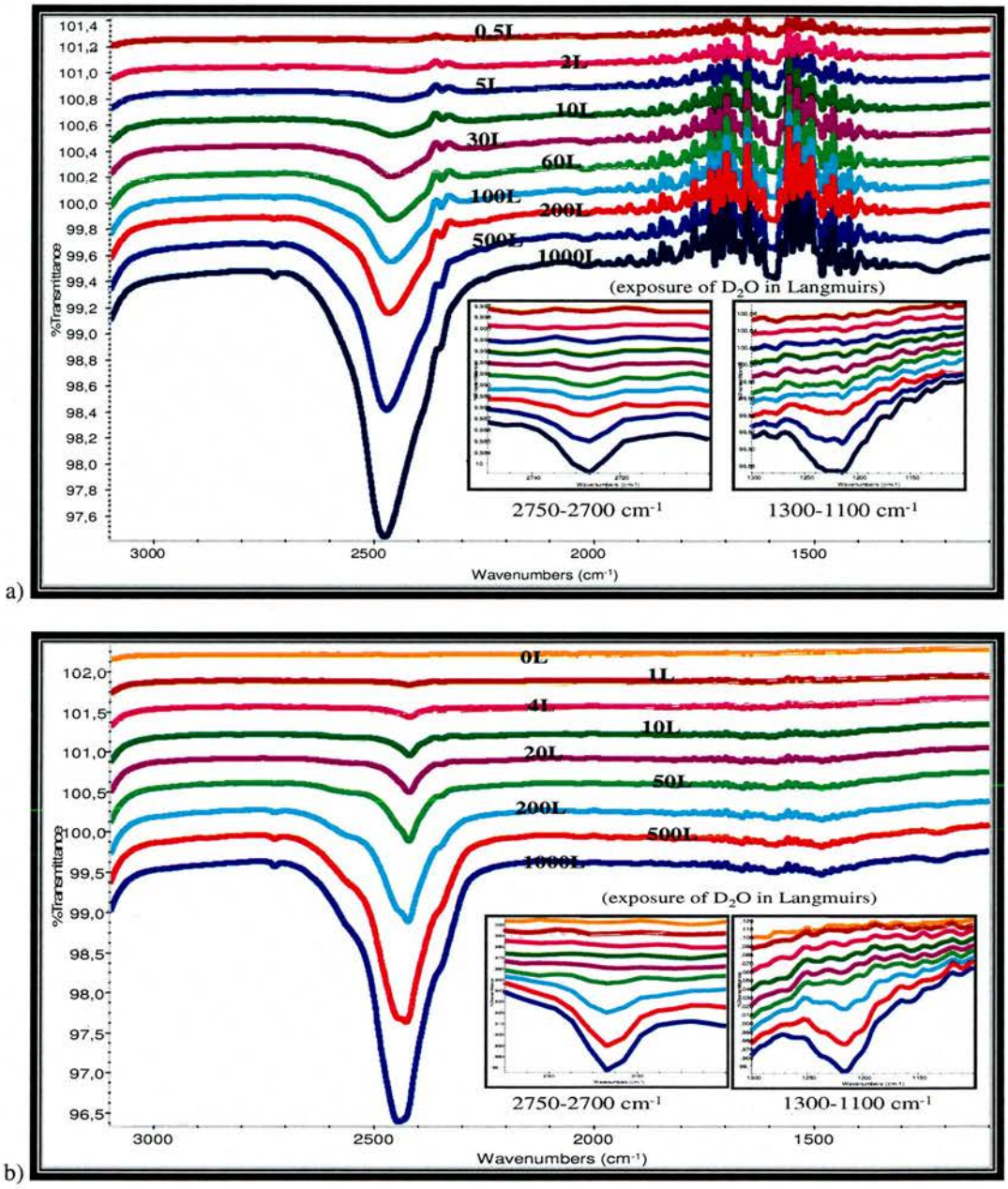

Figure 6-4. RAIRS spectra for increasing exposure of D_2O at low temperature (81-98 K) on a low coverage SAM of 2ME on Au(111).
a) 2ME applied after cooling to low temperatures. b) 2ME applied at room temperature before cooling.

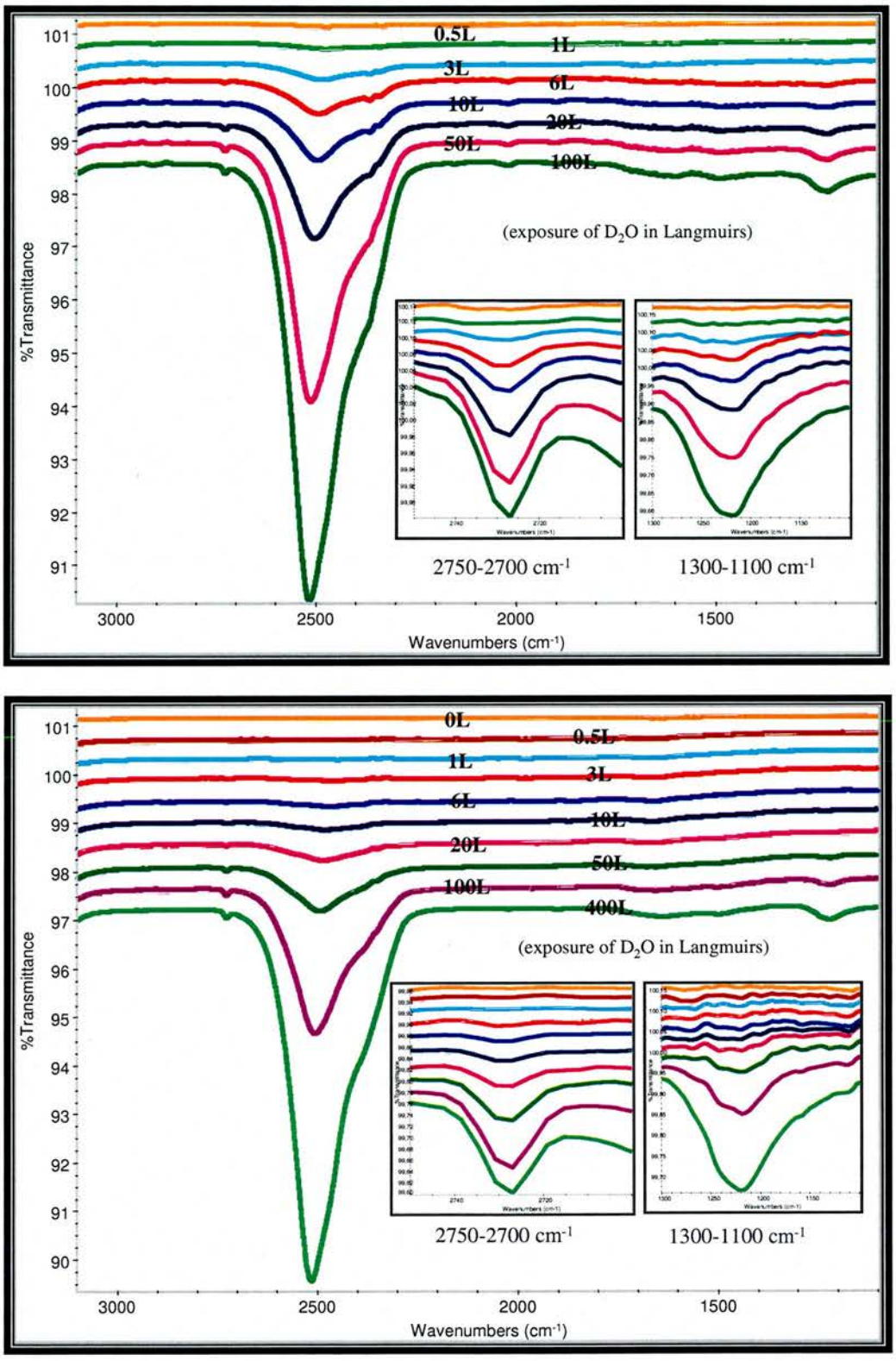

Figure 6-5. RAIRS spectra for different exposure of D_2O on a high coverage (one monolayer) SAM of 2ME on Au(111). a) 2ME applied after cooling to low temperature (81-88K). b) 2ME applied at room temperature before cooling.

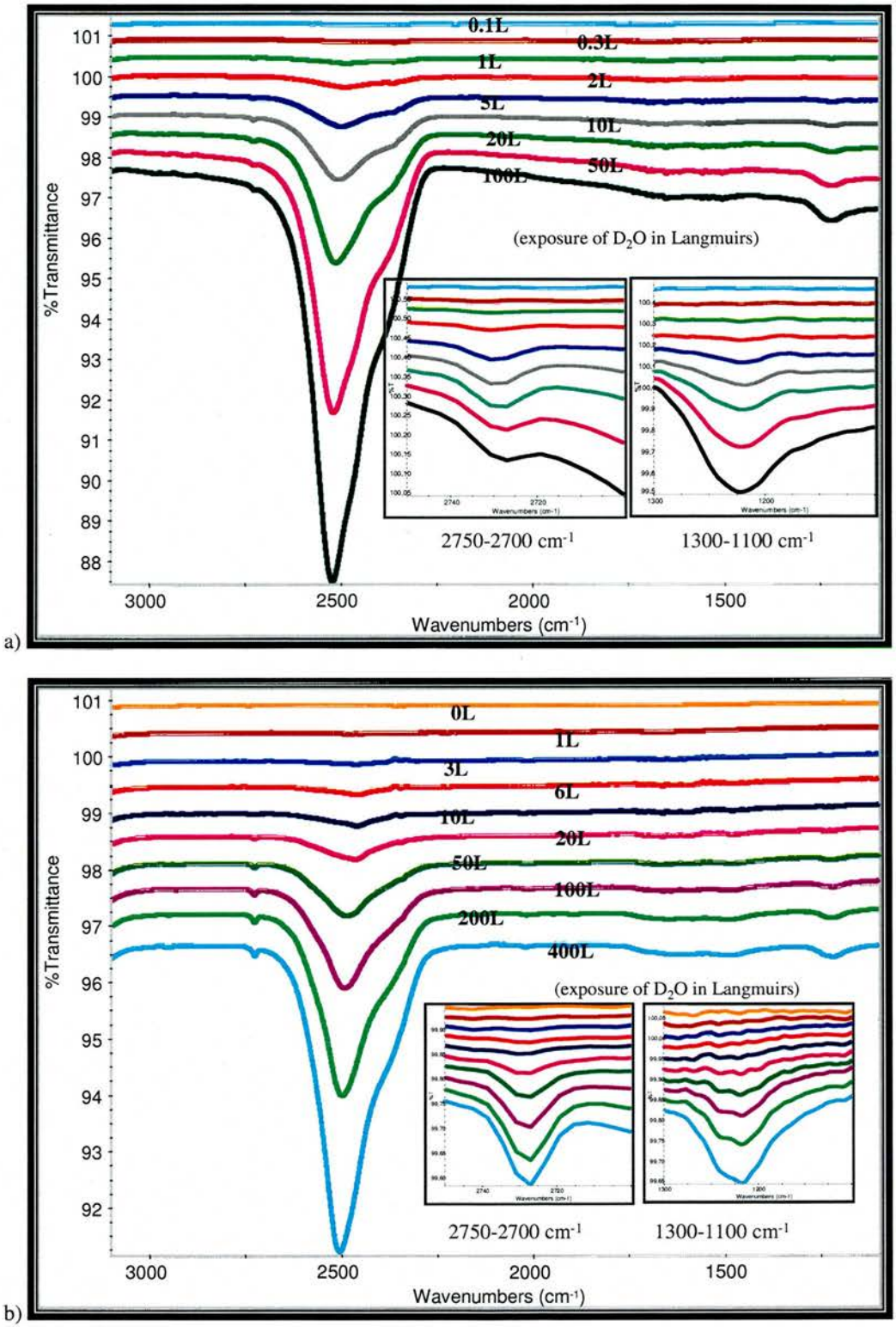

Figure 6-6. RAIRS spectra for different exposure of D_2O on multilayer of 2ME adsorbed on Au(111) at low temperatures. a) D_2O dosed directly after adding the thiol. b) The sample first warmed up to room temperature and then re-cooled before adding D_2O.

For all six cases, the wave numbers and the peak areas of the three peaks are plotted against the exposure of D_2O. First the variation in the wave number for the free O-D stretch mode against exposure of D_2O is shown in figure 6-7.

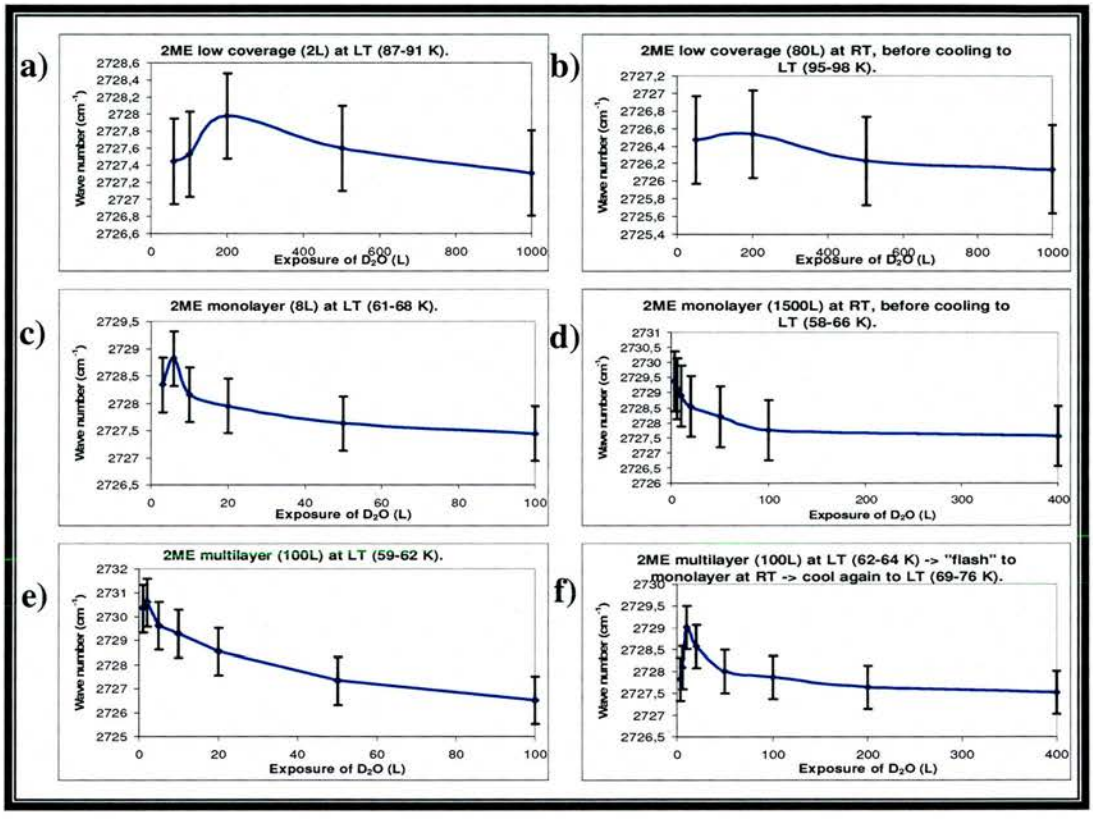

Figure 6-7: The wave number of the free O-D stretch mode versus exposure of D_2O above a SAM of 2ME of various coverages. a) Low coverage at reduced temperature, and b) at room temperature before cooling. c) High coverage (one monolayer) at reduced temperature, and d) at room temperature before cooling. e) Multilayer at reduced temperature and also at f) followed by heating to room temperature and re-cooled.

The variation of the wave number is very small, only 2 cm^{-1} for D_2O on the low coverage of 2ME, but up to 5 cm^{-1} for the higher coverage and multilayer. For the latter cases it decreases, first rapidly and then levels out. However, due to the large error in determining the peak (low signal to noise ratio, in particular the lower D_2O coverages), nothing can be concluded about any trendline.

In figure 6-8, the intensity of the free O-D stretch band is plotted against exposure of D_2O.

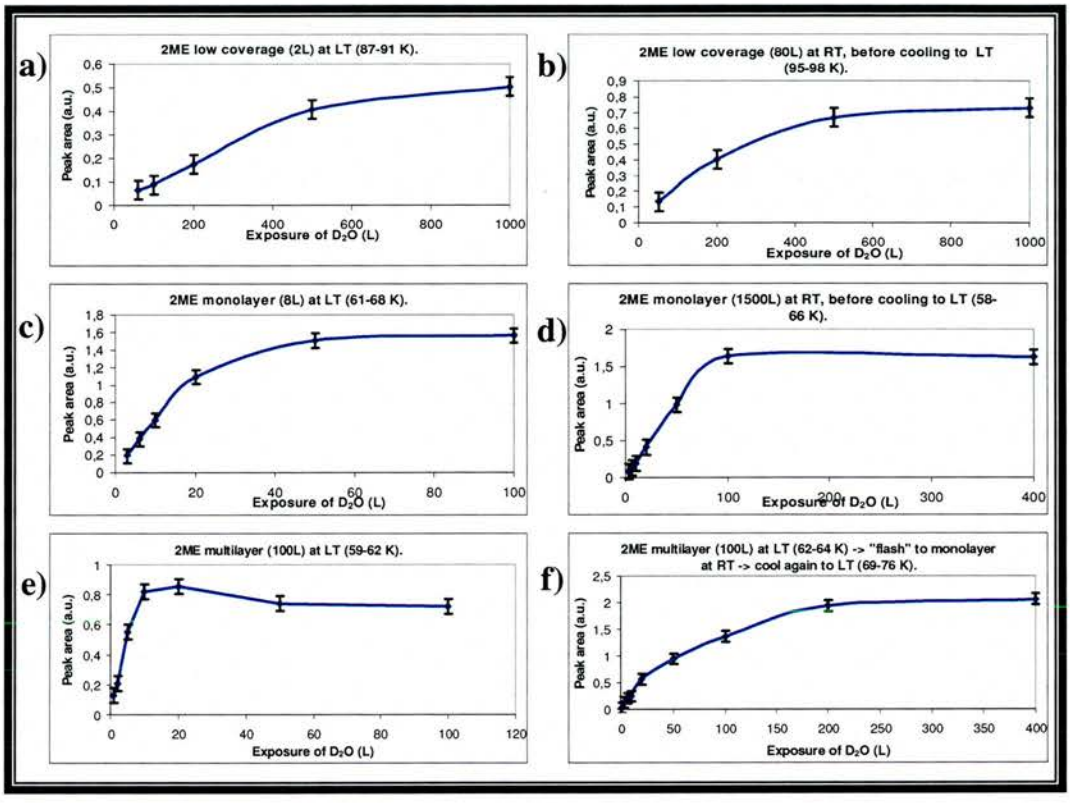

Figure 6-8: The peak area of the free O-D stretch mode versus exposure of D_2O above a SAM of 2ME of various coverages. a) Low coverage at reduced temperature, and b) at room temperature before cooling. c) High coverage (one monolayer) at reduced temperature, and d) at room temperature before cooling. e) Multilayer at reduced temperature and also at f) followed by heating to room temperature and re-cooled.

In all the different coverage of 2ME, the intensity (peak area) of the band rises steeply for small exposure of D_2O and then levels out. As with the D_2O adsorption directly on to the Au(111) surface, this is an indication that the first layer builds up the surface of the ice facing the vacuum containing the free O-D stretches. These are then replaced by hydrogen bonding O-D stretches when the next layer builds up. So the number of free O-D stretches remains the same, as it is only the outer surface of the ice that has free O-D stretches. The ice is

also saturated with this mode at lower exposure for the higher coverage of 2ME, and possible explanations is that either OH-groups of the thiol hydrogen bond with the free O-D on the side of the ice facing the 2ME layer or that deuterium atoms can be exchanged between the ice and the thiol.

$Au\text{-}S\text{-}(CH_2)_2\text{-}OH + D\text{-}O\text{-}D \Leftrightarrow Au\text{-}S\text{-}(CH_2)_2\text{-}OD + H\text{-}O\text{-}D$

For the next band, around 2500 cm^{-1}, the dependence of the wave number with the exposure of D_2O is shown in figure 6-9.

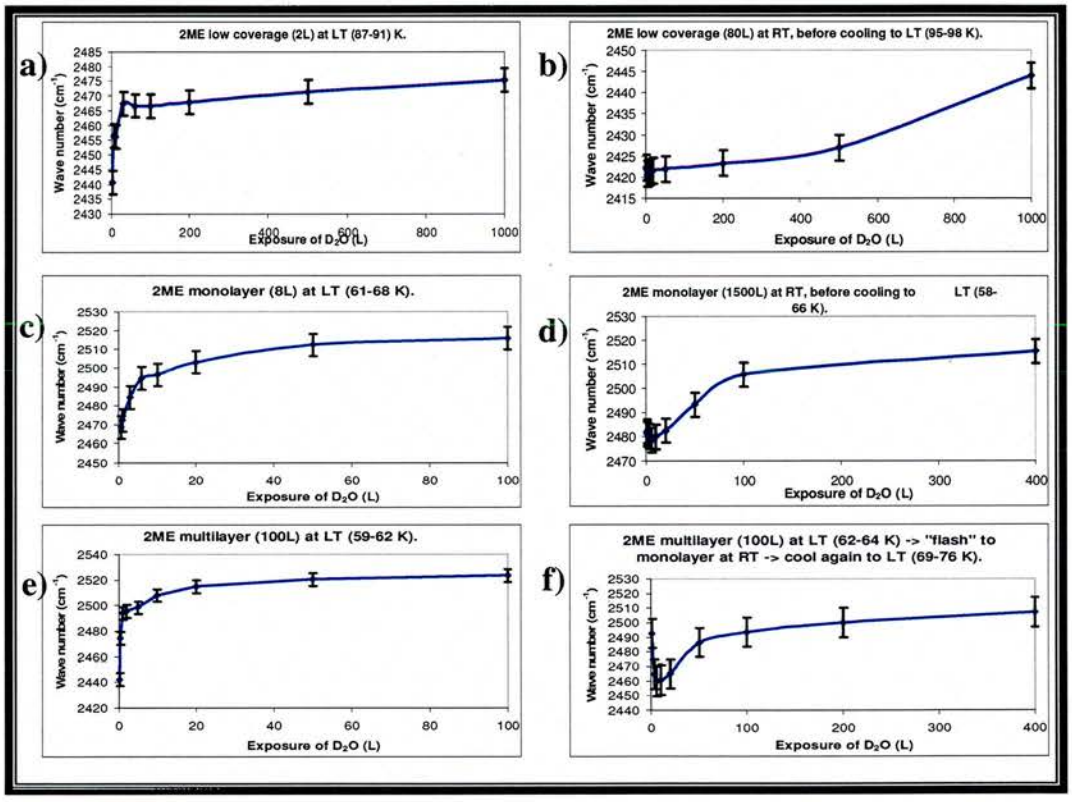

Figure 6-9: The wave number of the O-D hydrogen bonding stretch mode versus exposure of D_2O above a SAM of 2ME of various coverages. a) Low coverage at reduced temperature, and b) at room temperature before cooling. c) High coverage (one monolayer) at reduced temperature, and d) at room temperature before cooling. e) Multilayer at reduced temperature and also at f) followed by heating to room temperature and re-cooled.

For almost all the different coverages and for the different adsorption sequences of 2ME the wave number rises steeply in the beginning and for larger exposure levels out. But the maximum wave number is reached at a

higher exposure of D_2O, first around 100L, for both low and high coverage when the 2ME has been adsorbed at room temperature before cooling it down with liquid helium. Also the maximum value of the wavenumber is lower for both of the samples with low coverage 2ME in figure 6-9 (a and b) than for the mono- and multilayer ones (c to f). This suggests that the ice film may be somewhat more ordered when it is very thin but the subsequent layer of ice becomes somewhat amorphous but there is still a mixture of the phases. For the higher coverages of 2ME though this band both starts initially, and rises to, higher wave numbers suggesting the ice becomes more amorphous. Also, the gold atoms are more exposed at low coverage of 2ME and may also have an effect on the ice. Figure 6-10 shows how the peak area for this band varies with the D_2O exposure.

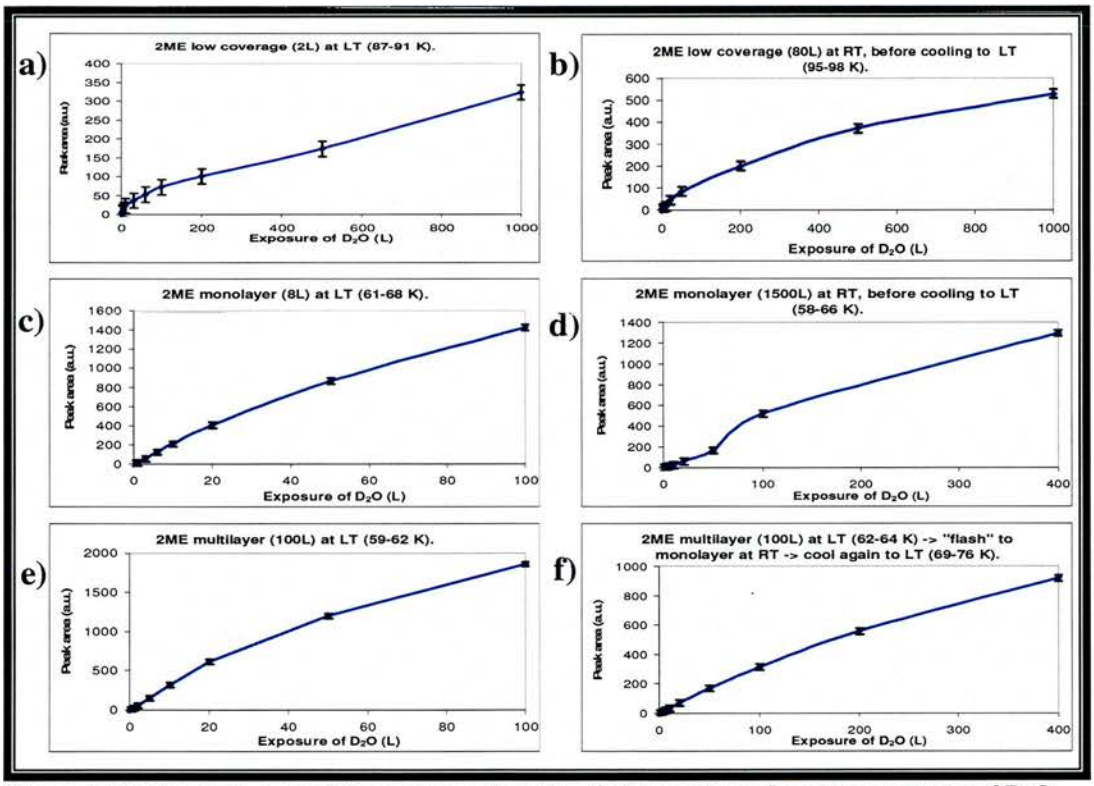

Figure 6-10: The peak area of the hydrogen bonding O-D stretch mode versus exposure of D_2O above a SAM of 2ME of various coverages. a) Low coverage at reduced temperature, and b) at room temperature before cooling. c) High coverage (one monolayer) at reduced temperature, and d) at room temperature before cooling. e) Multilayer at reduced temperature and also at f) followed by heating to room temperature and re-cooled.

For all coverages of 2ME and at all adsorption temperatures for the thiol (before or after cooling the gold substrate to low temperature) the peak area versus the exposure of D_2O shows the same linear growth as the ice build up on to bare Au(111). So we suggest this is an indication of that the thickness of the ice is proportional to the exposure. The low coverage cases (a) and (b) both have an initially slightly steeper slope. It may depend on a higher sticking probability on exposed gold atoms between the 2ME domains on the partly covered Au(111) surface.

As for the bare Au(111), the O-D bending mode did not show any variation in wave number with coverage and a linearly growing ice layer with the D_2O exposure was obtained.

No C-H stretching band (either positive or negative) in the range 2800-3000 cm^{-1} appeared for any coverage of 2ME and exposure of D_2O, so there were no sign of any change in orientation of the 2ME molecules in the monolayer caused by the build up of the ice overlayer.

There was no other distinct change in the intensity (peak area) of the hydrogen bonding O-D stretch or bend apart from the linear rise with exposure of D_2O. So the ice formed must be amorphous which agree with earlier findings at these temperatures [24].

6.6 FTIR studies of D_2O ice film growth on a self-assembled monolayer of benzyl mercaptan on Au(111).

6.6.1 Experimental details.

Similar experiments were performed for adsorption of an overlayer of D_2O above a SAM of benzyl mercaptan (BM), with the same variations of coverage of the thiol and temperature for adsorption, although the multilayer adsorption at low temperature is not included, and the saturated monolayer at room temperature has limited data due to some instrumental faults.

6.6.2 Results and discussion.

The spectra from the various experiments are summarized in figures 6-11 to 6-13. All these are reprocessed against a background spectrum containing the Au(111) and the thiol before the first addition of D_2O.

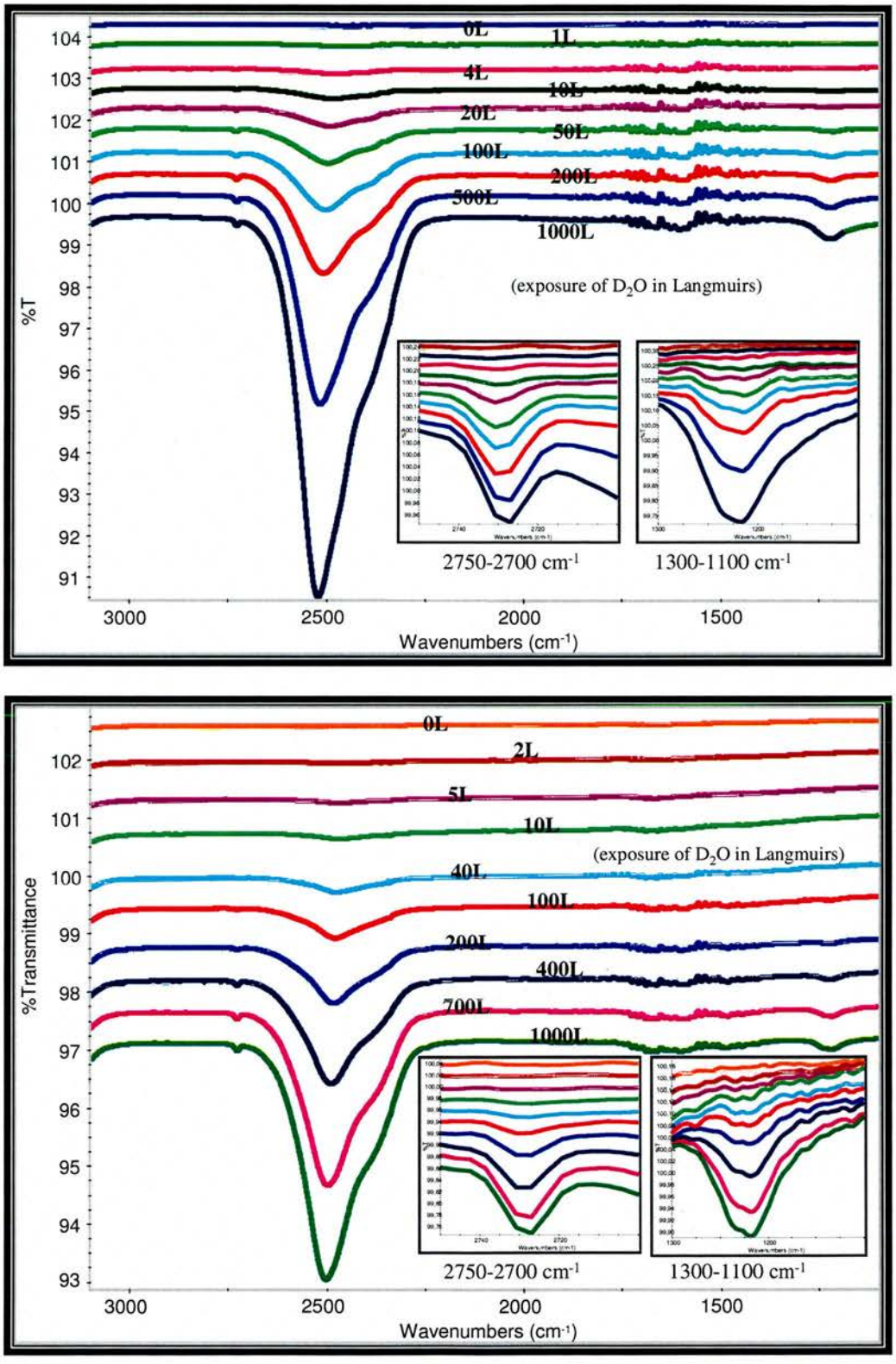

Figure 6-11. RAIR spectra for different exposure of D_2O on a low coverage SAM of 2BM on Au(111).
a) BM applied after cooling to ca 57-68K temperatures. b) BM applied at room temperature before cooling (75-85K).

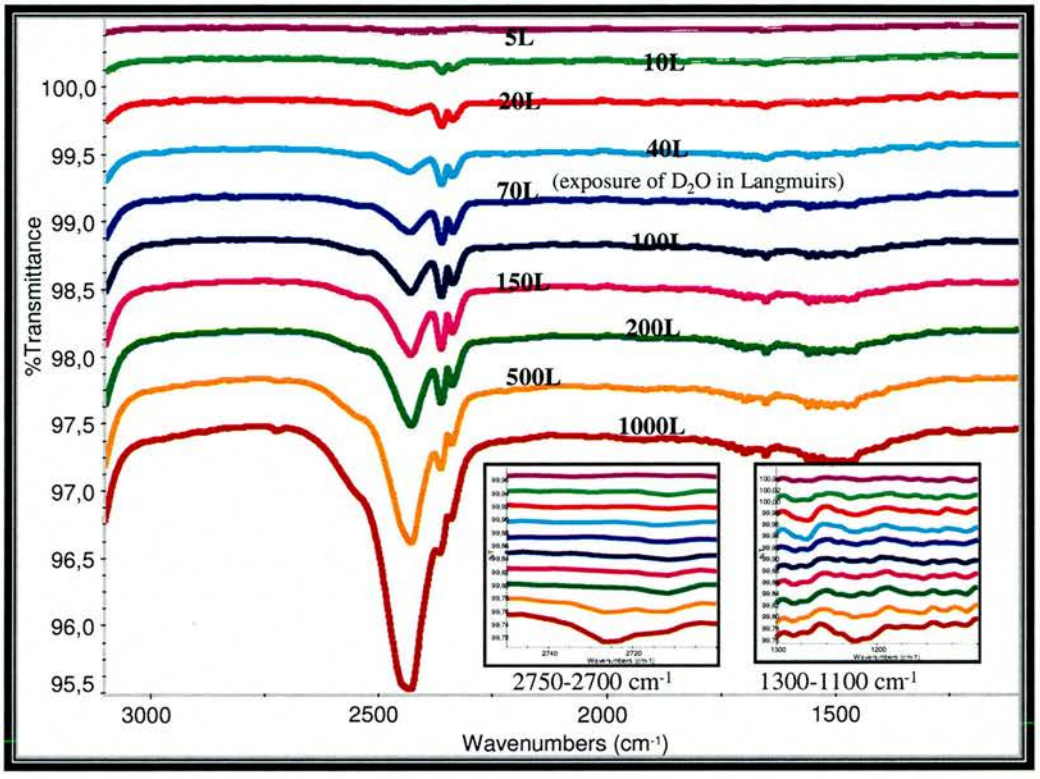

a)

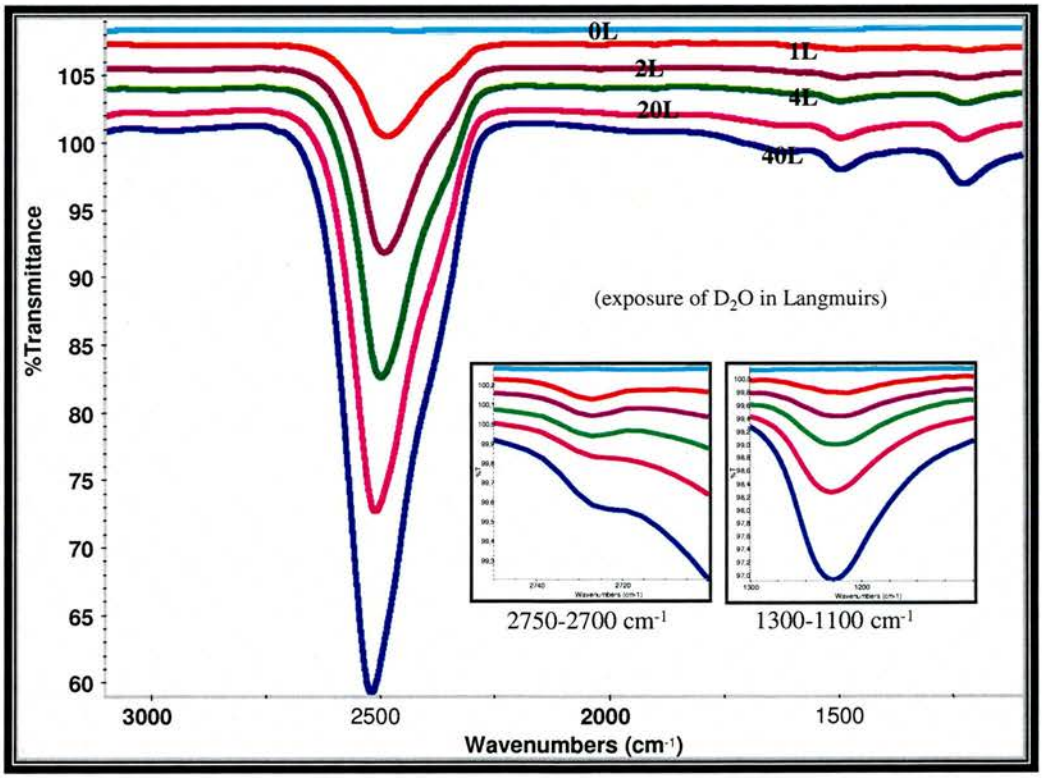

b)

Figure 6-12. RAIRS spectra for different exposure of D_2O on a high coverage (one monolayer) SAM of BM on Au(111). a) BM applied after cooling to low temperatures (74-86K). b) BM applied at room temperature before cooling (56-73K).

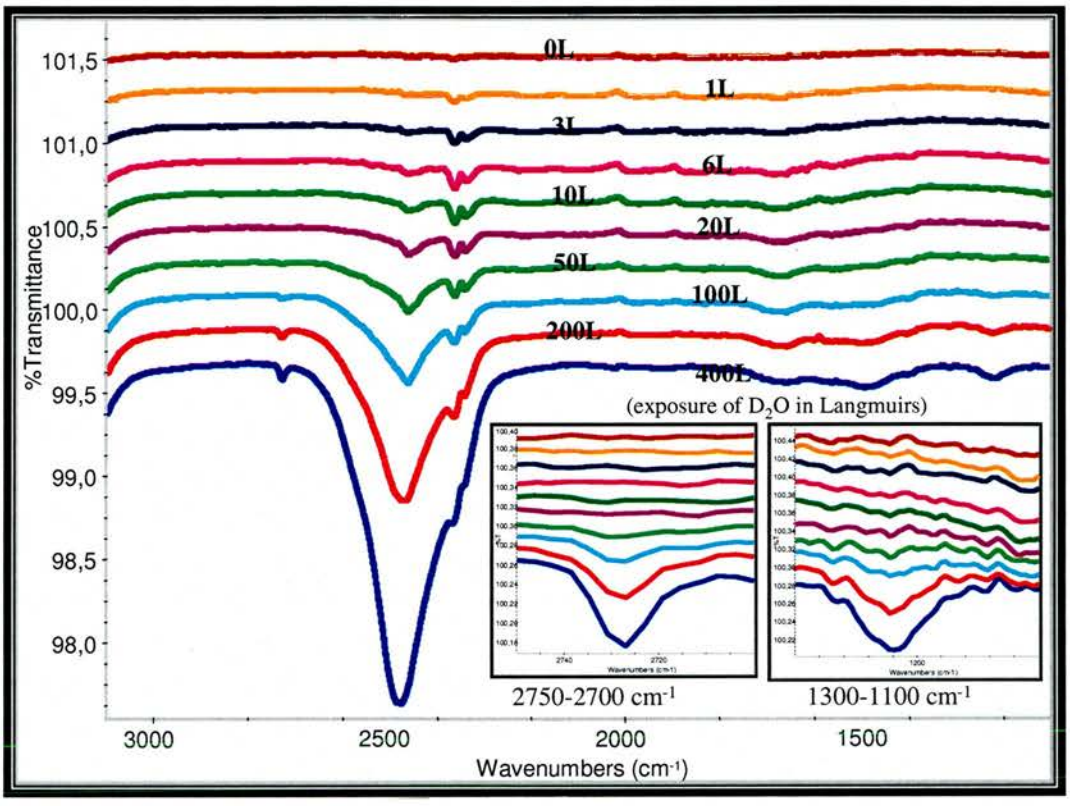

Figure 6-13. RAIRS spectra for different exposure of D_2O on multilayer of BM adsorbed on Au(111) at low temperatures (69-75K). The sample was first warmed up to room temperature and then re-cooled before adding D_2O.

The wavenumbers and the peak areas for the bands were again obtained in the same way as for 2ME using the tools in the Omnic software. The same three characteristic bands were found which vary with the exposure of the D_2O. When plotting the wave number and the peak area against the exposure (dose) of D_2O for each of the bands, the shape of the curves are very similar for all coverages and temperature of adsorption of the BM, only the absolute values differs somewhat.

First, the free O-D stretch does not change much in wavenumber with the increased exposure of D_2O, only up to 5 cm^{-1}, which is shown in figure 6-14.

Although there is a slight decrease in a) the error is large and for the other coverages of BM there are no significant change of wave number is this band.

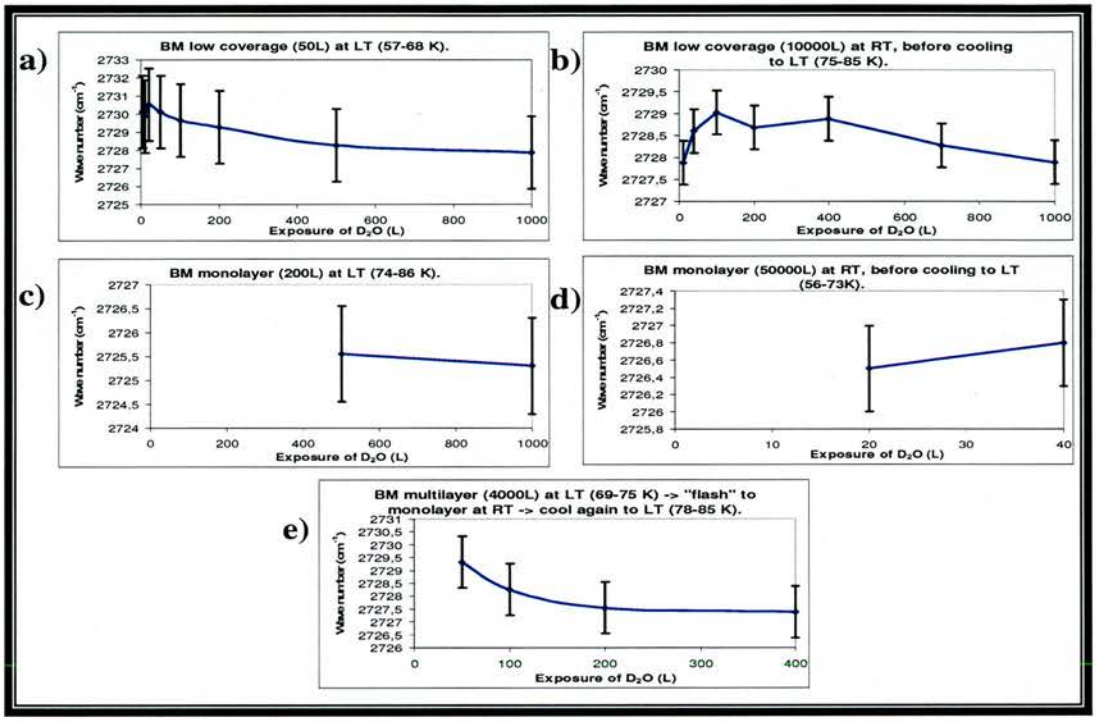

Figure 6-14: The wave number of the free O-D stretch mode versus exposure of D_2O above BM of various coverages on Au(111). a) Low coverage at reduced temperature, and b) at room temperature before cooling. c) High coverage (one monolayer) at reduced temperature, and d) at room temperature before cooling. e) Multilayer at reduced temperature followed by heating to room temperature and re-cooled.

The dependence of the peak area for the same band is shown in figure 6-15. For low coverage it follows the same pattern as for 2ME and saturation is obtained after some 600L of exposure. In contrast, for the higher coverage cases, this levelling out of the curve is not that obvious. In contrast to 2ME, BM has no OH-groups to engage in hydrogen bonding or H/D exchange with the D_2O. In addition, the hydrophobic nature of the aromatic ring could cause the ice to cluster to smaller units which contributes to larger surface area and hence more free O-D stretches for the ice layer.

It can be noted that the absolute value of the intensity varies considerably from one experiment from another, so they should not be comparable between each other. But the shape if the curve is more reproducible.

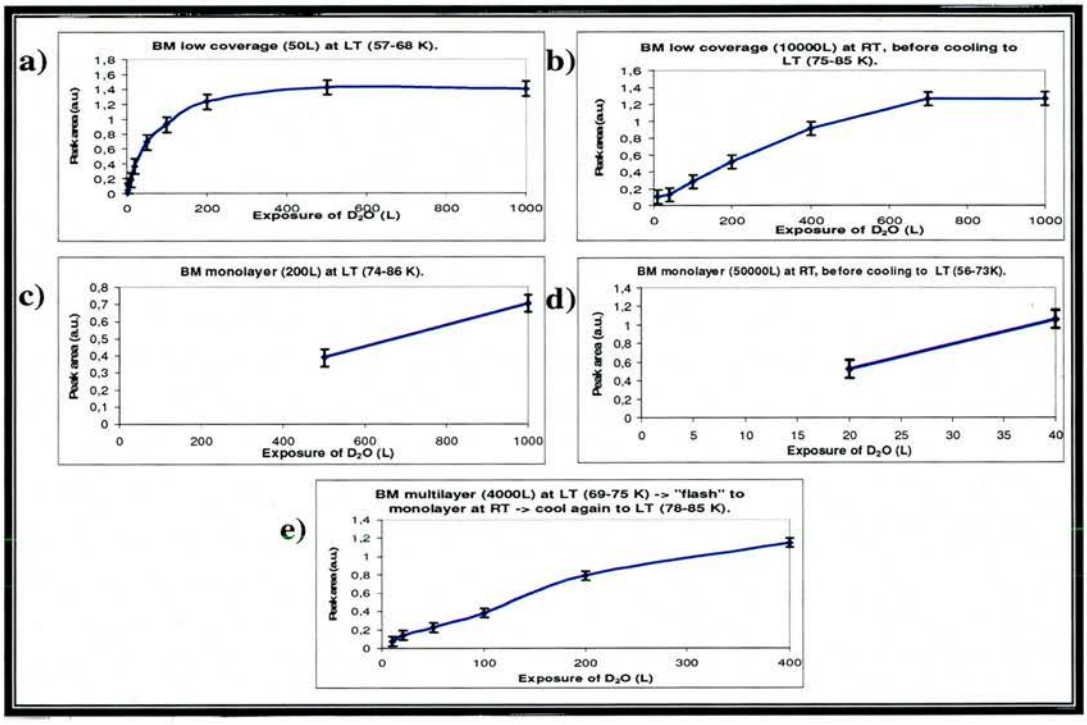

Figure 6-15: The peak area of the free O-D stretch mode versus exposure of D_2O above BM of various coverages on Au(111). a) Low coverage at reduced temperature, and b) at room temperature before cooling. c) High coverage (one monolayer) at reduced temperature, and d) at room temperature before cooling. e) Multilayer at reduced temperature followed by heating to room temperature and re-cooled.

The hydrogen bonding O-D stretch for ice on BM shows a similar profile versus the exposure of D_2O as in the cases of 2ME and bare gold. The wave number rises with the exposure, first steeply and then levels out as seen in figure 6-16. In contrast however, here the wavenumber is shifted to a slightly lower value (2430 to 2460 cm^{-1}) for the higher than for the lower coverage (around 2500 cm^{-1}), which is the reverse compared to the 2ME. Possibly a more ordered than amorphous ice is favoured on the hydrophobic BM surface and it ranges for the most of the ice layer. In comparison, Engquist et al. discovered

some polycrystalline phases of ice for the more hydrophobic part of their range of mixed SAM containing OH- and CH_3-terminated thiols, although at a higher temperature (120K and above) [24].

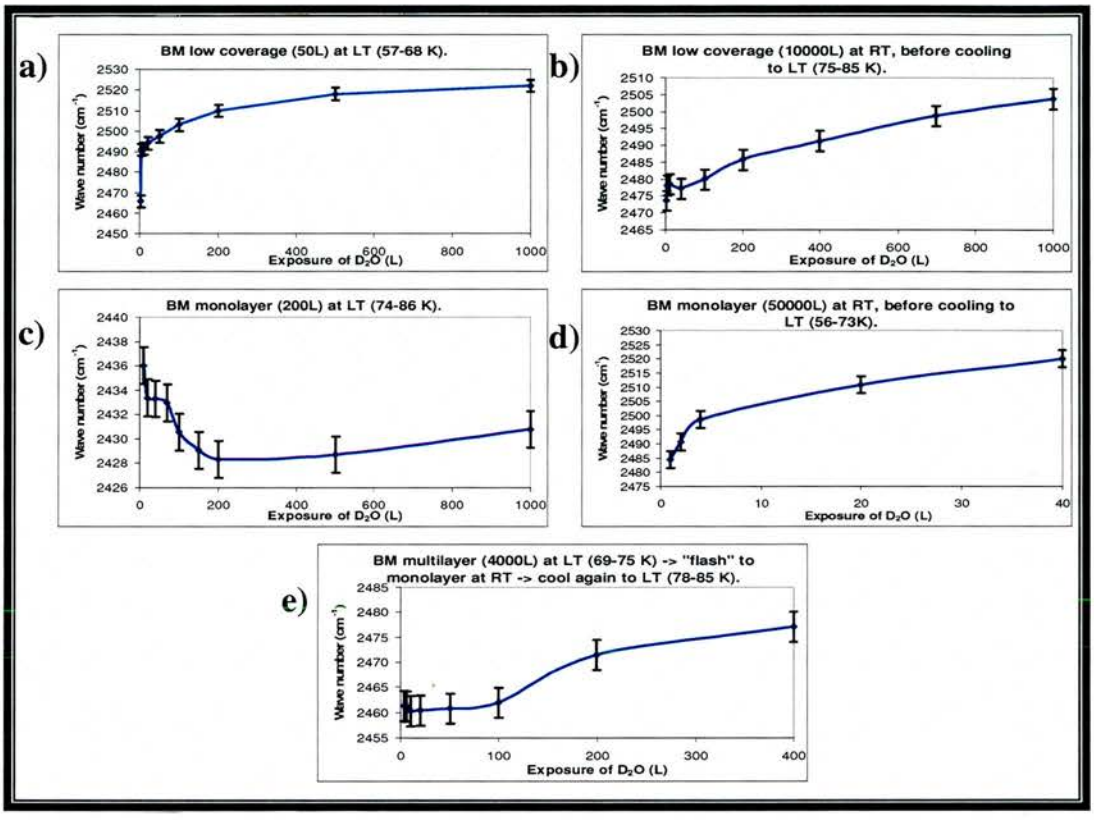

Figure 6-16: The wave number of the hydrogen bonding O-D stretch mode versus exposure of D_2O above BM of various coverages on Au(111). a) Low coverage at reduced temperature, and b) at room temperature before cooling. c) High coverage (one monolayer) at reduced temperature, and d) at room temperature before cooling. e) Multilayer at reduced temperature followed by heating to room temperature and re-cooled.

The range of the variation in the wave number is also smaller for the lower coverage.

The peak area is proportional to the exposure of D_2O for the most coverages of BM. Figure 6-17 show this. So also here this is an indication that the thickness of the ice increases linearly with the exposure of D_2O. Just a comment of the very large absolute values in figure 6-17 d, there were some

trouble with the D_2O leak valve in that run which may have caused an overdose. However it still shows an almost linear growth.

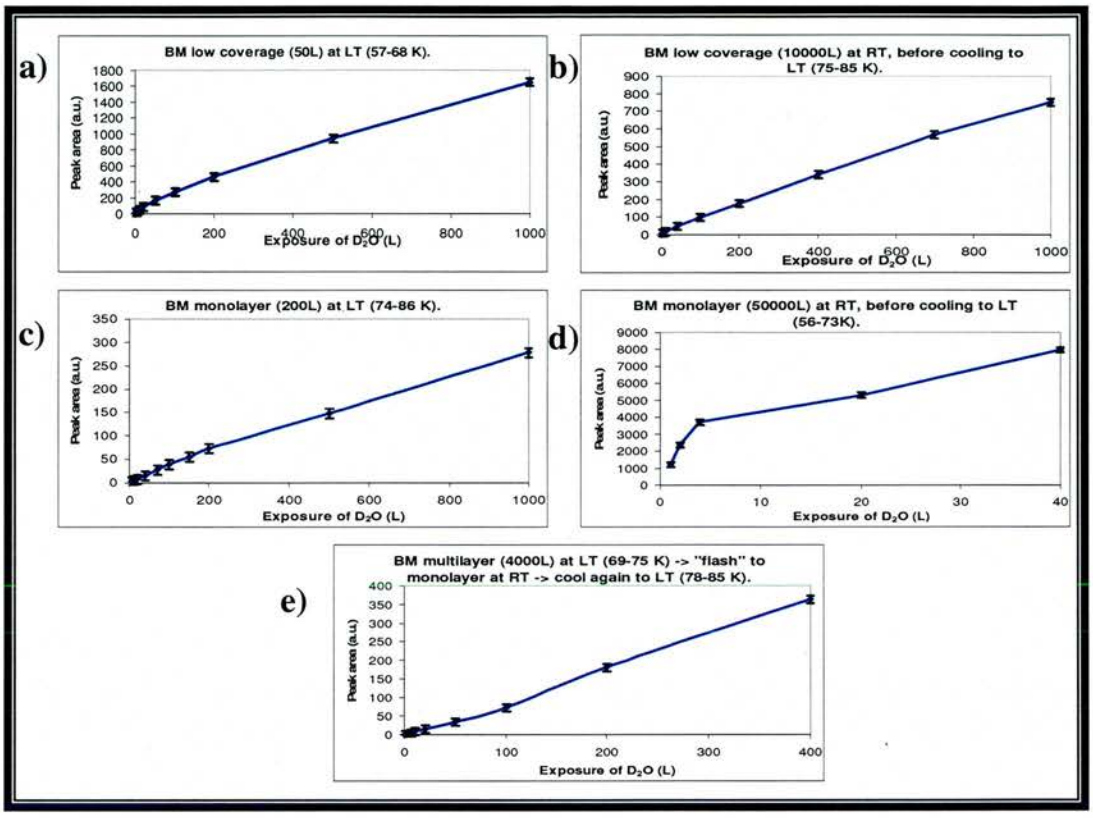

Figure 6-17: The peak area of the hydrogen bonding O-D stretch mode versus exposure of D_2O above BM of various coverages on Au(111). a) Low coverage at reduced temperature, and b) at room temperature before cooling. c) High coverage (one monolayer) at reduced temperature, and d) at room temperature before cooling. e) Multilayer at reduced temperature followed by heating to room temperature and re-cooled.

Finally, the profile of the O-D bending mode followed the same pattern also for BM: No specific trend line for the wave number and a linear growth of the ice layer versus exposure of D_2O.

As in the case of 2ME, there were no sign of structural change in orientation for the CH_2-group of BM molecules on the Au(111) surface as no aliphatic C-H stretches bands appeared in the 2800-3000 cm^{-1} region. However, some bands appear around 1500-1600 cm^{-1} (which can be assigned to the C-C

in-plane stretch) for the higher coverage of BM with the increasing exposure of D_2O. This could be caused by the D_2O molecules which prefer to bind to themselves rather than the hydrophobic BM ring, and hence the cluster may cause the aromatic rings to be distorted. In the low BM coverage case these bands were not seen because the aromatic ring is lying flat, parallel to the surface [9] and the C-C aromatic stretches are not visible due to the selection rule and also there is more space for the D_2O molecules to bind to the surface and therefore not distort the BM molecules so much.

6.7 STM imaging of water on Au(111) and benzyl mercaptan

6.7.1 Experimental details.

The imaging of water by STM was performed with UHV conditions at low temperature. Liquid nitrogen causes too much noise due to the violent boiling of the liquid. Therefore liquid helium was used as coolant instead. However, even when using this as coolant, the system was more sensitive to disturbances than at room temperature, so the outcome of STM images of the adsorption of the water molecules is quite limited. Water adsorption directly onto Au(111) that has been imaged well, and some successful studies of water adsorption on a BM monolayer on Au(111) have been carried out. For these experiments, H_2O, rather than D_2O has been used here as there are none of the difficulties in STM of the type, which required the use of D_2O for the RAIRS experiments.

6.7.2 Results and discussions.

First, the adsorption of water on the bare Au(111) at low temperature gives rise to some interesting features as shown in figure 6-18 . At low coverage at 15K (read by the thermocouple), these STM images show how the hexamers of water molecules diffuse on the surface and join together to form larger clusters. The circle at a) and b) in figure 6-18 shows a cluster increasing in size from 5 to 6 hexamers of water.

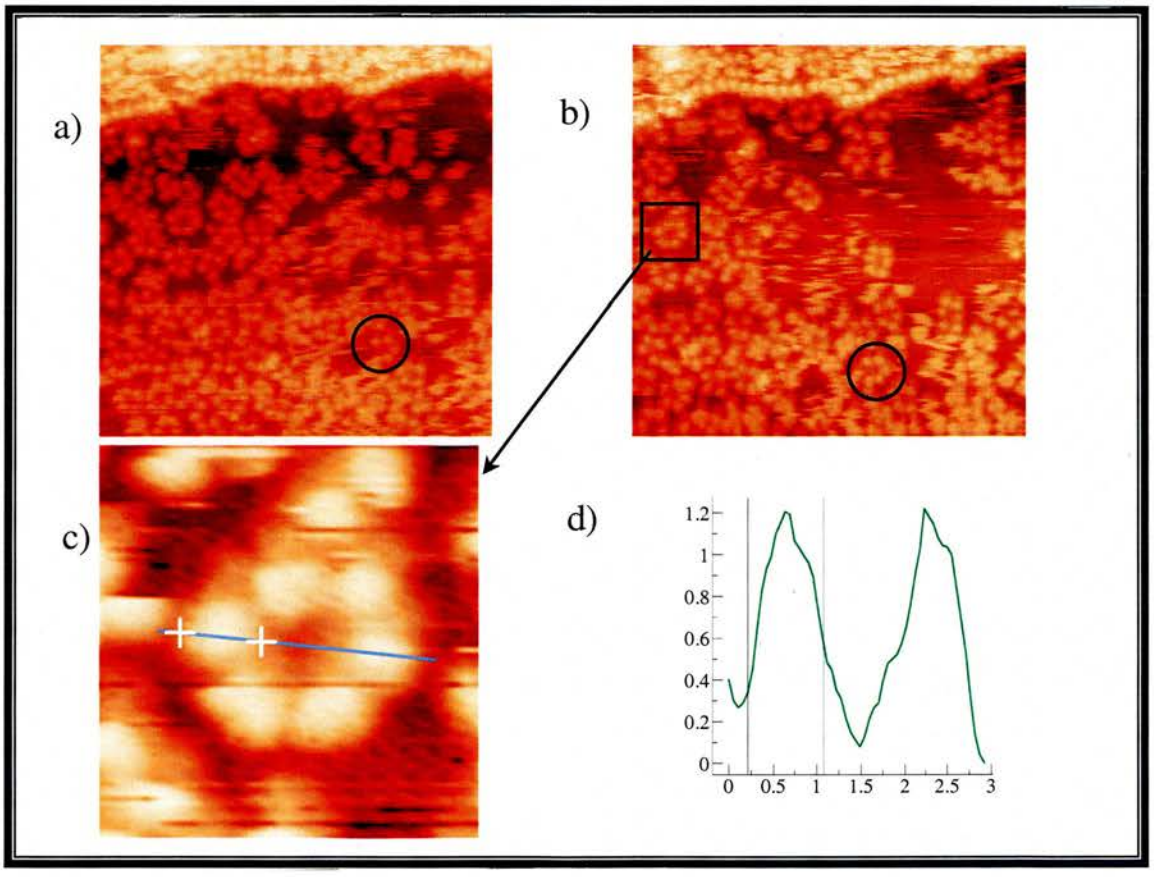

Figure 6-18: a) and b) are STM images obtained two minutes after each other following the adsorption of water onto a clean Au(111) surface at 15K (read by thermocouple). 27nm x 27 nm, bias -358 mV, tunnelling current 114pA. c) Enlargement of one sextet of a water hexamers, 4.1nm x 4.2 nm. d) Line profile of the sextet, X (horizontal) in nm and Z (vertical) in Å.

Similar cluster formation, where smaller clusters form larger clusters, has been found for water molecules on Pd(111) at 40K [6] and cyclic hexamers of water has been found to be the most stable cluster.

The distance between the markers on line profile in figure 6-18 c) is 8.63Å, which is equivalent for 8.63Å/2.88Å = 3 gold atoms. This means that the diameter of one water hexamer is the same as the diameter of a hexagonal unit of seven gold atoms. One suggestion is that each water molecule binds on top of a gold atom, but they have alternating orientation to allow hydrogen bonding between them. This is shown in figure 6-19. One water molecule is orientated horizontal while its neighbour is vertical with the hydrogen atoms pointing up.

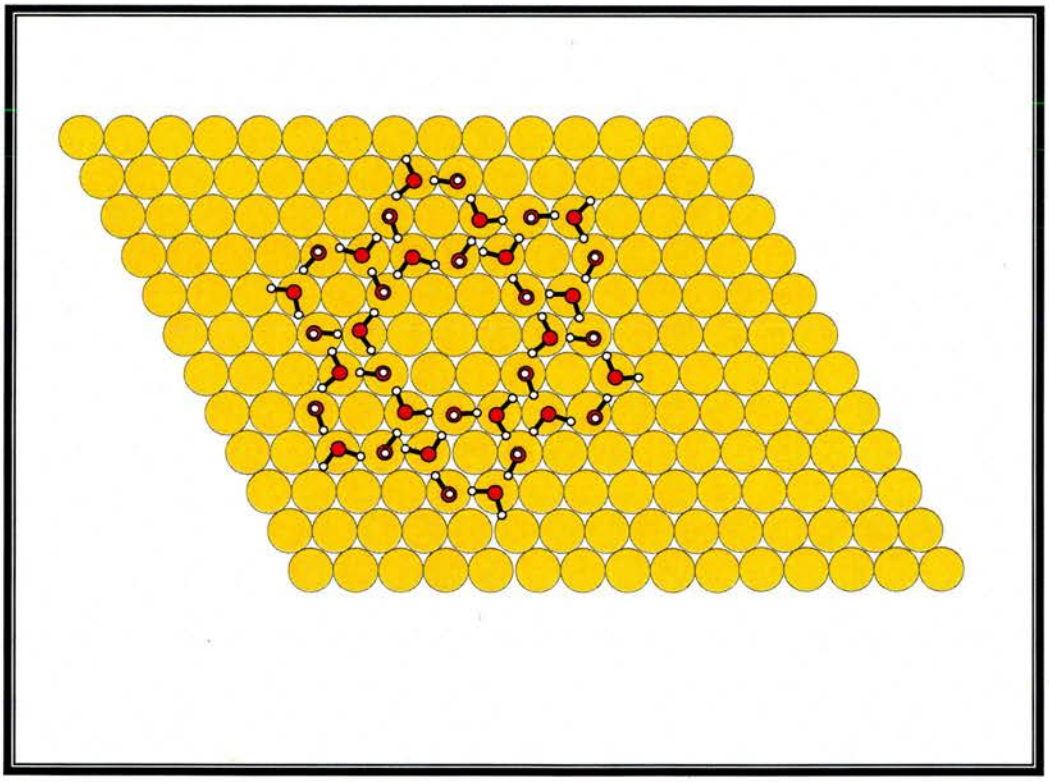

Figure 6-19: Schematic illustration how the water molecules bind on top of the gold atoms during adsorption. They are alternating, one orientated horizontal and the next vertical.

The diameter of the gold atom and lattice constant for gold (2.88Å) is very close to the O- - -O distance of water at 2.82Å [2]. So the on top

adsorptions on the gold atoms are slightly further apart than the ideal hydrogen bonding length. But the small difference in radii means that there is just a very small increase of 2% from the ideal hydrogen bonding. This compares with water on Ag(111), (lattice constant 2,89Å) and Cu(111) (lattice constant 2.56 Å) where the clusters of water hexamers are 7% stretched and 7% compressed respectively [18]. It was also found that the interaction of the H_2O molecules and Au atoms is weak enough not to cause any change of the reconstructed surface of the Au(111). The adsorption process was found to occur in one step, with the height of the clusters of about 1.5Å above the gold surface being the same as for a film of H_2O on Au(111) [13]. Also earlier TPD measurements showed only one distinct peak for desorption [10, 14, 18].

Finally, a low coverage of H_2O were dosed at 15K (read by the thermocouple) onto a low coverage of BM (28000L dosed at room temperature) on Au(111) and imaged by STM. This is shown in figure 6-20.

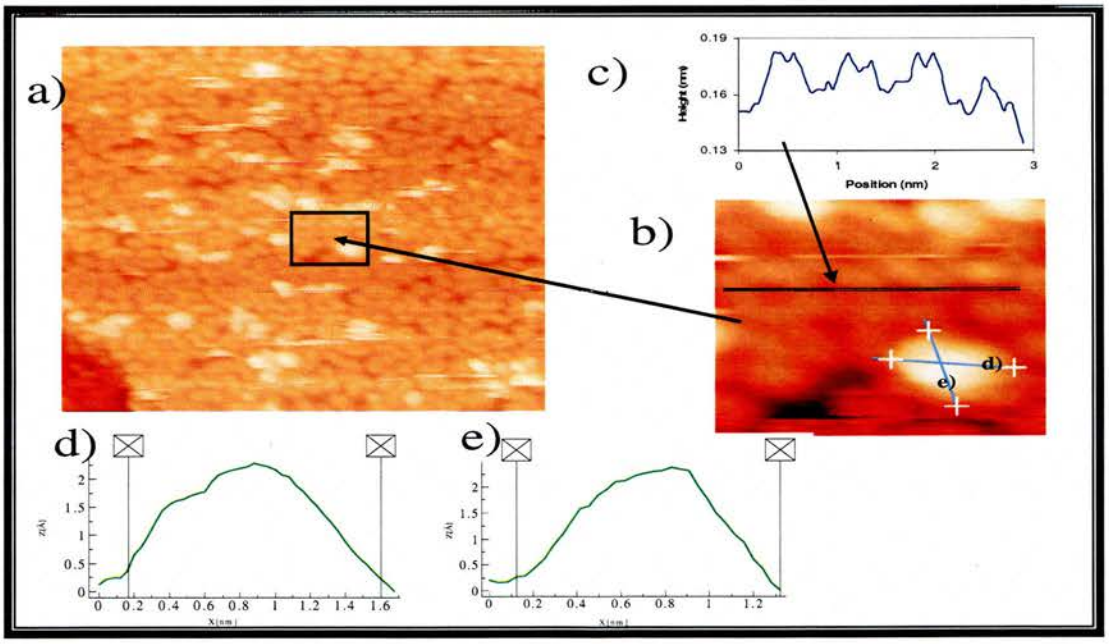

Figure 6-20. STM image of benzyl mercaptan on Au(111) with low coverage water at 15 K. Tip conditions bias 0.05 V and tunnelling current 0.1 nA. a) Full image 20.4 nm x 10.4 nm, b) inset 3.7 nm x 3.5 nm. Line profile from the inset is shown above, c) for some BM molecules and d), e) across a water cluster. The horizontal direction (X) is given in nm and the height (Z) in Å.

The brightest spots are clusters of water above the BM layer. With the dimensions of 14Å x 12Å and a height of around 2Å above the BM layer, it is possible that it is a trimer of hexamers of water [30]. The line profile in Figure 6-20 is drawn over a row of four flat lying molecules of BM, where the higher double peaks corresponds to the aromatic ring and the lower "satellite" the methylene group. So taking this together, the trimer of $(H_2O)_6$ is adsorbed on or near a low covered domain of BM molecules shown schematically in figure 6-21. They are not ordered but possibly form an "island" which could be a precursor to a more ordered monolayer of BM with the unit cell of $(\sqrt{7}x\sqrt{7})R19.1^o$ relative to the Au(111) lattice. This could be formed if the adsorption of BM were allowed to continue at higher exposure.

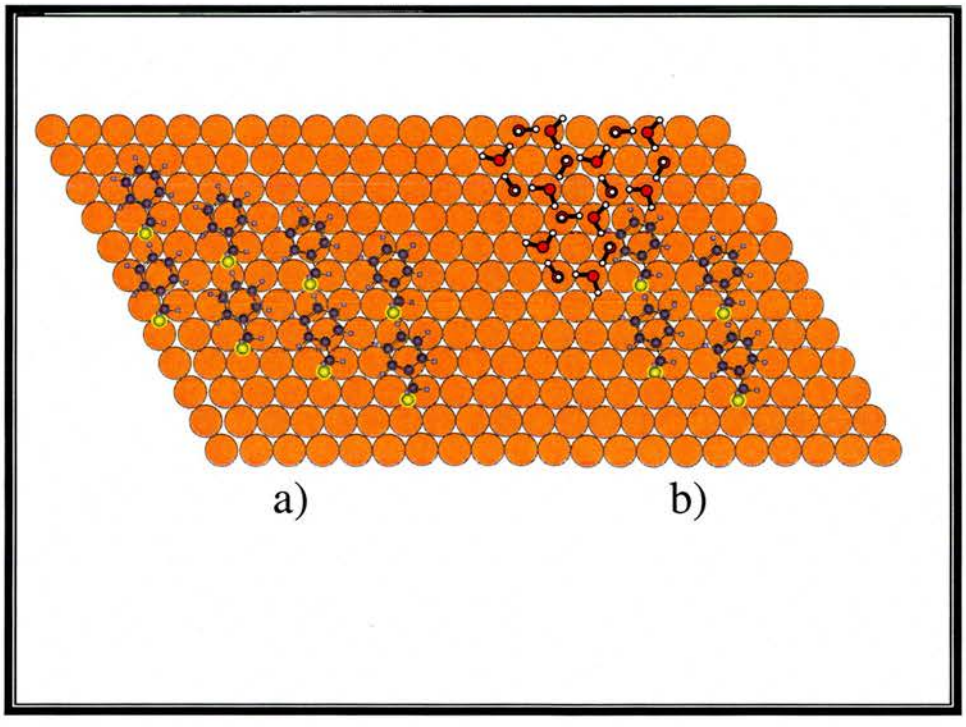

Figure 6-21. a) Schematic illustration of a domain of low coverage BM on Au(111) and b) with the co-adsorption of water above it.

This water cluster should be the most favourable structure of water as each of the water molecules can form hydrogen bonds to four others (only those able to link clusters) [2]. However it is not known if the hydrophobic nature of the aromatic ring can favour the water molecules to adsorb directly on to the gold surface between the BM molecules. This will hopefully be possible to be revealed in future work.

6.8 Conclusions

First, contact angle measurements give an idea about the relative sticking probability between BM and 2ME when adsorption takes place in atmosphere from solution. Here the BM seems to stick better that 2ME.

The RAIRS spectra show some interesting information about the structure of the D_2O ice adsorbed on Au(111) and SAMs of 2ME and BM, as well as some difference between these surfaces. In particular the hydrogen bonding O-D stretch band around 2400-2500 cm^{-1} contains a mixture of bands for amorphous and polycrystalline ice and its maximum can give a rough idea about the order of the bulk ice.

In the case of D_2O on bare Au(111) there is a rapid growth in intensity of the free O-D stretch up to a certain exposure and then it levels out. During this growth, the first layer of water (surface facing out to the vacuum) builds up. Then the ice continues to build multilayers. This profile was also the case for D_2O adsorbed onto the SAM of 2ME at all coverages and also for low coverage BM. For higher coverage BM however, the intensity did not level out suggesting

that the hydrophobic nature of the aromatic ring causes the D_2O molecules to form smaller clusters with larger area of free O-D bonds.

The frequency of hydrogen bonding O-D stretch showed that there are more features of ordered structure in the ice at low coverage SAM of 2ME and high coverage SAM of BM. This seems then that more hydrophobic surfaces lead to more ordered ice adsorbed on it. The intensity of the same band increases linearly with the exposure of D_2O which probably depend on that the ice film grow proportionally.

Finally STM imaging of water on bare Au(111) shows that hexamers of water molecules on the surface cluster together and form stable rings of six hexamers. And on a low coverage domain of BM the water molecules adsorb possibly as a trimer above or near these BM molecules.

6.9 References

1. M.F. Chaplin, ***Biochemistry and Molecular Biology Education*** 29 (2001) 54.
2. M.F. Chaplin, ***Biophysical Chemistry*** 83 (1999) 211.
3. A. Henderson, ***Surface Science Reports*** 46 (2002) 1.
4. E.A. Vogler, ***Advances in Colloid and Interface Science*** 74 (1998) 69.
5. S. Meng, E.G. Wang, S. Gao, Physical Review B. 69 (2004) 195404
6. T.Mitsui, M.K.Rose, E.Fomin, D.F.Ogletree, M.Salmeron, ***Science*** 297 (2002) 1850.
7. K. Morgenstern, K.-H. Rieder, ***Journal of Chemical Physics*** 116 (2002) 5746.
8. K. Morgenstern, ***Surface Science*** 504 (2002) 293.

9. J. Harnett, S. Haq, A. Hodgson, ***Surface Science*** 528 (2003) 15.

10. S. Haq, J. Harnett, A. Hodgson, ***Surface Science*** 505 (2002) 171.

11. N. Materer, U. Starke, A. Barbieri, M.A. Van Hove, G.A. Somorjai, G.J. Kroes, C. Minot, ***Surface Science*** 381 (1997) 190.

12. A.L. Glebov, A.P. Graham, A. Menzel, ***Surface Science*** 427/428 (1999) 22.

13. N. Ikemiya, A.A. Gewirth, ***Journal of Americal Chemical Society*** 119 (1997) 9919.

14. B.D Kay, K.R. Lykke, J.R. Creighton, S.J. Ward, ***Journal of Chemical Physics*** 91 (1989) 5120.

15. R.S. Smith, C. Huang, E.K.L. Wong, B.D. Kay, ***Surface Science*** 367 (1996) L13.

16. P. Löfgren, P. Ahlström, D.V. Chakarov, J. Lausmaa, B. Kasemo, ***Surface Science*** 367 (1996) L19

17. G. Pirug, H.P. Bonzel, ***Surface Science*** 405 (1998) 87.

18. P.A. Thiel, T.E. Madey, ***Surface Science Reports*** 7 (1987) 211.

19. H. Dubois, B.R. Zegarski, R.G. Nuzzo, ***Journal of Americal Chemical Society*** 112 (1990) 570.

20. J.V. Barth, H. Brune, G. Ertl, R.J. Behm, ***Physical Review B*** 42 (1990) 9307.

21. D.D. Chambliss, R.J. Wilson, S. Chiang, ***Physical Review Letters*** 66 (1991) 1721.

22. M. Hara, H. Sasabe, W. Knoll, ***Thin Solid Films*** 273 (1996) 66.

23. T. Boland, B.D. Ratner, ***Langmuir*** 10 (1994) 3845.

24. I. Engquist, I. Lundström, B. Liedberg, A.N. Parikh, D.L. Allara, ***Journal of Chemical Physics*** 106 (1997) 3038.

25. I. Engquist, I. Lundström, B. Liedberg, ***Journal of Physical Chemistry*** 99 (1995) 12257.

26. B. Mate´, A. Medialdea, M.A. Moreno, R. Escribano, V.J. Herrero, ***Journal of Physical Chemistry B*** 107 (2003) 11098.

27. A.S. Bolina, A.J. Wolff, W.A. Brown, ***Journal of Physical Chemistry B*** 109 (2005) 16836.

28. F. Bensebaa, T.H. Ellis, Progress In Surface Science 50 (1995) 173.

29. E.J. Sturrock, Q. Chen, P.H. Borchardt, N.V. Richardson, ***Journal of Electron Spectroscopy And Related Phenomena*** 135 (2004) 127.

30. E.J. Sturrock, P.H. Borchardt, N.V. Richardson, "STM study of water and benzyl mercaptan on Au(111)" – unpublished work 2004.

Chapter 7: General conclusions.

7.1 Introduction

Finally, I will here summarize all the conclusions from the monolayers of benzylmercaptan (BM), 2-mercaptoethanol (2ME) and water grown on Au(111). First the results from the adsorption of the two thiols on Au(111) will be described and compared to each other, including any similarities and differences between them. Second, the adsorption of water onto clean Au(111) and SAM of each of these thiols will be described and the possible structure of the adsorbed water molecules will be discussed.

7.2 Adsorption of benzylmercaptan and 2-mercaptoethanol on Au(111).

The SAMs of both these thiols show interesting properties regarding the orientation and structure of the molecules. There are both similarities between BM and 2ME like the coverage dependence of the molecular orientation and deprotonation of the molecules upon adsorption, and differences like sticking probability and ordered structure of the SAMs.

There is a great difference in sticking probability between the two thiols, and the adsorption process and environment (gaseous in UHV or solution at atmospheric pressure) where the SAMs are formed also has a big influence on

that. When the thiols were applied to the surface by gaseous exposure in UHV, their sticking probability were just a fraction of unity, but much higher for 2ME than for BM. An exposure of around 400L was required for a full monolayer of 2ME while over 50000L was needed for BM. These observations were found by vibrational spectroscopy (HREELS and RAIRS). For SAMs formed in ethanol solution on the other hand, contact angle measurements resulted in much better sticking probability for BM than for 2ME. This result however may also depend on the different shape on these molecules.

The orientation of the molecules in the SAMs of both BM and 2ME formed by gaseous deposition in UHV is obviously coverage dependent as verified by vibrational spectroscopy (HREELS and RAIRS). Both these molecules are orientated parallel to the surface at low coverage while they are more vertical at high coverage (saturated monolayer). A possible explanation is the interaction between the aromatic ring (BM) or OH-group (2ME) with the surface at low coverage and intermolecular interactions between the rings (BM) [1] and hydrogen bonding (2ME) respectively [2] together with steric hindrance at high coverage. For BM just two orientations of the molecules were found, with the plane of the aromatic ring parallel and perpendicular to the surface at low (around 20000L) and high coverage respectively (50000L). Similarly the 2ME molecules are orientated with the C-C-O plane parallel to the surface at low coverage (100L) and perpendicular to it at saturated monolayer. In addition, an intermediate orientation of the 2ME molecules was found at around 200L coverage with the C-C backbone orientated along the surface but the hydroxyl group standing up. At low temperatures multilayers were formed of both BM and 2ME for exposures beyond that for one full monolayer. These additional layers

did not show any specific molecular orientation and their molecules were not deprotonated as all peaks increased equally and the spectra looked much the same as their corresponding ones for the gas phase [3].

A ordered structure of BM on Au(111) was obtained by gaseous deposition of the thiol in UHV at high coverage (saturated monolayer). The result was a $(\sqrt{7}x\sqrt{7})R19.1^0$ structure which was clearly observed by LEED [1] and STM [4]. This structure is common for molecular adsorption on most (111) metal surfaces [5-7]. At low coverage, there were no long range order for BM on Au(111), just only islands of BM hexamers as a result from the STM images. For 2ME adsorbed on Au(111) STM was performed but the images were not sharp enough to evaluate line profiles and hence get any structural information, although one of them showed a striped pattern similar to the structures found by Hyun & Rhee [2].

7.3 Adsorption of water (D_2O) on Au(111) and SAMs of benzylmercaptan and 2-mercaptoethanol.

Once the molecular orientations and structures of the SAMs of BM and 2ME are known, the next step is to study the adsorbed water molecule above these monolayers and onto clean Au(111). There are some interesting results for adsorbed water (or D_2O), in particular from the RAIRS spectra but also a few STM images.

In RAIRS D_2O was used instead H_2O to avoid that the interesting peaks "drown" into the interfering bands from the detector ice and trace of water

vapour in the IR beam line. There were three interesting bands which appeared after D_2O was added, a small peak at 2730 cm^{-1} (free O-D stretch), a strong broad peak at 2450-2550 cm^{-1} (hydrogen bonded O-D stretch) and a small peak at 1220 cm^{-1} (O-D bend). The free O-D stretch (2730 cm^{-1}) was an indication of the build up of the first layer. The area for this band increased linearly with exposure and then levelled out at a maximum indicating a full monolayer. Then the next layer builds up and the free O-D stretches in the first layer become hydrogen bonded and are replaces by free O-D in the new layer, and so on. Also the peak area maximum is lower for water adsorption on more hydrophilic surfaces (2ME) and higher on more hydrophobic ones (BM) with adsorption on clean Au(111) somewhat in between. This is probably because the more hydrophobic surfaces cause the adsorbed water molecules to form smaller clusters and hence increase the surface of free O-D stretches.

The peak areas for the hydrogen bonded O-D stretches and O-H bending increase linearly with exposure, indicating a linear grown of the ice thickness with exposure. This is the case for all surfaces – the clean Au(111) and all coverages of both BM and 2ME.

The only band of which the wavenumber changed noticeably with the exposure was the hydrogen bonded O-D stretch. This had a variation between 2420 and 2530 cm^{-1}, more or less for each surface. It consists of a number of peaks, each assigned to a specific crystal or amorphous phase of the ice [8]. As these are not separated in our spectrometer, the wavenumber of the peak maximum is used in each case to tell whether the polycrystalline or amorphous ice dominates. The wavenumber for this band were lower for D_2O adsorbed on surfaces of low coverage 2ME and high coverage BM. As a result of these

rough estimations it seems that the more hydrophilic surface the more polycrystalline is the adsorbed ice layer. Similar conclusions were found for other hydrophilic and hydrophobic thiols (and their mixtures) by Engquist et al. [9]

Finally, the structures of water adsorbed on some surfaces were imaged by STM. On clean Au(111) the water molecules adsorb form stable clusters of six hexamers. The only other surface which was successfully imaged was low coverage of BM on Au(111), on which the water molecules seem to adsorb as trimers of hexamers units [4].

7.4 Final words and possible future work.

To round up everything I would like to say that there are many interesting results from all these experiments. The molecular orientations in the SAMs of both BM and 2ME are coverage dependent, and for BM an ordered structure for high coverage (one monolayer) is found. In addition, when water adsorbs on these SAMs and clean Au(111) in UHV at low temperature, the resulting structure of the ice is also dependent of the well defined surface.

All these interesting findings though, I would like to suggest some further work to be done in the future.

- Try to perform LEED and STM experiments for 2ME (in the same way as for BM) in order to find an ordered structure on Au(111).
- Grow SAMs of BM and 2ME (and mixtures of them) on Au(111) from solution in atmospheric pressure (in a box with nitrogen

atmosphere) and then transfer the substrate into the UHV system via a fast entry lock for analyses with RAIRS, HREELS, STM, LEED etc, and compare the results with the gas phase deposition experiments.

- Try to improve the liquid helium cooling system and resistive heater for better temperature control, i.e. to reach a desired temperature and stabilise the substrate at it more quickly.
- Grow a SAM of a mixture of BM and 2ME by gaseous dosing. However the exact molar ratio can be difficult to know. Although the mixture can be easily measured when mixing and filling the glass tube, the molar ratio may change during the purification (freeze-pump-thaw procedure) due to different boiling points.
- Experiment with the settings on the RAIRS, or use another better spectrometer, in trying to resolve the bands for different phases of the D_2O ice.
- Acquire RAIRS spectra quicker by much less number of scans and slowly increase temperature while getting the spectra. This "simple TPD" could give information of phase changes in the ice versus temperature and also desorption temperature.

These suggestions are just speculative for me today. But I hope I get the chance to try any of them in the future.

7.5 References.

1. E.J. Sturrock, Q. Chen, P.H. Borchardt, N.V. Richardson, ***Journal of Electron Spectroscopy And Related Phenomena*** 135 (2004) 127.
2. M. Hyun and C.K. Rhee, ***Bulletin of Korean Chemical Society*** 22 (2001) 213.
3. ***National Institute of Standards & Technology***, Standard Reference Database Number 69, July 2005 Release. http://webbook.nist.gov/chemistry (accessed Sep 2005).
4. E.J. Sturrock, P.H. Borchardt, N.V. Richardson, "STM study of water and benzyl mercaptan on Au(111)" – unpublished work 2004.
5. R. Heinz, J.P. Rabe, ***Langmuir*** 11 (1995) 506.
6. T. Müller, D. Heuer, H. Pfnür, U. Köhler, ***Surface Science*** 347 (1996) 80.
7. G.J. Jackson, S.M. Driver, D.P. Woodruff, B.C.C. Cowie, R.G. Jones, ***Surface Science*** 453 (2000) 183.
8. F. Bensebaa, T.H. Ellis, Progress In Surface Science 50 (1995) 173.
9. I. Engquist, I. Lundström, B. Liedberg, A.N. Parikh, D.L. Allara, ***Journal of Chemical Physics*** 106 (1997) 3038.